



Self-Cleaning and Anti-Reflective Microtextured Fluoropolymer Cover Films for Photovoltaics

Zur Erlangung des akademischen Grades eines
DOKTORS DER INGENIEURWISSENSCHAFTEN (Dr.-Ing.)

von der KIT-Fakultät für Maschinenbau des
Karlsruher Institut für Technologie (KIT)
angenommene

DISSERTATION

von

M.Sc. Aiman bin Roslizar

Tag der mündlichen Prüfung : 06.03.2024
Hauptreferent : Prof. Dr. Hendrik Hölscher
Korreferenten : Prof. Dr. Bryce S. Richards
Prof. Dr. Christian Greiner



This document is licensed under a Creative Commons Attribution-ShareAlike 4.0 International License (CC BY-SA 4.0): <https://creativecommons.org/licenses/by-sa/4.0/deed.en>

Table of Contents

Abstract	6
Kurzfassung	7
List of Abbreviations	8
List of Symbols	9
List of Figures	10
1	Introduction	13
2	Fundamentals	17
2.1	Fundamentals of Photovoltaics	17
2.1.1	Solar Cell Working Principle	17
2.1.2	Solar Cell Performance Parameters	17
2.1.3	Application of PV	18
2.2	PV Soiling Mitigation	19
2.3	Self-Cleaning by Microtexturing	22
2.3.1	Observation of Superhydrophobicity from Nature	22
2.3.2	Fundamentals of Wetting Property	22
2.3.3	Artificial Structures to Induce Superhydrophobicity	24
2.4	Fundamentals of Light Management in PV	25
2.5	Light Management by Microtextures	27
2.6	Fluoropolymers as PV Module Front Cover Material	28
3	Methods	31
3.1	Fabrication of Microtextured Cover Films	31
3.1.1	Hot-Embossing Fundamentals	33
3.1.2	Mold Fabrication	35
3.1.3	Microtextures Design	35
3.1.3.1	Random Microtextures	36
3.1.3.2	Periodic Cone-Shaped Microtextures	36
3.1.4	Up-Scaling to Large-Area Microtextures	37
3.2	Cover Film Material: Fluorinated Ethylene Propylene	38
3.3	Microtextured Cover Film on PV Devices	38
3.3.1	PV Devices	38
3.3.2	Temporary: Index Matching Gel	39
3.3.3	Permanent: Lamination	40
3.4	Characterization	40
3.4.1	Wetting property	40

3.4.2	Microscopy.....	40
3.4.2.1	Optical Microscope	40
3.4.2.2	Scanning Electron Microscope.....	41
3.4.3	Reflectance and Transmittance.....	41
3.4.4	Solar Cell Characteristics	41
3.4.5	Self-Cleaning	41
3.4.5.1	Dust Contaminants.....	42
3.4.5.2	Impact of Self-Cleaning on Photocurrent Generation.....	43
3.4.6	Dust Removal by Wind	44
3.4.7	Durability of Microtextures.....	45
4	Random Microtextured PV Module Cover Film	47
4.1	Influence of Random Microtextured FEP Film on Properties Relevant for PV Applications	48
4.1.1	Wetting Properties.....	48
4.1.2	Optical Properties	52
4.2	Morphological Analysis of the Random Microtextures	56
4.3	Application as PV Module Front Covers	60
4.3.1	Electrical Properties	60
4.3.2	Self-Cleaning Capability.....	62
4.4	Summary.....	64
5	Periodic Cone-Shaped Microtextured PV Module Cover Film	65
5.1	Influence of Aspect Ratio on the Wetting Property of Cone-Shaped Microtextured Surfaces.....	66
5.2	Morphological Analysis of Periodic Microtextures and Durability Towards Imperfections.....	68
5.3	Microtextured FEP as Anti-Reflective PV Module Covers	71
5.4	Periodic Microtextured FEP as Self-Cleaning Covers	75
5.5	Multifunctional Integrity Under Fabrication and Abrasion Defects.....	82
5.6	Comparing Random and Cone-Shaped Microtextured FEP	85
5.7	Summary.....	88
6	Wind as an Alternative Force for Self-cleaning Soiled PV Modules	89
6.1	Self-Cleaning of Dust Under the Influence of Wind	92
6.1.1	Removal of Large Dust Particles.....	92
6.1.2	Removal of Small Dust Particles.....	94
6.1.3	Dust Particle Removal Behavior	95
6.2	Comparing Dust Particle Removal from Microtextured PV Module Cover Films	96
6.3	Wind for Self-Cleaning PV Module Applications.....	99
6.3.1	PV Module Performance Recovery.....	99

6.3.2	Wind Speed Requirements in Real-World Conditions	101
6.3.3	Limitations of Investigation.....	101
6.4	Summary.....	102
7	Summary and Outlook	105
References	109
List of Publications.....		122

Abstract

Solar photovoltaic (PV) is increasingly becoming an alternative source of renewable energy generation. Nevertheless, there exist potential issues that could hinder its power generation performance. One issue that significantly reduces a PV system's performance is soiling where dust contaminants on the surface prevents light from entering the PV module and thus reduce power generation up to 78%. This study focuses on the development of a PV module front cover as a mitigation solution to the issue of PV soiling, utilizing rainfall. A random microtextured front cover was first developed using a suitable fluoropolymer material – fluorinated ethylene propylene (FEP) – to introduce superhydrophobic properties to the PV module top surface. This simple random microtexturing resulted in a superhydrophobic surface (contact angle of $156\pm 1^\circ$ and a roll-off angle of $8\pm 3^\circ$) and an improved J_{sc} by 1.3% compared to a reference PV mini-module. The self-cleaning performance of the random microtextured FEP front cover demonstrated a 93.6% recovery in terms of J_{sc} . The PV module front cover was further improved by introducing periodic cone-shaped microtextures onto the FEP front cover films and managed to demonstrate significant enhancement in both self-cleaning and anti-reflective properties. The final cone-shaped design, having an aspect ratio of 0.7, successfully retained the superhydrophobic properties (contact angle = $161\pm 3^\circ$ and roll-off angle = $6\pm 4^\circ$) and further improved the light in-coupling. It significantly reduced the front reflectance and achieved a significant 3.1% relative improvement in J_{sc} . The self-cleaning performance was also enhanced where a recovery ratio of 100% and 65.8% were achieved when soiled with sea sand and Arizona test dust, respectively. Further investigations were conducted to determine whether wind could be utilized as a driving force for the self-cleaning mechanism in the case where rainfall was absent. It was successfully shown that wind can be utilized for dust removal but would require relatively high wind speeds. Moreover, the introduction of microtextures made the wind requirement higher compared to a planar surface. For this option of utilizing wind for dust removal to be a practical solution, the result presented becomes a good starting point for further research to be conducted. In any case, this research work presents the successful development of a multifunctional (self-cleaning and anti-reflective) superhydrophobic microtextured PV module front cover that addresses the issue of PV soiling and enhances photocurrent generation.

Kurzfassung

Solar-Photovoltaik (PV) wird zunehmend zu einer alternativen Quelle der erneuerbaren Energieerzeugung. Dennoch gibt es potenzielle Probleme, die die Leistung der Stromerzeugung beeinträchtigen könnten. Ein Problem, das die Leistung einer PV-Anlage erheblich beeinträchtigt, ist die PV-Verschmutzung. Der Ph.D. Die in dieser Dissertation vorgestellten Forschungsarbeiten konzentrieren sich auf die Entwicklung einer Frontabdeckung für PV-Module als Lösung zur Eindämmung des Problems der PV-Verschmutzung unter Ausnutzung von Regenfällen. Zunächst wurde eine zufällige mikrotexturierte Frontabdeckung unter Verwendung eines geeigneten Fluorpolymermaterials – fluoriertem Ethylenpropylen (FEP) – entwickelt, um der Oberseite des PV-Moduls superhydrophobe Eigenschaften zu verleihen. Diese einfache zufällige Mikrotexturierung führte zu einer superhydrophoben Oberfläche (Kontaktwinkel von $156\pm 1^\circ$ und einem Abrollwinkel von $8\pm 3^\circ$) und einem um 1.3% verbesserten J_{sc} im Vergleich zu einem Referenz-PV-Minimodul. Die Selbstreinigungsleistung der zufällig mikrotexturierten FEP-Frontabdeckung zeigte eine Rückgewinnung von 93.6% in Bezug auf J_{sc} . Die Frontabdeckung des PV-Moduls wurde durch die Einführung periodischer kegelförmiger Mikrotexturen auf den FEP-Frontabdeckungsfolien weiter verbessert und konnte eine deutliche Verbesserung sowohl der Selbstreinigungs- als auch der Antireflexionseigenschaften nachweisen. Das endgültige kegelförmige Design mit einem Seitenverhältnis von 0.7 behielt erfolgreich die superhydrophoben Eigenschaften bei (Kontaktwinkel = $161\pm 3^\circ$ und Roll-Off-Winkel = $6\pm 4^\circ$) und verbesserte die Lichteinkopplung weiter. Es reduzierte das Reflexionsvermögen an der Vorderseite erheblich und erzielte eine erhebliche relative Verbesserung von 3.1% im J_{sc} . Auch die Selbstreinigungsleistung wurde verbessert, wobei bei Verschmutzung mit Seesand und Teststaub aus Arizona eine Rückgewinnungsrate von 100% bzw. 65.8% erreicht wurde. Weitere Untersuchungen wurden durchgeführt, um festzustellen, ob der Wind als treibende Kraft für den Selbstreinigungsmechanismus genutzt werden könnte, wenn es nicht regnete. Es konnte erfolgreich gezeigt werden, dass Wind tatsächlich zur Staubentfernung genutzt werden kann, dafür aber relativ hohe Windgeschwindigkeiten erforderlich wären. Darüber hinaus wurde durch die Einführung von Mikrotexturen der Windbedarf im Vergleich zu einer ebenen Oberfläche erhöht. Damit diese Option der Nutzung von Wind zur Staubentfernung eine praktische Lösung darstellt, stellen die präsentierten Ergebnisse einen guten Ausgangspunkt für weitere Forschungsarbeiten dar. Die Forschungsarbeit präsentiert die erfolgreiche Entwicklung einer multifunktionalen (selbstreinigenden und entspiegelnden) superhydrophoben mikrotexturierten PV-Modul-Frontabdeckung, die das Problem der PV-Verschmutzung angeht und die Photostromerzeugung verbessert.

List of Abbreviations

PV	Photovoltaics
IEA	International Energy Agency
MPP	Maximum Power Point
PDMS	Polydimethylsiloxane
IMPS	Inverted Micro-Pyramidal Structures
mc-Si	Multicrystalline Silicon
FEP	Fluorinated Ethylene Propylene
EVA	Ethylene Vinyl Acetate
IMT	Institute of Microstructure Technology
KIT	Karlsruhe Institute of Technology
PTFE	Polytetrafluoroethylene
PC	Polycarbonate
CIGS	Copper Indium Gallium Diselenide
SEM	Scanning Electron Microscopy
UV-vis-NIR	Ultraviolet–Visible–Near Infrared
INGV	Istituto Nazionale di Geofisica e Vulcanologia

List of Symbols

$I-V$	Current–Voltage
$J-V$	Current Density–Voltage
J_{SC}	Short-Circuit Current Density
V_{OC}	Open-Circuit Voltage
ϑ	Contact Angle
J_{MPP}	Current Density
V_{MPP}	Voltage
PCE	Power Conversion Efficiency
P_{out}	Output Power
P_{in}	Input Power
FF	Fill Factor
η	Solar Cell Efficiency
λ	Wavelength
Ra	Average Roughness
n	Refractive Index
RR	Recovery Ratio
t	Time
v	Velocity

List of Figures

- Figure 1.1 Soiled PV modules
- Figure 2.1 J - V characteristic curve quantifying the performance of a solar cell
- Figure 2.2 Examples of mitigation methods for PV module cleaning
- Figure 2.3 Definition of contact angle of a water droplet resting on a surface
- Figure 2.4 Definition of wetting property based on contact angle of water droplet resting on a planar surface
- Figure 2.5 Different wetting states when water droplet rests on a textured surface
- Figure 2.6 Fundamental interaction of light when hitting a surface
- Figure 2.7 Light trapping in a PV device due to the presence of microtextures
- Figure 3.1 Hot-embossing set-up for microtextured sample fabrication
- Figure 3.2 Defects during hot-embossing of microtextures
- Figure 3.3 Phases and parameters throughout the hot-embossing process
- Figure 3.4 Hot-embossed random microtextures
- Figure 3.5 Hot-embossed cone-shaped microtextures
- Figure 3.6 Development of large area microtextured mold insert
- Figure 3.7 Conceptual illustration of PV device architectures
- Figure 3.8 Dust contaminants used to investigate self-cleaning capability
- Figure 3.9 Wind tunnel test set-up
- Figure 4.1 Influence of fabrication parameters on the wetting properties of hot-embossed random microtextured FEP
- Figure 4.2 Water droplet on untextured FEP and microtextured FEP surfaces
- Figure 4.3 Bouncing of water droplets on untextured FEP and microtextured FEP surfaces
- Figure 4.4 Reflectance measurements of various microtextured FEP samples
- Figure 4.5 Full reflectance spectra for the various fabricated microtextured FEP samples
- Figure 4.6 Full transmittance spectra for the various fabricated microtextured FEP samples
- Figure 4.7 SEM images of nickel mold insert for random microtextures
- Figure 4.8 Surface morphology of all fabricated random microtextured FEP samples
- Figure 4.9 Interferometry images for surface roughness evaluation
- Figure 4.10 J - V characteristic curves of PV mini-module comparing influence of various top covers
- Figure 4.11 Absorbance of index matching gel
- Figure 4.12 Self-cleaning of soiled surface demonstrated visually and quantitatively
- Figure 4.13 Visual demonstration of self-cleaning mechanism on random microtextured FEP
- Figure 5.1 Hexagonally arranged cone-shaped microtextures
- Figure 5.2 Influence of aspect ratio on wetting properties
- Figure 5.3 All fabricated periodic cone-shaped microtextured samples having different aspect ratio
- Figure 5.4 Defects in fabricated cone-shaped microtextures
- Figure 5.5 Impact of height loss on the wetting properties of microtextured surface

Figure 5.6	Influence of aspect ratio on the reflectance of microtextured FEP top covers when applied to CIGS solar cells
Figure 5.7	$J-V$ characteristic curves of CIGS solar cells with the application of planar untextured FEP and microtextured FEP as front covers
Figure 5.8	Relative improvement of CIGS solar cell by different aspect ratio microtextured FEP covers
Figure 5.9	Self-cleaning performance of different front covers attached to a glass encapsulated mc-Si solar cell
Figure 5.10	Dust particles used for self-cleaning investigations
Figure 5.11	Fine dust particles that still remains on the microtextured surfaces after self-cleaning
Figure 5.12	Illustration of microcones and dust particles that could potentially be trapped within the cavities
Figure 5.13	Impact of multiple soiling-cleaning cycles on self-cleaning performance
Figure 5.14	$J-V$ characteristic of PV mini-module with microtextured FEP covers showing the result of multiple soiling-cleaning cycles
Figure 5.15	Dust particles used in abrasion tests
Figure 5.16	Impact of abrasion on cone-shaped microtextured FEP films
Figure 5.17	Impact of abrasion on contact angle of microtextured FEP films
Figure 5.18	Impact of abrasion on reflectance of microtextured FEP films
Figure 5.19	Impact of different microtextured front covers on $J-V$ characteristic when attached to a mc-Si PV mini-module
Figure 5.20	Self-cleaning performance of different front surfaces comparing random microtextured FEP and cone-shaped microtextured FEP as PV module front cover
Figure 6.1	Bouncing of falling water droplets on different surfaces
Figure 6.2	Influence of wind velocity on the removal of large dust particles
Figure 6.3	Influence of wind velocity on the removal of small dust particles
Figure 6.4	Visual observation of dust removal behavior
Figure 6.5	Trendlines of large dust particle removal behavior
Figure 6.6	Trendlines of small dust particle removal behavior
Figure 6.7	Impact of dust removal on PV output in terms of J_{sc}
Table 2.1	Main advantages (+) and disadvantages (–) of various mitigation methods

1 Introduction

Solar Photovoltaics (PV) is gaining more support as an alternative source of energy with 14,458 GW of potential power generation capacity projected (Net Zero Emission scenario) to be installed globally by the year 2050 [1]. The exponential increase of commissioned solar PV installations in recent years has resulted in a total installed capacity of 1,185 GW at the end of 2022 [2]. Moreover, with the rising cost of fossil fuel and its limited reserves, a renewable energy source such as solar PV becomes more appealing. Apart from being a renewable and cleaner source of energy, solar PV is also attractive since it can generate electricity from anywhere, as long as sufficient sunlight is available. Furthermore, a stand-alone PV system can be installed in remote and hard to reach locations – and thus not having to rely on electricity from a power grid.

PV modules, which operate on the principle of converting sunlight into electricity, are commonly designed to have a lifespan >20 years. Such PV devices are considered as a mature and stable technology, but throughout their expected lifetime, there are potential defects and failures that could affect the solar energy generation. Some are due to technical defects that depend on the PV module condition such as flawed devices, device cracks, various degradations, delamination of components, corrosion and discoloration [3], [4]. Meanwhile some are due to external factors such as the weather conditions leading to reduced sunlight, shadowing due to surrounding objects or activities and also soiling, where all of these reduce the performance of PV systems [3], [4]. Among these potential problems, PV soiling is the main focus of this research study.

PV soiling occurs when dust contaminants, of various possible origins, are deposited on the surface of PV modules and reduces the incident light that hits the active area of the solar cell. The reduced photon flux reaching the solar cells via spectral losses (absorption and reflection) – due to the soiling – will thus reduce the photocurrent generation [5]–[7]. Deposited dust contaminants on the surface also results in the shadowing of the underlying solar cells which significantly reduces the energy yield of the PV modules to perform below their expected capacity rating [6], [8]–[12].

Figure 1.1 demonstrates two separate examples of soiled PV modules. In both cases, dried up soil contaminants can be observed deposited on the surface. In Figure 1.1b, there seems to be signs of dust removal either from wind or rain but was minimal and most of the soiling remains deposited on the surface. Without proper maintenance or dust mitigation procedures, the PV soiling will affect the power generation performance of the PV modules.



Figure 1.1 Soiled PV modules with dust contaminants deposited on the surface showing (a) dried up soil deposits and (b) soiled PV modules with minimal dust removal without maintenance.

The problem of PV soiling is highly dependent on a wide range of factors, including the local climate, properties of dust and its concentration, as well as whether a mitigation strategy is employed [10], [13], [14]. Furthermore, the complex nature of the dust deposition and dust removal also depends on the properties of the dust contaminants (dust composition and particle size distribution), as well as environmental factors such as temperature, rainfall, and radiation-induced aging [15]. Moreover, for investigation of a self-cleaning solution for the problem of PV soiling, the adhesion of dust to the surface plays an important role, which is governed by several aspects such as particle shape, roughness, chemistry and size [15]. These real-world conditions are taken into consideration, where necessary, in this research work.

PV modules in different regions of the world are subjected to various kinds of soiling. In fact, locations within the same region can have very different dust profiles depending on the surrounding geography, weather conditions and industrial activities [14]. Dust contaminants in the PV soiling issue can appear in various forms such as loose geological minerals like sand and limestone, from combustion exhausts of the industrial and transportation sector, and also as biological matters such as pollens and bird droppings [16], [17].

The problem of PV soiling is more prominent in arid or semi-arid areas, such as the Middle East and North Africa, where dust accumulation is very high due to the high amount of suspended particles in the air [13], [18]. Unfortunately, those areas are also among the most potential for solar energy.

PV modules installed in urban locations (such as residential or rooftop installations) that are close to heavy traffics and industrial areas often suffer from carbon-based soiling agents such as grime and soot, which can worsen the performance of PV systems due to the high light absorbing properties of these types of soil [17]. When left un-cleaned and exposed to the environment over time, these carbon-based soiling can become hard to remove due to formation of cement-like films that adheres to the surface of the PV modules [17].

Volcano eruptions are another interesting phenomenon that can impact the performance of PV systems in a very wide area, with volcanic tephra being deposited on any exposed surface. Even though the volcano eruption occurs in a certain region, it can be a far-reaching effect and contributes towards PV soiling, with volcanic ash having been detected on PV modules that were located ≈ 2700 km away [19], [20]. This is made worse by the fact that volcanic pollutants can remain in the atmosphere for months due to the resuspension of deposited volcanic ash, thus potentially soiling PV modules again [21].

In terms of dust profiles, there is a wide range of dust sizes available in the environment. The majority of dust particles deposited on PV modules have diameters in the scale of tens of micrometers [22]–[25]. Similarly, dust particles of up to $400 \mu\text{m}$ in diameter have also been collected and reported from PV modules, although in smaller quantities [23], [26]–[29]. Furthermore, the dust contaminant type is crucial since the performance of a PV device is spectrally sensitive whereby different dusts can have different colored pigmentations, such as carbon (black) or iron oxide (red) [30].

PV soiling has been shown to severely reduce the performance of PV modules. Outdoor soiling tests, reported in the literature, demonstrated a reduction in PV module performance by up to 78% over a period of one year, where modules were exposed to soiling and no cleaning was implemented [17], [31]. Meanwhile, a few studies have reported specifically on the impact of volcano ash on PV systems. There are severe cases that can result in the PV modules no longer producing any solar power such as the study based on the 2010 eruption of Eyjafjallajökull volcano in Iceland where PV modules within a 300 km radius would have a high chance of being fully covered by volcanic tephra deposits [19]. From a different study, a 60 kW PV system situated ≈ 50 km away from the Shinmoedake volcano, suffered a $\approx 67\%$ performance drop due to volcanic ash deposition [32]. It is thus necessary to address the issue of PV soiling to prevent these solar energy generation losses.

One approach to reduce the effect of PV soiling is through functional surface modification. This Ph.D. study proposes the development of a multifunctional microtextured self-cleaning fluoropolymer PV module front cover. This is an attractive approach since it is a passive solution which reduces any maintenance required and reduces the negative impact of PV soiling. A superhydrophobic cover film attached on top of the glass superstrate of a PV module has the potential to remove dust from the soiled surface assisted by rainfall. The cleaning mechanism occurs via water droplets picking up the dust as they roll down the surface leaving behind a clean PV module. Furthermore, a selective design of the microtextures will also enable the enhancement of light in-coupling by introducing an anti-reflective function. For application as a multifunctional PV module front cover, an ideal microtextured cover would maximize enhancement of both self-cleaning and anti-reflective properties.

This thesis summarizes my Ph.D. work conducted from Oct 2015 to Jan 2020 at the KIT which resulted in the development of a multifunctional PV module front cover to address the issue of PV soiling. There was a delay until the submission of the thesis due to personal problems faced especially worsen by the Covid-19 issue. Since leaving KIT, two journal publications, one conference attended, and finally the thesis was successfully completed based on the Ph.D. work. In Chapter 2, the theoretical background related to the proposed solution is presented. While in Chapter 3, the key methods used in this research work are shortly explained. Chapter 4 presents the development of a

random microtextured fluoropolymer PV module front cover. The main focus of the chapter is to investigate how it would be possible to combine a low energy material and microtexturing such that it achieves superhydrophobicity in order to address the PV soiling issue and at the same time suitable for PV applications. Further improvement to the self-cleaning front cover is presented in Chapter 5 by investigating how it would be possible to enhance the optical benefits through optimizing the microtextures design, while also maintaining the superhydrophobic properties resulting in a multifunctional front cover (anti-reflective and self-cleaning). Since the superhydrophobic self-cleaning front cover to address the issue of PV soiling relies on rainfall or water droplets, Chapter 6 presents the potential of using wind as an alternative force for cleaning soiled PV modules and how the microtextured superhydrophobic self-cleaning front cover influences dust removal by wind. Finally in Chapter 7, a summary is followed by an outlook for further improvement and research opportunities are discussed.

2 Fundamentals

The fundamental theoretical background relevant to the key topics in this research study are first introduced to provide better understanding for the work that is presented in the following chapters. This chapter begins by introducing the topic of PV that is the targeted application area relevant to the work presented in this dissertation.

2.1 Fundamentals of Photovoltaics

2.1.1 Solar Cell Working Principle

The basic unit of a PV device is the solar cell, whose working principle is the direct conversion of light into electricity. A conventional solar cell architecture consists of an n-type (electron-conducting) and a p-type (hole-conducting) semiconductor. This excess of electrons or donors in the n-type material and the excess of holes or acceptors in the p-type material is achieved by means of doping. The photovoltaic effect occurs when energy from incident light is absorbed by the p-n semiconductor which is the active solar cell area. The absorption of energy from a photon promotes an electron into an excited state to create an electron-hole pair, with a requirement that the energy absorbed is larger than the energy bandgap. Photons with energy smaller than the bandgap will simply pass through since they cannot be absorbed. The free electrons and holes generated are then collected at opposite electrodes of the device, and when the circuit is completed, electric power can be harnessed. A PV device is generally completed with additional components such as metal contacts, anti-reflective coatings (ARC), encapsulations, back sheets, and glass front covers – depending on the specific technology. There are various types of PV devices that have been and are still being developed with silicon PV devices currently the most widely installed PV technology, having >95% market of PV production capacity in 2022 based on the International Energy Agency (IEA) report [33]. All functioning based on the same working principle – the photovoltaic effect.

2.1.2 Solar Cell Performance Parameters

A solar cell's performance is evaluated based on its electrical parameters. The performance is most commonly measured from their current–voltage (I – V) characteristics, where normalizing to a solar cell area (usually in cm^2) results in the current density–voltage (J – V) characteristics as illustrated in Figure 2.1.

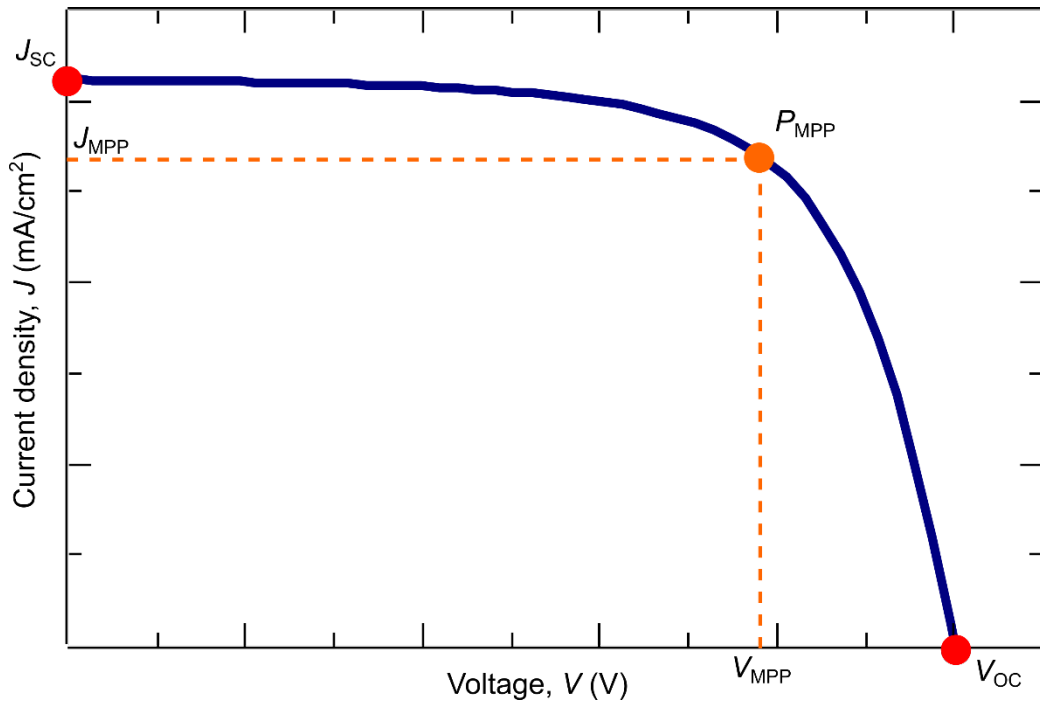


Figure 2.1 J - V characteristic curve quantifying the performance of a solar cell; demonstrating the short-circuit current density (J_{sc}), the open-circuit voltage (V_{oc}) as well as the current density (J_{MPP}) and voltage (V_{MPP}) at the maximum power point (MPP).

From the I - V / J - V characteristic curve, the main performance criteria of a solar cell can be determined – the power conversion efficiency (PCE). The PCE gives the ratio of output power (P_{out}) generated from the solar cell to the incident radiant input power (P_{in})

$$PCE = \frac{P_{out}}{P_{in}} = \frac{J_{sc} \times V_{oc} \times FF}{P_{in}}$$

with the Fill Factor (FF) defined as

$$FF = \frac{(J \times V)_{max}}{J_{sc} \times V_{oc}}$$

The short-circuit current density (J_{sc}) is the maximum current generated in an area of the solar cell when there is no load ($V = 0$ V), measured in a short-circuit configuration. Meanwhile, the open-circuit voltage (V_{oc}) is the cell voltage when there is zero current ($I = 0$ mA or $J = 0$ mA/cm²) flowing through the cell measured in an open-circuit configuration.

2.1.3 Application of PV

PV modules, which are devices that consist of a number of solar cells, have been utilized for various conditions and locations. They can be installed in residential areas on rooftops; or in urban areas on the top or sides of buildings; in open space fields as PV power plants and also in hard-to-reach remote areas as stand-alone PV systems. Each application has its own requirements and limitations. The beauty of a PV system is that as long as sufficient solar irradiation shines on the area,

there is potential for solar energy. Nevertheless, an assessment must always be conducted to determine the suitability and viability of that specific location which would then be used to determine the optimum position and orientation of the PV installation. As previously discussed in Chapter 1, the geographical location highly affects the performance of a PV system. There might be potential factors such as surrounding human activities, vegetation growth, the weather conditions or potential dust contaminant sources that could affect the PV system. Any inhibition of solar irradiation will result in a loss in power generation. Therefore, understanding the location is crucial before installing any PV modules for power generation.

2.2 PV Soiling Mitigation

As also highlighted in Chapter 1, the problem of PV soiling can severely reduce the power output of a PV system unless a mitigation strategy is implemented. There are various soiling mitigation methods that have been used that can be categorized into either preventive (prevents or reduces dust from depositing onto PV modules) or restorative (removes dust that has deposited on PV modules) approaches [6], [31]. Several review papers provide a good overview of the wide range of mitigation strategies that have been explored [6], [9], [15], [31], [34]. Different PV systems might have more suitable mitigation methods depending on the specific PV system technology and the external conditions of application.

Established mitigation methods include: i) manual cleaning [9], [13], [18], [35]; ii) stowing of PV arrays [6]; iii) automated or semi-automated mechanical cleaning devices [6], [9], [13], [18], [35]; iv) the incorporation of electrodynamic screens to repel dust [36], [37]; and v) surface modification [6], [9], [18], [35], [38]. The application of several established mitigation methods is summarized in Figure 2.2.

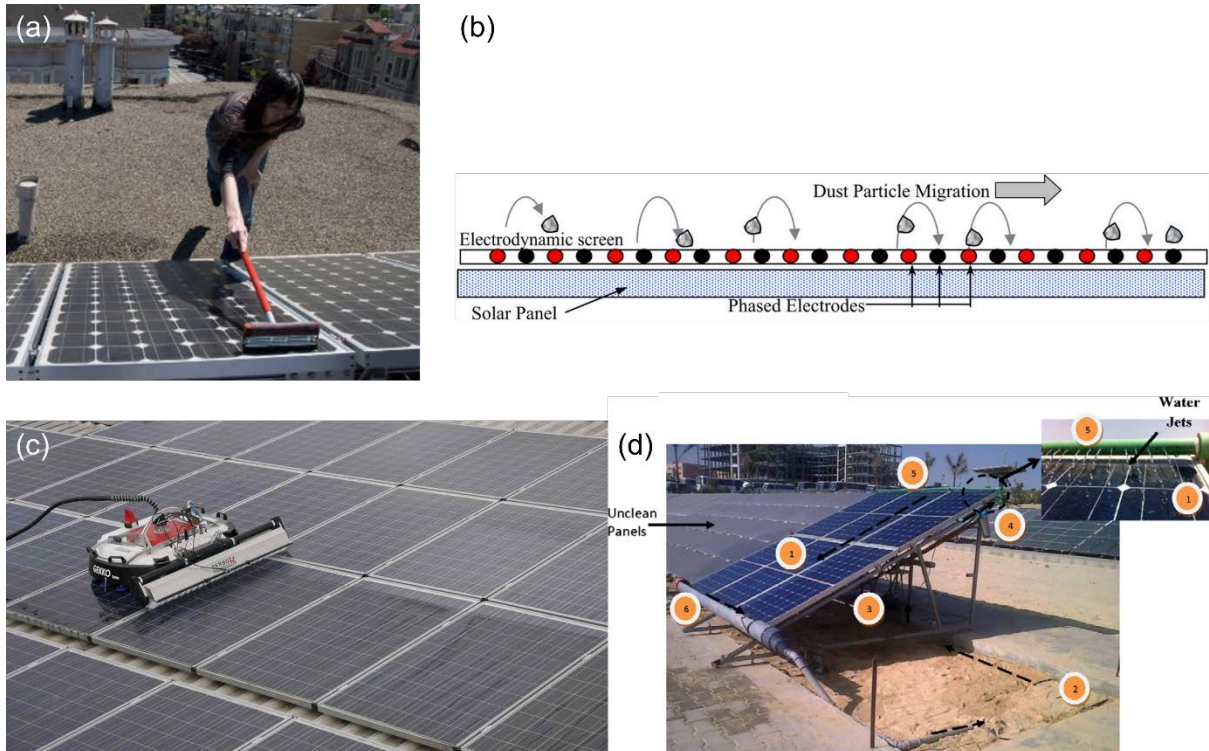


Figure 2.2 Examples of mitigation methods for PV module cleaning: (a) Manual cleaning [39], (b) electrodynamic screens to push dust particles off PV modules [40], (c) PV module cleaning robots [41], and (d) auxiliary water irrigation systems [42]. (Photos and graphics adapted are from their respective references)

The most common mitigation method is manual cleaning; which entails that operators physically clean the surface of the PV modules, leading to high labor cost [6], [9], [18], [35]. Stowing of PV arrays, such that they are protected in bad weather or when not in use, requires less human attention, but in some cases the activation and operation are still operated manually [6]. Automated or semi-automated mitigation devices such as cleaning robots, auxiliary water irrigation systems or mechanical wipers can be implemented by utilizing additional components or systems. An electrodynamic screen functions automatically and utilizes electromagnetic forces to move dust off the PV modules but is only viable for dry conditions. Fully automated systems are attractive since minimal monitoring is usually required but would most likely be economical only for large PV installation due to the higher initial and operating costs, apart from the power requirements for operation [9]. For example, an automatic cleaning system equipped with motorized brush and water flow components consumes $\approx 6\%$ of generated power, but when the water consumption is also taken into consideration, the economic benefits of the system reduces even further [7]. Surface modification is conducted to achieve a self-cleaning function by changing the wetting property of the surface to be either superhydrophobic [43] or superhydrophilic [38] by way of a chemical coating [38] or through an additional textured surface [31]. The main advantages and disadvantages of each mitigation method are listed in Table 2.1.

2 Fundamentals

Table 2.1 Main advantages (+) and disadvantages (–) of various mitigation methods (adopted from [44])

Mitigation Method	Advantages (+)	Disadvantages (–)
Manual cleaning	+ Fully restores PV module to as-clean condition [45]	– Labor and resource intensive [6], [45], [46] – Requires frequent cleaning cycles. In most cases, weekly cycles but immediate cleaning for severe cases of soiling [47]
Stowing of PV arrays	+ Protects from soiling when not in use (nighttime, dust storms)	– Ineffective during daytime if sudden dust storm approaches (insufficient stowage time) [6]
Surface modification	+ Passive self-cleaning method	– Depends on rainfall to function [38], [43]
Mechanical cleaning	+ Performance not as good as manual cleaning, but little labor required	– High initial and maintenance cost; Better suited for large systems [7] – Electrical power required as the components are auxiliary systems [7] – Potential abrasive damage [35]
Electrodynamic screens	+ Removes 90% of soiling [36] + Less power consumption; as low as 0.003% of generated power [36]	– Requires dry condition to work effectively [36]

A self-cleaning surface obtained from surface modification offers a particularly attractive approach due to it being neither labor nor resource intensive [6], [11]. This mitigation approach can reduce maintenance and labor costs due to its passive nature. Not relying on an auxiliary system for the cleaning process also means that it does not consume any of the solar power that was generated. A passive self-cleaning front cover makes it suitable for remote areas and hard-to-reach locations. Apart from reducing the requirement for manual maintenance, it can also keep the performance output of the PV module at a higher level over a longer period of time due to the consistent removal of dust from the surface.

One option for surface modification is to apply a chemical layer on top of the PV modules' surface. Nevertheless, a chemical layer can be easily eroded when exposed to the weather or scratched from external forces. Thus, the surface would no longer retain the self-cleaning function and the chemical layer would need to be reapplied; in some cases, as early as after a few months [38]. Unfortunately, applying the chemical coating in the field is itself not a viable option. Another interesting approach for surface modification is to attach a front cover that alters the PV module surface to introduce a self-cleaning function. The main strategy of this approach is to enhance the wetting property to become either superhydrophobic or superhydrophilic. This can be achieved by

selecting a suitable material that already has superhydrophobic/superhydrophilic properties or introducing textures to enhance the prevalent wetting property.

2.3 Self-Cleaning by Microtexturing

A self-cleaning surface can be achieved by introducing textures on a surface. This section discusses the fundamentals relating textures to the intended self-cleaning function from this work.

2.3.1 Observation of Superhydrophobicity from Nature

Self-cleaning can be achieved by having water droplets from rainfall rolling down the soiled PV modules, picking up the deposited soil, which can be observed on superhydrophobic surfaces. Superhydrophobicity is a state of strong water repellence, where the surface tends to prevent wetting and results in the water droplets rolling off the surface at an inclined angle [48]–[52].

This phenomenon can be easily observed in nature where water droplets bead up and rolls off the leaves of some plant species. Most commonly referred to as the “Lotus effect” in the literature, it describes the concept of a self-cleaning, superhydrophobic surface [51]. The superhydrophobic properties observed are partially due to the multiscale textures on the surface of the leaves [51]. Historically, the fundamental analysis of water repellence due to multiscale roughness and porosity of solid surfaces were studied and initially reported by Wenzel (1936) as well as Cassie and Baxter (1944) [49], [52]. The key finding from the work of Wenzel and Cassie-Baxter most relevant to this research work is that a superhydrophobic behavior can be induced by introducing textures on surfaces [49], [52].

2.3.2 Fundamentals of Wetting Property

The self-cleaning capability is evaluated by measuring the wetting property of a surface. The wetting property defines the interaction between a water droplet and a surface, resulting from the intermolecular interactions. The balance between these intermolecular forces (adhesion and cohesion) will result in a steady state three-phase interaction (liquid, solid and gas) which is classically defined by the Young’s equation [53]

$$\gamma_{LV} \cos \theta = \gamma_{SV} - \gamma_{SL}$$

Here, the equilibrium between the interfacial surface tensions γ_{LV} , γ_{SV} and γ_{SL} – respectively the liquid–vapor, solid–vapor and solid–liquid interface – will govern the contact angle (θ) of a water droplet on the surface. Research works are still being conducted to develop further understanding about wetting property [53]. Nevertheless, the most classical quantification of a wetting property can be determined by looking at the contact angle of a water droplet resting on the surface, as demonstrated in Figure 2.3.

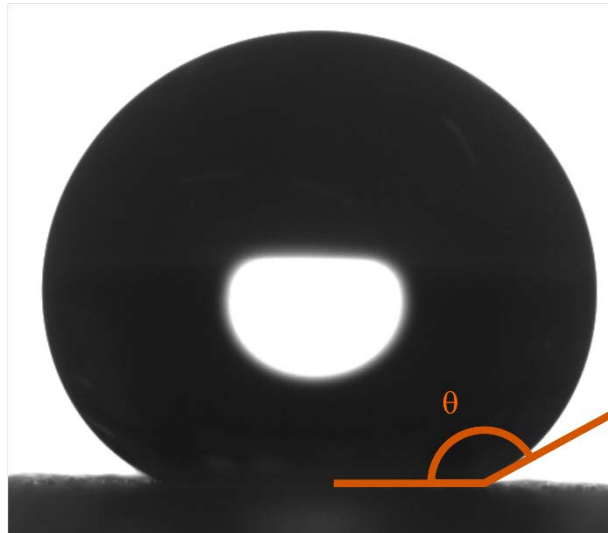


Figure 2.3 Definition of the contact angle (θ) of a water droplet resting on a surface.

The wetting property is an indicator for the general behavior of water droplets deposited on a surface. When a water droplet rests on a surface, the water would either tend to spread (indication of hydrophilic behavior) or repelled by the surface (indication of hydrophobic behavior). The basic definition, based on contact angle, of different wetting properties are given in Figure 2.4.

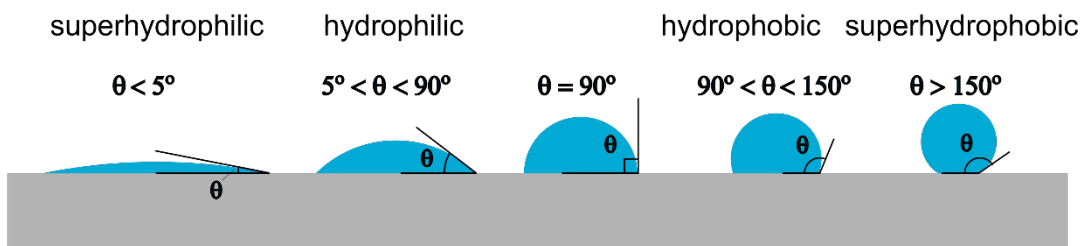


Figure 2.4 Definition of wetting property based on contact angle of water droplet resting on a planar surface.

The conventional definition for superhydrophobicity is if it exhibits a water contact angle $>150^\circ$ [48], [54]. Development in the research of wetting properties has led to further definitions being introduced. Depending on the context of study and application, other characteristics has also been used to further define superhydrophobicity such as contact angle hysteresis [55], roll-off angle [56] or bouncing of water droplets [55], [57], [58]. Since this work focuses on a self-cleaning function by way of water droplets rolling-off from a superhydrophobic microtextured surface, only the water contact angle and the roll-off angle will be used to define the superhydrophobicity of a surface. A surface needs to exhibit both a contact angle $>150^\circ$ as well as a roll-off angle $<10^\circ$ in order to be classified as superhydrophobic [59]. Furthermore, this roll-off angle is compatible with the minimum installed tilt angles of PV modules, which, even near the Equator is 10° [60].

A closer observation of the water droplets resting on a textured surface would reveal that there exist different wetting states. A textured surface might have the same wetting property but would have different wetting conditions or states which also determine the eventual behavior of the

water droplet. For example, two textured surfaces might both be superhydrophobic but on one surface, the water rolls-off at an angle; and on the other, the water droplet would stick to the surface. The basic wetting states of interest to the context of this work can be classified into i) the Wenzel state; and ii) the Cassie-Baxter state [48], [61]. The critical difference between the Cassie-Baxter state and the Wenzel state is whether water penetrates or fills the cavities of the microtextures and whether air is trapped inside the cavities as illustrated in Figure 2.5.

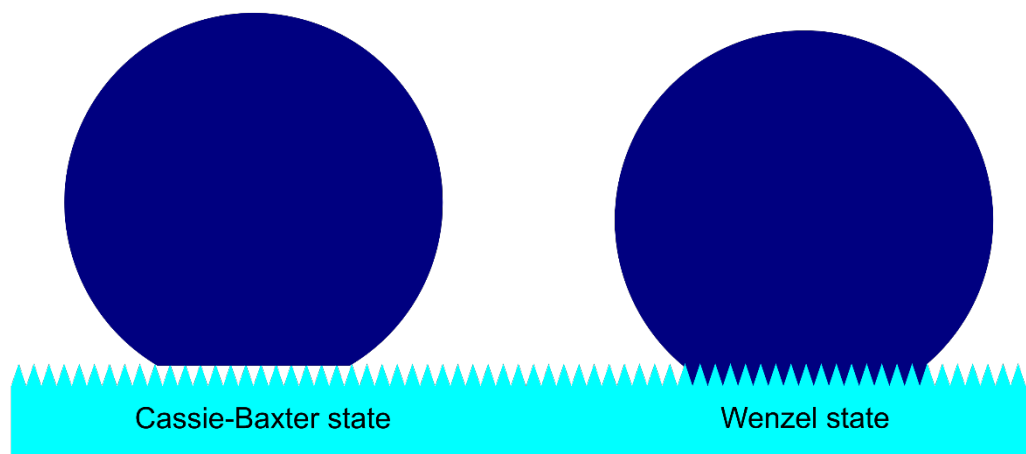


Figure 2.5 Different wetting states when water droplet rests on a textured surface. The Cassie-Baxter and Wenzel state are illustrated.

Subsequently, in the case of a Wenzel state, a high contact angle is observed but the water droplets will stick to the surface even if the surface is tilted $>90^\circ$ [56], [62]. This observation is also known as the “Rose petal effect” [56], [62]. While in the Cassie-Baxter state, a water droplet usually rolls-off at an inclined angle – the previously discussed “Lotus effect” [48], [49]. Introducing carefully designed textures on a surface would enable control of the desired wetting behavior of that surface.

2.3.3 Artificial Structures to Induce Superhydrophobicity

As stated in Section 2.3.1, the main approach that will be taken to achieve a soiling mitigation solution is by introducing a superhydrophobic surface that would assist dust removal with the presence of water droplets. Theoretically, several approaches are possible to achieve a superhydrophobic top surface: i) modifying the top surface bulk material to become superhydrophobic [63]; ii) applying a superhydrophobic coating on the top surface [64]; or by iii) introducing artificial textures to modify the liquid–solid surface contact area [65]–[67].

Various artificial textures that can achieve superhydrophobicity were already demonstrated in the literature. For example: random microcavities [44], periodic morphologies such as grooves [68], pillars [69] or cones [65], [70], hierarchical structures [71]–[75] as well as unique bioinspired structures such as nanofur [76] and flower petal surface textures [51], [77]; with each design having their own specific characteristics and governing features. In general, in order to induce superhydrophobicity, the key aim for the texture design is to minimize the surface contact area.

As this research work will involve achieving superhydrophobic surface from texturing, some notable results in the literature are highlighted further where various superhydrophobic textures have been studied for PV applications. It was shown that superhydrophobic polydimethylsiloxane (PDMS) microshell arrays will exhibit a contact angle of $\approx 151^\circ$, and when applied on monocrystalline silicon solar cells achieved a 71.8% recovery ratio (*RR*) in terms of solar cell efficiency (η) after washing with water droplets (going from $\eta = 6.6\%$ when soiled to $\eta = 9.8\%$ after self-cleaning compared to initial $\eta = 11.2\%$) [78]. Meanwhile, PDMS nanocones realized a superhydrophobic contact angle of $\approx 155^\circ$ and a roll-off angle of $\approx 13^\circ$; and when applied on perovskite solar cells, achieved a 1.1% efficiency improvement [70]. Another study that used inverted micro-pyramidal structures (IMPS)–PDMS required a fluoro-octyltrichlorosilane treatment for it to achieve superhydrophobicity (contact angle $>150^\circ$) [79]. When applied on Perovskite solar cells, a 3.3% improvement was achieved ($J_{sc} = 21.3 \text{ mA/cm}^2$) compared to a reference device ($J_{sc} = 20.6 \text{ mA/cm}^2$), while a flat PDMS cover exhibited a J_{sc} of 20.9 mA/cm^2 [79]. Vüllers et al. showed that by using a high surface energy material, it was also possible to exhibit a superhydrophobic behavior demonstrating a contact angle of $\approx 166^\circ$ and a roll-off angle of $<6^\circ$ [76]. This was achieved by introducing bioinspired nanofur textures on polycarbonate (PC) films, achieving a 5.8% relative gain in terms of J_{sc} compared to a bare multicrystalline silicon solar cell (mc-Si) [76]. These reported achievements demonstrate that the introduction of textures can lead to superhydrophobicity that when applied as self-cleaning superhydrophobic cover films, will improve the performance of PV devices. Unfortunately, there were not many reports on the self-cleaning performance evaluation of PV devices having a microtextured top cover. In the few literatures that does report on the self-cleaning performance, not many include the optical benefits. For example, in a study by Park et al., superhydrophobic PDMS microshell pillar arrays demonstrated significant self-cleaning performance, but the authors did not analyze the direct optical benefits of the pillar arrays that can improve the *PCE* of a PV module [78].

For application as a self-cleaning PV module cover, an ideal microtextured cover should maximize enhancement of both self-cleaning and anti-reflective properties. Therefore, this research work will report on the development of a superhydrophobic microtextured cover film for PV modules that exhibits both properties – thus a multifunctional PV module cover.

2.4 Fundamentals of Light Management in PV

The behavior of incident light plays a central role in the function of PV devices, since the main working principle is about converting light into electricity. The amount of light that a PV module absorbs directly impacts its ability to generate electricity. Therefore, light management is a key factor that determines the efficiency of a PV module. It can either increase the efficiency of PV modules or be a source of performance loss.

When incident light hits the surface of a PV module, several effects can happen – the light can either be reflected, transmitted, or absorbed as shown in Figure 2.6. What is desired is to maximize the light in-coupling that reaches the active solar cell area and thus potentially be absorbed for photocurrent generation.

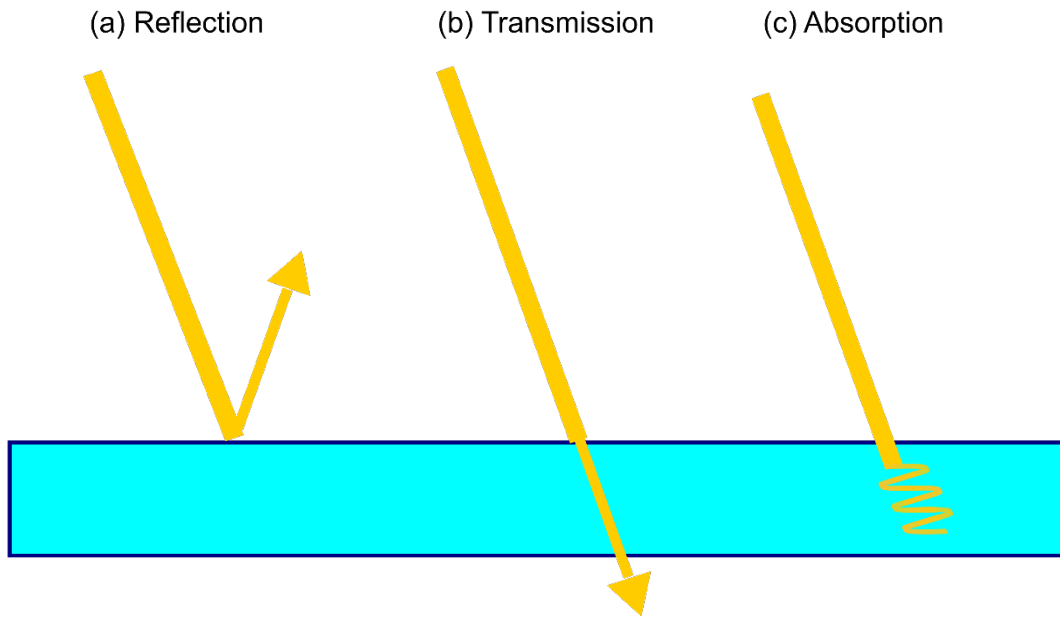


Figure 2.6 Fundamental interaction of light when hitting a surface. It can either be (a) reflected, (b) transmitted through the material or (c) absorbed.

The three key light management strategies, which addresses different sources of optical losses, can be attacked individually to enhance the photocurrent generation (quantified by J_{sc}): (1) Front-surface reflection, (2) parasitic absorption, and (3) light trapping.

Front-surface reflection occurs when in-coming light interacts with an interface, whether when light propagates from air to the superstrate or between any interlayer in the PV module. Light is reflected mainly due to a mismatch in refractive indices between the mediums – more commonly referred to as the Fresnel reflection losses – reducing potential light in-coupling and thus the potential for photocurrent generation. There are several strategies/approaches taken to reduce front-surface reflection. On a solar cell level, it is common for solar cell manufacturers to include wafer texturing or by applying an anti-reflection coating on the solar cells [80]–[82]. Meanwhile, on a PV module level, steps taken should reduce parasitic reflection losses. One option is by selecting suitable materials for each layer of the device or apply a textured layer such that there is a smoother transition in the refractive indices that would then reduce the Fresnel reflection losses [70], [83].

Parasitic absorption refers to the absorption of incident light by materials other than the active solar cell area in a PV module. For example, the glass cover or the encapsulation material of a PV module can absorb portions of the incident light, reducing the amount of light that is available to be absorbed by the solar cell. This in turn can reduce the overall efficiency of the PV module. To reduce parasitic absorption, it is important to use materials that have low absorption coefficients throughout the PV module architecture where absorption is not intended. For any additional layers to be added, such as a PV module front cover, a low absorption coefficient should be one of the requirements for material selection.

Light trapping strategies are used to increase the amount of light passing within the PV module. This allows more of the light to be absorbed by the solar cells, leading to an increase in the overall efficiency of the PV module. This can be achieved through path-length enhancement or a retro-reflection effect. Some common light trapping strategies include introducing light trapping structures such as diffraction gratings, textured surfaces, and multilayered structures. Interaction of light with the structures or textures leads to light diffraction into multiple paths or light scattering into multiple direction that will only serve to increase the path-length [82]. Textured surfaces also have the potential to redirect the outgoing reflected light back onto the active area of the solar cell, thus trapping the light within the PV module and increasing the potential absorption from the multiple passes [33], [84], [85].

2.5 Light Management by Microtextures

Introducing textures on the front surface has the potential to enhance light harvesting when applied as anti-reflective covers on PV modules. Incident light that hits optically large textures, relative to the wavelength (λ) of visible light, can improve light in-coupling through multiple interactions of light upon the surface, thereby reducing reflection losses [86]. Interaction of light with textures can change its path angle, which in turn can potentially increase the path length [86]. As a result, there will be an increase in the probability for the light to be absorbed. Moreover, introduction of textures can result in the front cover film having an effective refractive index (n) that would reduce the Fresnel reflection losses due to a smoother transition between the mediums of interest [70], [83]. This anti-reflective effect has been demonstrated in various texture morphologies such as random textures [44] and microshell pillar arrays [78]. Apart from the shape of the textures, the specific parameters of a texture design, such as aspect ratio, can also enhance transmission due to multiple impinges of light [85]. This will be reported further in Chapter 5 where the influence of aspect ratio was investigated.

The interaction of light with a surface does not only occur for in-coming light, but also for out-going light, which usually comes in the form of reflected light by the underlying substrate layer. With the introduction of textures, it is also possible to induce a light trapping effect where out-going light is retro-reflected back inside the PV device, as illustrated in Figure 2.7 [84], [85], [87].

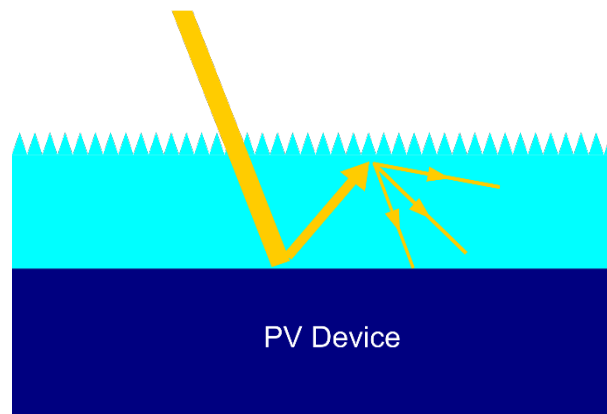


Figure 2.7 Outgoing light reflected back into the PV device due to the presence of microtextures increasing the potential photocurrent generation. This light trapping effect is known as the retro-reflection effect. Illustration not to scale.

The multiple passes of light onto the active area of the solar cell will enhance the photocurrent generation. This effect was observed in some textures found in nature such as the rose petal. An artificial texture based on the rose petal demonstrated a reduced reflection of 65%, which was proven to be partially contributed by the retro-reflection effect [77]. The ideal outcome to enhance the light harvesting with the retro-reflection effect is to minimize reflection of in-coming light and maximize reflection of out-going light. Therefore, this must be taken into consideration when selecting the morphology of the textures to be introduced.

All these examples serve to emphasize the importance of texture design selection to maximize the anti-reflective properties. For PV module cover applications, getting a balance of the multifunctional features is a challenge when designing the anti-reflective microtextured surface.

2.6 Fluoropolymers as PV Module Front Cover Material

A proposed polymeric film to be used as a front cover for PV modules must satisfy a list of requirements suitable for the intended functions. As a front cover for PV modules, it must exhibit high transmittance, which is challenging with microtextured surfaces as surface roughness usually results in opacity [88], [89]. To realize superhydrophobicity by microtexturing, the material of choice should also have low surface energy [90]. Further requirements, so that the front covers could withstand the same lifetime the PV modules, are mechanical strength and prolonged photostability (>20 years) under sunlight [89].

Fluoropolymers are one class of material that fulfils these requirements. It has suitable properties to be used in PV applications such as high optical transparency, high ultraviolet (UV)-stability, high mechanical strength and low water vapor permeability [91]. It is also known for their durability, chemical inertness and environmental resistance [92], [93]. The energy of photons at $\lambda = 300$ nm, corresponding to an energy of 397 kJ/mol, is not sufficient to break the bonds between carbon and fluorine molecules of the fluoropolymers, which has a bond disassociation energy varying between 452 and 544 kJ/mol [93]. Fluoropolymers have the potential to be applied as back sheets, front covers or encapsulation materials in the PV industry [92]. It has already been applied commercially in thin film PV devices [89]. Furthermore, fluoropolymers have been used as encapsulation materials to produce waterproof devices [94].

The cover material of choice in this work, fluorinated ethylene propylene (FEP), is already a common fluoropolymer studied for PV applications [88], [91], [95], [96]. In fact, FEP has a track record of being employed in PV modules and has also demonstrated the ability to perform as a superhydrophobic self-cleaning cover [44], [88]. It was reported that the solar transmission of FEP is comparable to low iron float glass over a 20-year period [97]. The reports also indicates that FEP exhibited: (i) a high transmittance and (ii) was also stable over a 20-year period, retaining over 90% of its initial transmittance [97]. Moreover, planar FEP meets the requirement of a low surface energy, leading to a large initial water contact angle (110°), which hydrophobicity can be enhanced further through texturing [44].

There were previously reports of different strategies that utilizes FEP as self-cleaning covers: (1) FEP was applied on a glass substrate using chemical vapor deposition to achieve a hydrophobic nanolayer that was further modified to achieve an anti-soiling dual hydrophobic–hydrophilic surface [98] and (2) laminating FEP films and then peeling it off to produce a nanolayer coating of FEP [99]. Although these approaches also use FEP as the cover material, but these different strategies rely on dew condensation that accumulates and rolls-off when a certain water droplet size threshold is reached [98], [99]. This differs from the research reported in this dissertation where dust removal relies on rainfall; thus, has different microtexture design requirements.

It should also be noted that there are some practical issues that should be considered before actual implementation. Here, a few of them are discussed briefly. Fluoropolymers, due to the low surface energy, are known for their anti-adhesive propensity which can be a challenge for attaching to any surface. Nevertheless, it is possible since the application of fluoropolymers as a top cover layer for PV modules has already been established in commercial applications [100], [101]. For permanent attachments in this work, a standard lamination method for PV modules was used with ethylene vinyl acetate (EVA) as the encapsulant. EVA is already used for PV modules encapsulation due to its low cost, high transparency and high adhesion strength [102]–[104].

The issue of cost for commercial applications as PV module front covers should also be considered. The cost of fluoropolymers is conventionally higher than other types of polymers [91], but there are several strategies that can potentially reduce the cost. For the development of a microtextured front cover in this work, a 125 μm thick planar FEP film was used. With the maximum height of our microtextures being $\approx 21 \mu\text{m}$, it is possible to use significantly thinner base FEP films ($< 50 \mu\text{m}$) that would significantly reduce costs. The fabrication cost can also be reduced with the potential of continuous roll-to-roll hot-embossing. Compared to the conventional hot-embossing process, the processing cost can be reduced due to the increased throughput [105], [106]. To identify the actual cost benefits of applying a microtextured FEP as PV module front covers, a more in-depth cost analysis study should be conducted.

There is also valid concerns about the usage of fluoropolymers due to health and environmental issues since they are a group of polymer that is part of the per- and polyfluoroalkyl substances (PFAS) class [107]. While the concern are true, the fluoropolymer group consists of a vast array of specific materials and some fluoropolymers are categorized as polymer of low concern (PLC) when considering the health and environmental issues [108]. Detailed studies should be conducted to better understand the toxicity, environmental and health issues, and the disposal or recycling potential to determine how it is possible to utilize the benefits of fluoropolymers. Nevertheless, the proposed concept to obtain superhydrophobic front cover film in this research work still holds for other types of polymers (as demonstrated in Section 5.1) since this work only manipulates the surface texturing and no chemistry modification was involved.

3 Methods

This chapter presents the most important experimental methods and materials utilized for the development of a self-cleaning PV module cover film. This includes hot-embossing as the main fabrication method, the cover film material, application of the microtextured films as PV module front covers and briefly all experimental methods used to characterize the microtextured cover films.

3.1 Fabrication of Microtextured Cover Films

The fabrication of microtextured films in this work revolves around hot-embossing, which was chosen since it is a well-established mechanical process and has the potential to be up-scaled to large areas using a roll-to-roll technique [109]. Moreover, the Institute of Microstructure Technology (IMT) at the Karlsruhe Institute of Technology (KIT), where the majority of this research work was conducted, had experienced personnel and resources relating to the process.

In this work, the main fabrication process to produce microtextured films was performed using a customized hot-embossing system (HEX 03, Jenoptik Mikrotechnik, Germany) as shown in Figure 3.1a. The commercial system, which mainly consists of a hot-embossing unit, was customized previously by colleagues at the IMT to include a vacuum unit (vacuum chamber and pump).

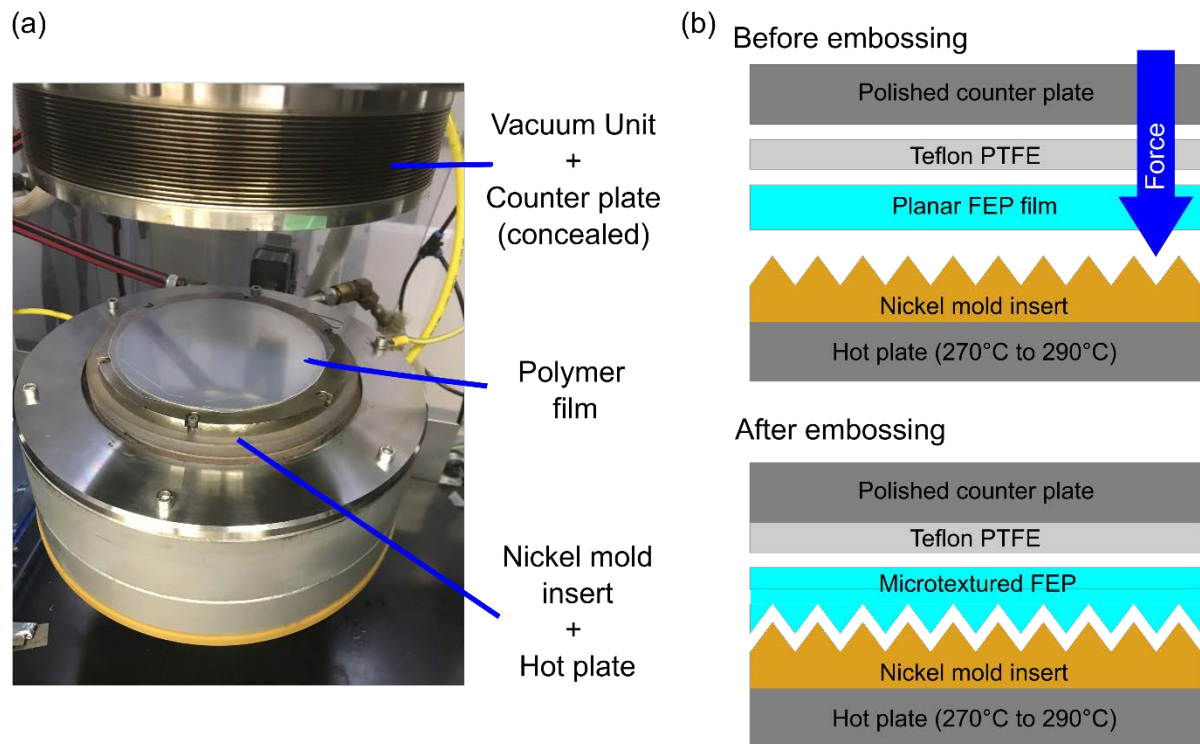


Figure 3.1 Hot-embossing set-up for microtextured film fabrication. (a) Main hot-embossing area with key elements labeled; (b) Simplified illustration of hot-embossing process conducted in this work where temperature and force were key parameters controlled. Temperature was introduced by the hot plate and force was exerted vertically through the counter plate. After the hot-embossing process is completed, the FEP film will have embossed microtextures on the underside.

As a general overview of the fabrication process, microtextures were imprinted in planar films using a hot-embossing system as illustrated in Figure 3.1b. Nickel mold inserts containing the desired microtextures were first developed and used as templates for the hot-embossing process. The fabrication parameters (temperature and force) were controlled and customized for each combination with the aim of obtaining perfect replicas based on the original mold inserts. Further detailed description of the hot-embossing fabrication process used will be discussed in Section 3.1.1.

Since the desired microtextures in this work are within the micron scale, and due to the morphology of some of the microtextures having sharp tips or miniscule cavities that could potentially trap air, the hot-embossing process was conducted in vacuum. Figure 3.2a demonstrates defects in microtextures (missing cone tips) partially due to trapped air during the fabrication process, compared to the near-perfect cones as shown in Figure 3.2b. In that specific case of defect, there was an error during the fabrication such that vacuum was not achieved during the hot-embossing process.

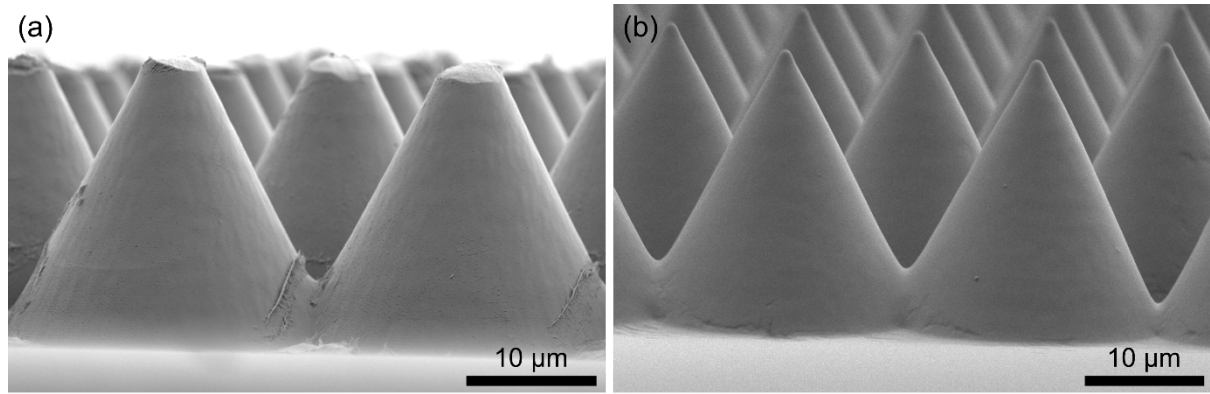


Figure 3.2 Defects that might occur during hot-embossing of microtextures. (a) Defects in microtextures due to fabrication errors and (b) near-perfect fabrication of cone-shaped microtextures.

3.1.1 Hot-Embossing Fundamentals

Hot-embossing is a common fabrication process to develop microtextured surfaces [109], [110]. It involves the replication of a pattern on a sheet of polymer film with the use of heat and force [110]. As explained in the previous section, the hot-embossing in this work was conducted in vacuum. The steps that occur throughout the hot-embossing process are illustrated in Figure 3.3.

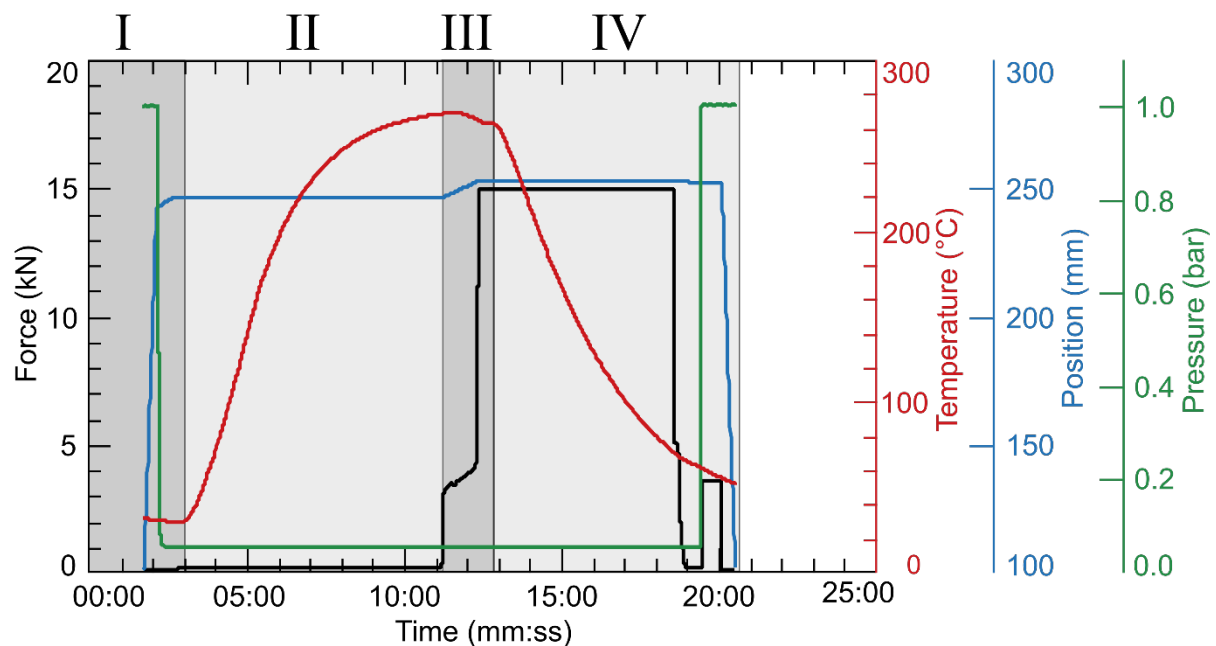


Figure 3.3 Phases and parameters versus time throughout hot-embossing process. Phases: (I) Initiation of process and setting-up vacuum condition; (II) Soften material by heating up until set-point temperature; (III) Emboss pattern into material by applying force and (IV) De-molding by reducing temperature to harden patterned material before removing finished sample.

Here, some key hot-embossing steps will be highlighted. After installing the mold inserts containing the desired pattern into the machine, the planar polymer film was placed in between the upper and lower molding tools. In phase (I), the process was initiated, and the molding tools close slowly until they just touch each other, controlled by setting an initial force threshold. The air was then evacuated until a vacuum condition was reached. After that, heat was applied in phase (II) until

the desired temperature to soften the polymer film was achieved. Force was then applied in phase (III) to emboss the pattern from the mold into the polymer film. Finally, in phase (IV), the film was cooled down until it reaches near-ambient temperature (well below the glass transition temperature), while maintaining the applied force to prevent shrinkage, before the machine was vented to de-vacuum the chamber and opened so that the microtextured films can be removed.

Planar polymer sheets used as the cover films were prepared by cutting them into suitable film sizes. The main material used for the self-cleaning cover films is a fluoropolymer (FEP), which will be discussed further in Section 3.3. Since several different microtextured mold insert sizes were used in this work, the thin FEP films were cut into sizes slightly larger than the microtextured area for further handling purposes. As an example, the random microtextured mold insert used in this work has a 20 mm x 20 mm microtextured area and a \approx 30 mm x 30mm FEP film was thus prepared. Prior to inserting into the hot-embossing machine, the FEP films were cleaned with isopropanol and nitrogen gas to ensure that it is free of any dust or residues.

Mold inserts prepared are coupled to a hot plate using a mechanical connection such that heat is translated to the polymer films. In this set-up, the mold inserts are installed on the bottom for easy removal of the hot-embossed film without the need to take out the mold inserts. This reduces the time taken for the continuous production of multiple samples. Meanwhile, a polished steel counter plate was positioned on top that applies force onto the FEP film. A 3 mm thick Polytetrafluoroethylene (PTFE) layer was placed in between the polished steel plate and the FEP film to prevent: i) back side texturing of the FEP; and ii) the textured FEP from sticking to the counter plate, as it will be heated above its melting point temperature.

The two key fabrication parameters, force and temperature, were varied and eventually a relatively narrow temperature window of 270°C to 290°C was identified to be used for surface texturing in our case [96]. 260°C was initially used as the lower reference given the glass transition temperature of FEP, nevertheless the work in Chapter 4 will demonstrate that insufficient texturing was achieved at that temperature. Meanwhile, hot-embossing at temperatures $>300^\circ\text{C}$ have been shown to result in opacity [88], and therefore this high temperature was not suitable for producing highly transmissive films as required for PV applications. There is also a risk of destroying the mold inserts when using temperatures higher than 290°C as the FEP was irreversibly stuck in the microtextures as was found out in initial tests that were conducted.

The work presented in Chapter 4 also investigates what are the suitable forces to be used for the hot embossing process. A wide range of forces (500 N, 1500 N, 5000 N, 15000 N, and 50000 N) were used in the hot-embossing process to identify the optimum force needed to afford superhydrophobic microtextures. A lower force of 50 N was initially investigated, but the resulting sample was mostly untextured, thus this force was omitted from further processes. An optimization process was conducted to identify the suitable combination of temperature and force settings for different microtexture designs. As will be presented in this work, an optimal combination of temperature and force results in perfect replicas of the microtextures.

Briefly, several hot-embossing fabrication parameters were used to produce the various samples in this research work:

- 1) Random microtextures: The range of temperature (270°C to 290°C) and force (500 N, 1500 N, 5000 N, 15000 N and 50000 N) were investigated.
- 2) Periodic cone-shaped microtextures: FEP samples were produced using 15 kN at 280°C. Meanwhile, for PC samples (250 µm film thickness), the hot embossing was conducted with a force of 15 kN at 160°C. The parameters (force and temperature) for the hot-embossing processes were selected based on an optimization exercise to obtain near-perfect sharp cone shape microtextures.
- 3) Large area samples (both random and cone-shaped microtextures): the microtextured pattern from the large-area mold was transferred onto FEP films at temperatures of 270°C with a force of 15 kN.

3.1.2 Mold Fabrication

The desired microtextures were based on masters that would then be transferred into mold inserts. The nickel mold inserts, also sometimes called nickel shims, were developed using an electroforming process as reported in [44]. This process was conducted with the kind support of Dr. Markus Guttman and the mold insert working group at the IMT.

A substrate sandwich was prepared before the electroforming process could be conducted by first attaching a microtexture master to a polished silicon wafer. Then the preparation was completed by evaporating 8 nm of chromium (as an adhesion layer) and 100 nm of gold (as a conductive plating base) on top of the microtexture master.

The substrate sandwich was masked with nonconductive tape to create a centric plating area, defining the shape and size of the resulting mold insert. The masked substrate was then immersed into a galvanic bath using a special plating holder. The nickel electroplating system with a standard boric acid containing nickel sulfamate electrolyte ($T = 52^\circ\text{C}$, pH 3.4 to 3.6) was developed especially for the nickel electroforming of micro- and nanostructures [111]. The current density was increased gradually from 0.1 A/dm^2 up to 1.0 A/dm^2 to ensure a slow growth of the nickel layer and to achieve a defect-free filling of the microtextured surface area until the nickel layers reached a thickness of at least $600 \text{ }\mu\text{m}$. This process leads to a stiff homogenous metallic shim which can withstand the forces applied in the hot-embossing process. Finally, the nickel mold insert was cleaned using oxygen plasma (STP2020, R3T, Germany) for 120 min at 22°C , 800 W, 450 mTorr before it can be used.

3.1.3 Microtextures Design

In general, the microtexture designs for this work were chosen to enhance the wetting and optical properties of a planar cover film. The two designs – (1) random microtextures and (2) periodic cone-shaped microtextures – will be discussed in this section.

3.1.3.1 Random Microtextures

The bio-inspired random microtextures design was based on the study of the leaves from water plants (*Silvinia* and *Pistia*) [43], [76]. The previous work by Vüllers et al. developed superhydrophobic multiscale textured PC films described as nanofur, consisting of a dense layer of micro- and nanohairs on top of random microhemispherical base textures [76]. In a further work, it was found that the major optical benefits actually originated from the microhemispherical base textures [43].

Thus, due to the optical benefit that was attributed to the micron-scaled base textures, a similar random microhemispherical microtextures was chosen to produce the desired self-cleaning cover films, as will be presented in Chapter 4. Figure 3.4 shows an example of the random microtextures that were fabricated in this work; with Figure 3.4a and 3.4b showing side- and plan views of the sample. The micro- and nanohairs – which were essential for achieving superhydrophobicity in PC – was not required to achieve superhydrophobicity in FEP [43]. The random hemispherical microcavities can be produced by sand-blasting a nickel plate using $\approx 75\text{--}150\ \mu\text{m}$ sized spherical silica particles, which would then be used as a master to produce the mold inserts.

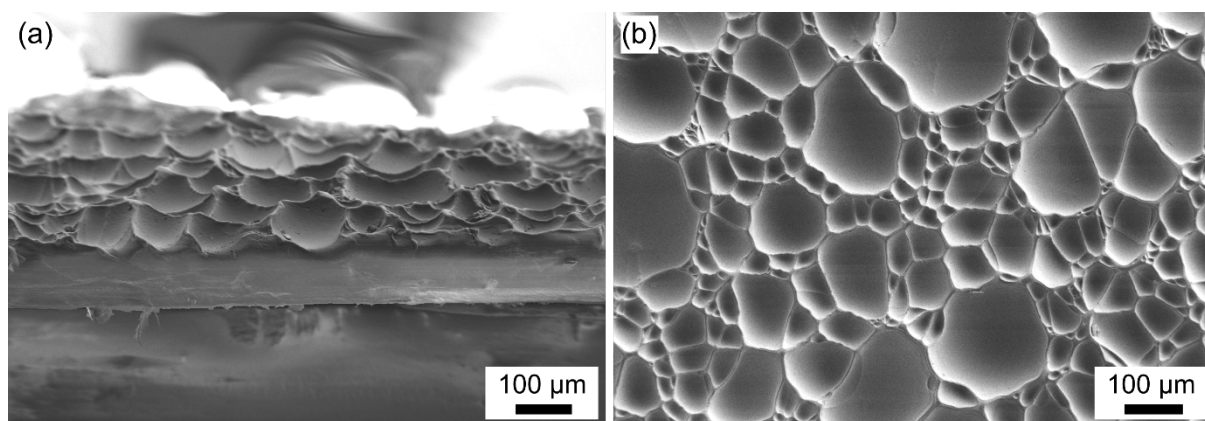


Figure 3.4 Hot-embossed random microtextures showing (a) tilted side view and (b) plan view.

3.1.3.2 Periodic Cone-Shaped Microtextures

To further enhance the optical benefits of the self-cleaning cover films, periodic cone-shaped microtextures were introduced as the texturing, apart from the design being suitable to induce superhydrophobicity as will be discussed in Chapter 5. Master textures of hexagonally arranged periodic microcones were prototyped using a commercial direct laser writing system (Photonic Professional GT, Nanoscribe, Germany). All microcones have individual base diameters of $30\ \mu\text{m}$ with center-to-center spacings of $25\ \mu\text{m}$. Textures with various aspect ratios (0.3, 0.5, 0.7, 1.0 & 1.4) were prepared by modifying the height of the microcones accordingly. The eventual cone-shaped microtextures are demonstrated in Figure 3.5. The initial masters were developed using a direct laser writing procedure with the help of a colleague, Dr. Stephan Dottermusch. A similar detailed procedure was described in a previous work by Dottermusch et al. [85].

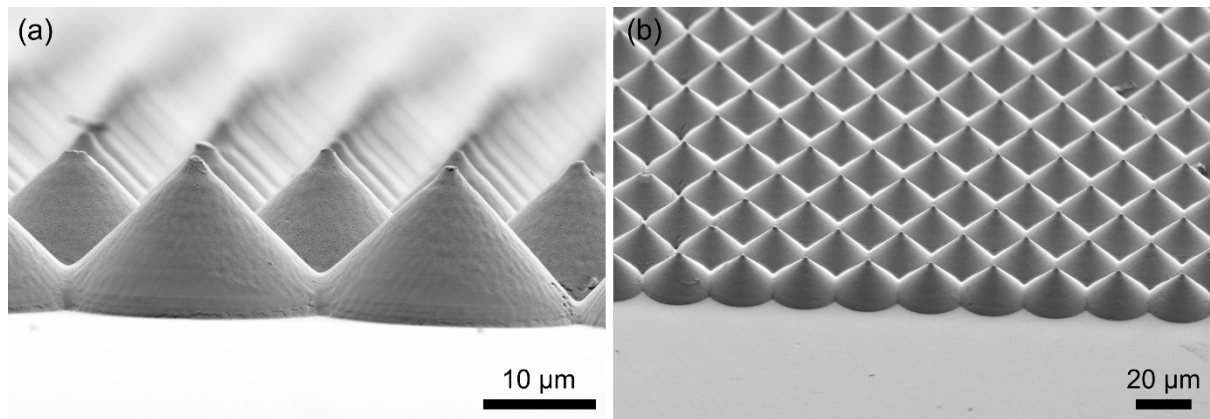


Figure 3.5 Hot-embossed cone-shaped microtextures showing (a) a side view and (b) an angled view.

3.1.4 Up-Scaling to Large-Area Microtextures

For the work in Chapter 6, a large area microtextured film was required. The small-area cone-shaped microtextures (1.1 cm × 1.1 cm) from the work in Chapter 5 was scaled up to a ≈10 cm × 10 cm area using a process as illustrated in Figure 3.6. The large-area master was obtained by fabricating a huge number of the small-area samples and manually stitching them together. The small-area samples were carefully arranged and attached together on a silicon wafer. The large area master was then used to develop a mold insert to produce the large area microtextured films. Again, using the hot-embossing process, the microtextured pattern from the large-area mold was transferred onto FEP films (thickness = 250 μm). This process was again conducted in vacuum to prevent defects due to trapped air bubbles between the cavities of the mold.

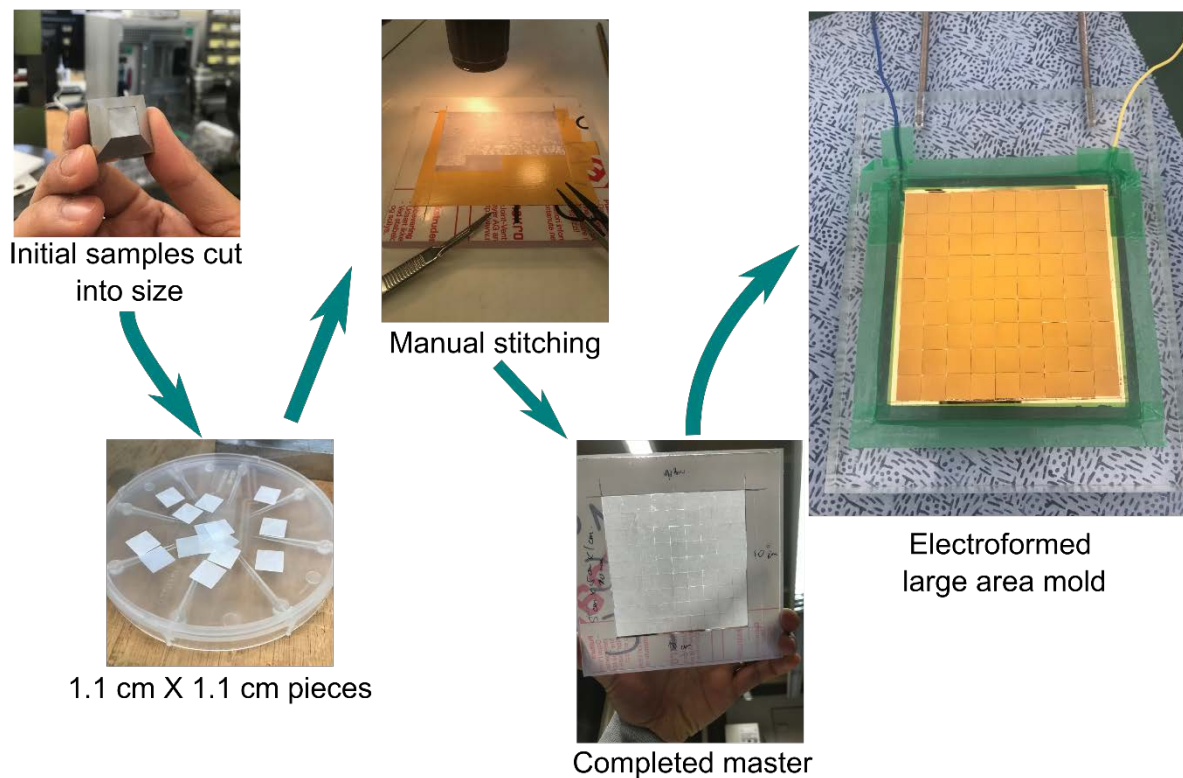


Figure 3.6 Development of a large area microtextured mold insert through manual stitching.

3.2 Cover Film Material: Fluorinated Ethylene Propylene

The material of choice for the PV module front cover has to meet specific requirements in terms of the surface energy and also transmissivity, apart from satisfying the requirements for PV applications. FEP films (thickness = 127 μm), sourced from DuPont Chemours (Teflon FEP Fluorocarbon, DuPont), were chosen as the main cover film material investigated in this work since it meets the necessary requirements. Its high optical transmittance will allow light to pass through, low surface energy will make FEP more susceptible to becoming superhydrophobic from texturing and it also has a favorable refractive index. The refractive index of $n = 1.34$ at $\lambda = 589 \text{ nm}$ is highly beneficial when applied as a front cover since it already reduces the Fresnel reflection losses [96]. FEP was also reported to be mechanically strong as well as being photostable under sunlight for more than 20 years, meeting the stability requirements for PV module applications [91]. Additionally, fluoropolymers have previously been used in PV modules as cover films [95], [112].

3.3 Microtextured Cover Film on PV Devices

For further investigations, the fabricated microtextured cover film samples were applied onto different surfaces depending on the intended characterization technique used. A majority of the samples would be applied onto PV devices to investigate the actual influence on photocurrent generation.

3.3.1 PV Devices

For that purpose, two types of PV devices were used in this work. First, a glass-encapsulated PV mini-modules comprised of a mc-Si solar cell (E-Ton Solar, Taiwan) was used. Crystalline silicon type solar cells holds the largest market share for PV technology currently being applied in the market, making it the preferred device to be investigated [113], [114]. The main PV device used in this work has an architecture that consists of a mc-Si solar cell having a silicon nitride anti-reflection coating (ARC), an EVA encapsulation layer, and low-iron float glass as front and back sheet layers as illustrated in Figure 3.7a. From initial tests, the PV mini-modules used has a J_{SC} of $\approx 31.2 \text{ mA/cm}^2$ and a PCE of $\approx 10.7\%$. Furthermore, the conceptual representation of a potential PV module equipped with the developed self-cleaning microtextured front cover is also illustrated in Figure 3.7b.

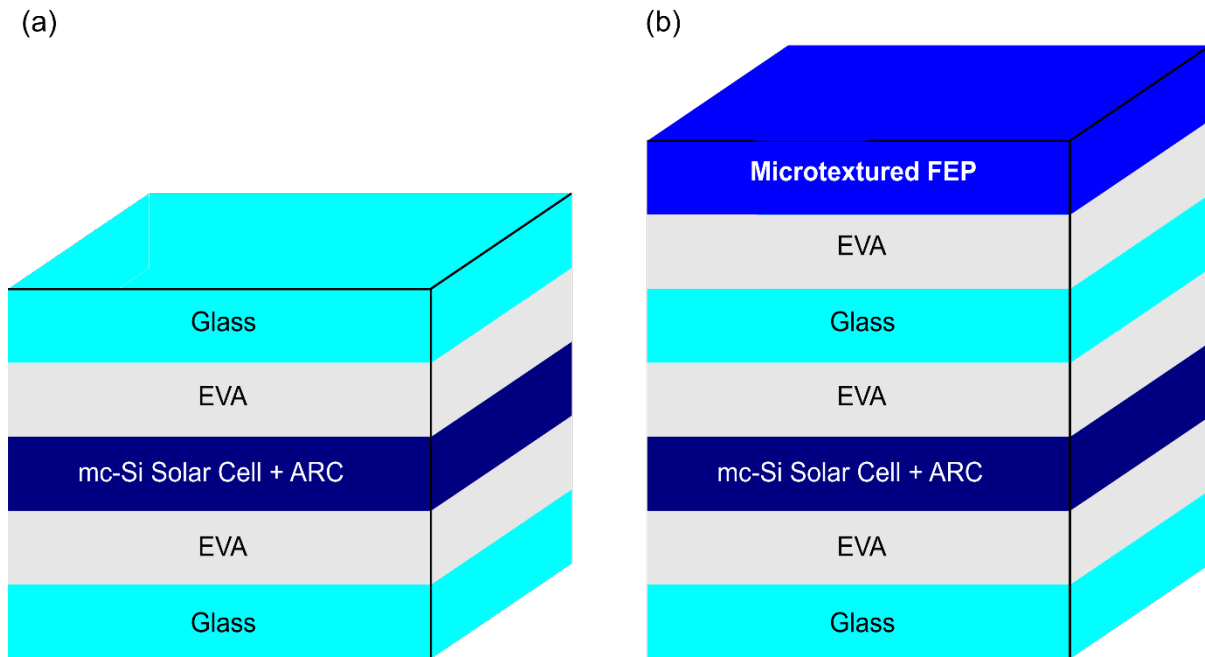


Figure 3.7 Conceptual illustration of PV device architecture showing (a) reference PV module and (b) PV module with self-cleaning microtextured FEP front covers. Illustrations are not-to-scale.

Other investigations conducted also involves the application of microtextured FEP cover films on Copper Indium Gallium Diselenide (Cu(In,Ga)Se_2 or CIGS) solar cells (2.0 cm x 0.5 cm) with a measured *PCE* of 12.7% (ZSW, Germany). The CIGS solar cells were chosen for the performance-oriented study, since they exhibited very little reflectance, thus making them suitable for highlighting the reduced reflectance at the air/FEP interface. Furthermore, the dimensions of the CIGS solar cells closely matched the textured area in length and width, while no interference of light occurred in the FEP layer of more than 100 μm thickness, making the optics highly comparable to those in a solar module, including the cover glass. The architecture of the CIGS solar cells consists of a molybdenum back contact, a CIGS absorber layer, a cadmium sulfide buffer layer, an undoped zinc oxide layer and an aluminum doped zinc oxide front contact. More information about these CIGS solar cells can be found in References [115], [116].

3.3.2 Temporary: Index Matching Gel

In several characterizations, the same area on the PV mini-module was investigated. To this end, a temporary optical coupling was required. This was achieved by using refractive index matching gel, applied between the microtextured FEP films and the glass, having a refractive index of 1.45 at $\lambda = 589 \text{ nm}$ (G608N3, Thorlabs, USA) [117]. It has to be noted that the gradual increase in refractive indices from air ($n = 1$), FEP ($n = 1.34$), gel ($n = 1.45$) and glass ($n = 1.5$) already reduces the Fresnel reflection losses. The gel was applied manually before covered with the microtextured FEP films. Force from a stream of nitrogen gas was used to ensure an even spread and no air bubbles were trapped in the gel.

3.3.3 Permanent: Lamination

For investigations requiring permanent application of the microtextured films, EVA foils (EVGuard, Folienwerk, Germany) – a commonly used adhesive interlayer in the PV industry – was used to provide the adhesion between the FEP covers to the solar cells or glass surface. The FEP covers, either planar or exhibiting the investigated microtextures, were laminated onto CIGS solar cells at 140°C with 4 mbar pressure using a vacuum laminator (Energy Environmental Technical Services, U.K.). The lamination parameters were held for 30 minutes before cooling to room temperature.

3.4 Characterization

As a reminder, the main purpose of this research is to develop a self-cleaning superhydrophobic microtextured FEP PV module front cover. The characterization techniques used for the investigations throughout this work will be presented in this section.

3.4.1 Wetting property

The wetting property was determined from contact angle and roll-off angle measurements using a contact angle goniometer (OCA 15Pro, Dataphysics, Germany) equipped with an electronic tilting base unit (TBU90E, Dataphysics, Germany). To measure the contact angle, 10 μL of distilled water was deposited on the sample and measurement taken in static condition. For the roll-off angle, the base was rotated at 1°/second until the droplet rolled-off at which the angle was taken. These measurements were repeated at three different spots for each sample.

3.4.2 Microscopy

For surface and particles analysis, different microscopy techniques and equipment were used depending on the purpose of the investigation. The general microscopy equipment used are summarized in the following.

3.4.2.1 *Optical Microscope*

An optical microscope (VHX-500, Keyence Corporation, Japan) was used to make observations of the fabricated microtextured surface and to characterize the dust particles especially the particle size distribution, apart from imaging for visualization purposes. Further analysis of relevant particle size distribution, based on the images taken, was conducted using the freely available image analysis software ImageJ [118].

3.4.2.2 Scanning Electron Microscope

Different microtextured surfaces were fabricated throughout this work. The microtextured FEP samples were imaged using a scanning electron microscope (SEM, Supra 60VP, Zeiss, Germany) to relate the resulting properties with their respective microtextures. Both plan and side views were taken for each sample. The samples were first prepared by coating with 10 nm of silver prior to insertion into the SEM.

3.4.3 Reflectance and Transmittance

The influence on the optical property by the microtextured cover films were evaluated using an ultraviolet–visible–near infrared (UV–vis–NIR) spectrophotometer (Lambda 950, PerkinElmer, USA) equipped with an integrating sphere. Depending on the investigation, the reflectance and transmittance were measured at three different areas and averaged to take into consideration the different areas of the microtextured film. In general, a beam size of ≈ 3 mm x 14 mm was used – most importantly, the beam size was kept constant for the same investigation.

3.4.4 Solar Cell Characteristics

The impact on the photocurrent generation was analyzed via the J – V characteristics. J – V characteristics were measured under an air-mass 1.5 global (AM1.5G) spectrum using a class AAA solar simulator (Oerlikon Solar, Liechtenstein).

In order to compare the influence of different microtextured samples, the same spot on a PV mini-module was used for evaluation. Since dimensions of the microtextured FEP samples were smaller than those of the PV mini-module, a mask with an active area relative to the samples dimension was used – resulting in a small reduction in the measured V_{OC} of the solar cells. The J – V measurements were made using three different areas of the microtextured FEP sample and the results were averaged to account for randomness of the microtextures and any difference in thickness of the manually applied gel.

For the case of permanently laminated microtextured films, the J – V characteristics of the solar cell having the different microtextured covers were compared with initial reference measurements.

3.4.5 Self-Cleaning

The self-cleaning function and impact on the photocurrent generation when microtextured FEP films were applied on a reference PV device were also investigated in this work. Several dust contaminants were used to consider different soiling environments. The dust contaminants were then merely deposited on the surfaces and washed away. Aging and other mechanisms that increase particle adhesion, such as cementation and caking [47], were not studied.

3.4.5.1 Dust Contaminants

Four different dust particles were employed as the dust contaminants throughout this work as presented in Figures 3.8a–3.8d, divided into two categories, coarse and fine: (a) coarse volcano ash collected from the Stromboli volcano (Italy) was sieved to have particle sizes between 125 and 250 μm ; (b) sea sand (Merck, Germany) having particle size rated between 100 and 300 μm ; (c) fine volcano ash collected from the Campi Flegrei volcano (Italy) filtered using a sieve to have particle sizes <63 μm ; and (d) Arizona test dust (A1 fine particles, Fiatec, Germany) having particle sizes <22 μm .

It should be noted that dust sizes in the environment greatly depend on the location. Previous studies reported that the majority of dust particles collected from PV modules have sizes <63 μm [27], [28]. Nevertheless, sizes up to 400 μm have also been collected [29], [30]. Thus, the range of dust particles employed in this work broadly represents those occurring in nature. Since the focus of this work is on the microtextured cover film, the selection of the dust sizes used was relative to the microtextures spacing – specifically the periodic cone-shaped microtextures. Coarse particles being significantly larger than 25 μm ; meanwhile fine particles were generally smaller than 25 μm .

The particle size distribution was measured using methods suitable for their respective sizes. The size distribution of the larger coarse dust particles was identified using microscopy analysis, captured by the previously mentioned optical microscope before analyzing using the image processing program, ImageJ. Meanwhile, the size distribution of the smaller fine dust particles was analyzed using dynamic light scattering (Litesizer 500, Anton Paar, Germany). The measured particle size distributions are presented in Figures 3.8a–3.8d, respectively.

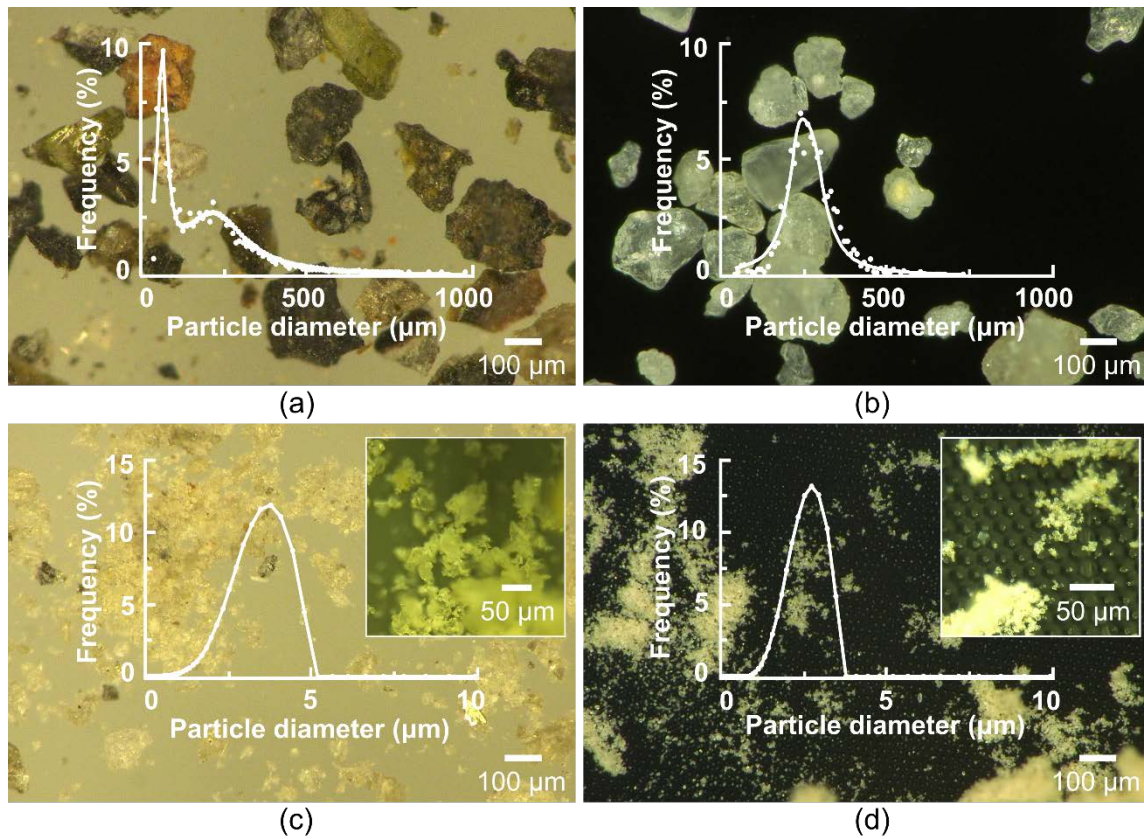


Figure 3.8 Dust contaminants used to investigate self-cleaning. Microscopy images showing the typical morphology of (a) coarse volcano ash, (b) sea sand, (c) fine volcano ash and (d) Arizona test dust with the particle size distributions plotted in the foreground. The insets are the respective dust particles viewed at a higher magnification. (Adapted from reference [119])

3.4.5.2 Impact of Self-Cleaning on Photocurrent Generation

The contact angle and the roll-off angle are good indicators for the self-cleaning potential of a surface. Nevertheless, the actual evaluation of the self-cleaning would provide a more conclusive investigation. To this extent, the self-cleaning function and impact on the photocurrent generation were evaluated from the J - V characteristics of a PV mini-module with various microtextured FEP cover films, measured similar as in Section 3.5.4, but with the additional soiled/cleaned conditions. The J_{SC} was used as the performance indicator. The key figure of merit used is the recovery ratio (RR) reported in percentage – the ratio between the performance loss after soiling ($J_{SC, loss}$) and the performance regained after cleaning ($J_{SC, recover}$) [78]:

$$RR = \frac{J_{SC, recover}}{J_{SC, loss}}$$

Again, apart from the reference conventional planar glass surface of a PV mini-module, different microtextured FEP covers were temporarily attached onto the masked PV mini-module using the refractive index matching gel described in Section 3.3.2.

Measurements of the J - V characteristics were conducted under the solar simulator with the PV mini-module tilted at a 10° angle (definition of superhydrophobic roll-off angle). The self-cleaning

performance was investigated by soiling and subsequently cleaning the soiled surface with water. Three different conditions were measured (initial, soiled and cleaned) to quantify the self-cleaning performance.

Soiling was performed *in situ* under the solar simulator by manually sprinkling the dry dust contaminants by hand from a distance of ≈ 3 cm above the tilted PV mini-module. To ensure reproducibility, the soiling was performed as homogeneously as possible and the same reduction in J_{SC} (in %) was targeted for the same set of experiments. For the investigation in Chapter 4, which used only the coarser sea sand particles as the dust contaminants, a reduction of $\approx 15 \pm 0.5\%$ in terms of J_{SC} were used. Meanwhile for Chapter 5, which used both coarse and fine dust contaminants for the investigation, a $\approx 22 \pm 1\%$ reduction in terms of J_{SC} was targeted. The J_{SC} reduction was controlled in such a manner to investigate the cleaning capability of each case by comparing similar soiling impacts with respect to the reference (clean) conditions. The reduction in J_{SC} , obtained after several initial trials, was chosen on the basis of achieving maximum reduction from the different dust contaminant types, while still maintaining enough exposed surface for the water droplets and top surface to come into contact. This situation corresponds to when the water droplets were observed to roll-off for the case of soiled superhydrophobic covers and thus could potentially clean the soiled surface.

For the cleaning step, a consistent amount of distilled water was used in the same set of experiments to eliminate the influence of water quantity on the self-cleaning capability. Droplets of distilled water were manually deposited across the soiled samples using a syringe from a ≈ 5 mm height to remove the dust. For the investigation in Chapter 4, ≈ 200 μl droplets of distilled water were used to remove the dust contaminants, which simulates a slight shower where 2 mm of rain is experienced [120]. Meanwhile, for the more refined investigation in Chapter 5, ≈ 300 μl droplets of distilled water was deposited dropwise to mimic moderate rain conditions [120].

3.4.6 Dust Removal by Wind

The influence of wind on the removal of dust contaminants was investigated inside a custom-built portable wind tunnel at the Istituto Nazionale di Geofisica e Vulcanologia (INGV), Rome. Figures 3.9a–3.9c portray how the test was set up and how the observation was possible through the transparent walls of the tunnel. The wind tunnel has a square cross-section of 12 cm \times 12 cm and an effective length of 110 cm. The experiment was set up such that the top surface of the samples was level with the tunnel's surface to prevent any unintentional resistance to the air flow. The dust particles were deposited onto the samples manually with ≈ 10 mg/cm² used for the coarse dust particles and ≈ 1 mg/cm² used for the fine dust particles as demonstrated in Figures 3.9d–3.9e. Plan view images were extracted from the video camera (FDR-AX 100E, Sony, Japan) and used to analyze the removal of dust particles under the influence of wind. The wind flow velocity, generated from an electric motor of a commercial leaf blower (EB-26D, Dream Power, Japan), was increased stepwise (0.5 m/s) and kept at each velocity step for at least 1 minute to allow the dust removal to stabilize before increasing the wind velocity again. The amount of dust removal was then correlated with the corresponding wind velocity, measured by an anemometer (PCE-423, PCE Instruments, Germany) inside the wind tunnel.

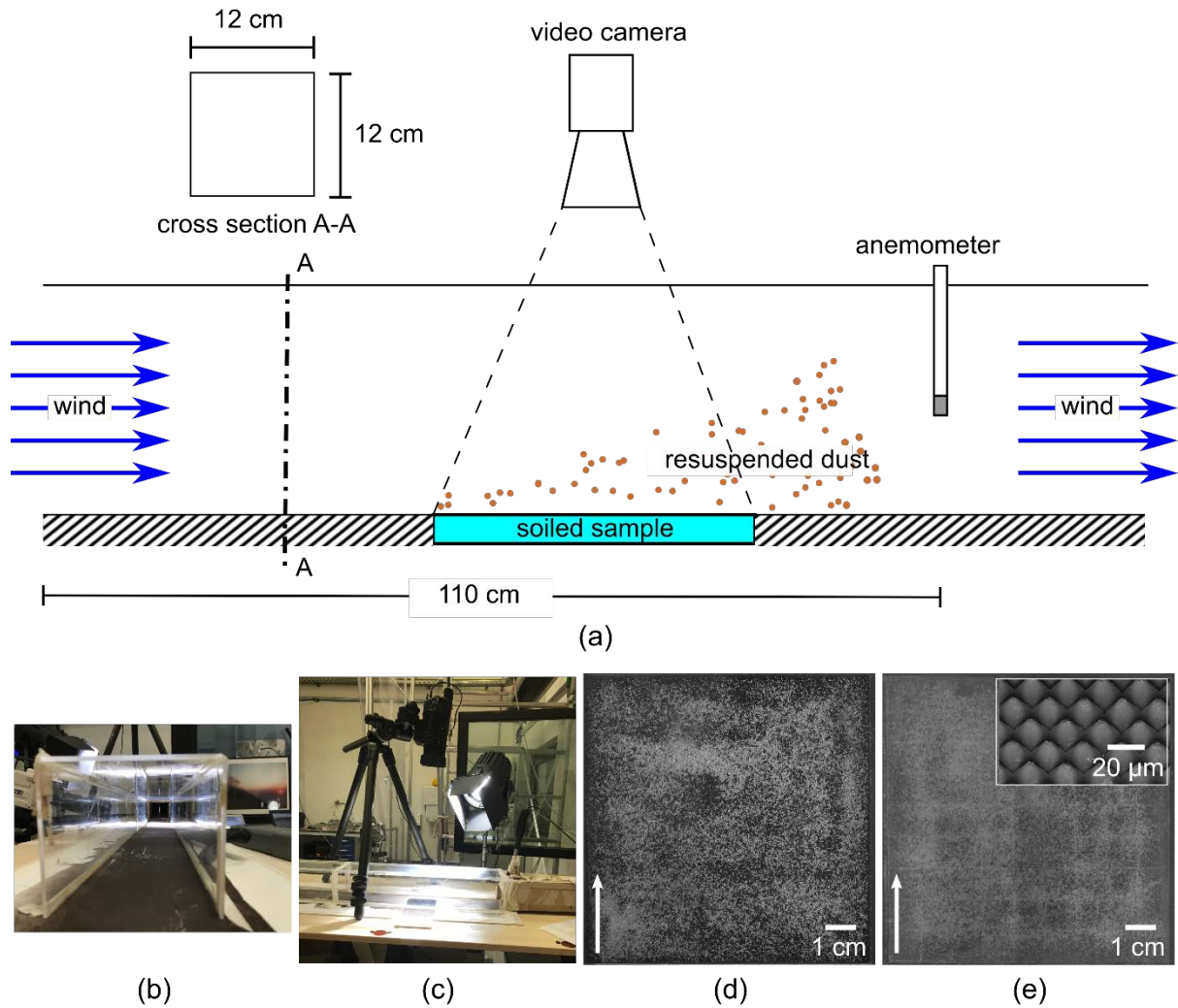


Figure 3.9 Wind tunnel test set-up. (a) Side view illustration during the wind tunnel operation, (b) view along mouth of wind tunnel, (c) main investigation area showing the sample and video camera placement. The dust particles were deposited on the investigated samples having different front surfaces: (d) planar glass and (f) microtextured FEP. The arrows illustrate the direction of the wind when placed inside the wind tunnel.

(Adapted from Reference [119])

3.4.7 Durability of Microtextures

The durability of the microtextured FEP PV module cover films is crucial for application in real world conditions, especially in relation to the long lifetime of PV modules. Abrasion tests based on relevant standards were conducted to demonstrate the durability of the microtextured FEP covers developed in this work [121]. Two categories of indoor abrasion test methods were selected: 1) falling dust particle test which imitates common low-velocity impact events and 2) forced dust impingement test that simulates intense dust storm occurrences.

For the falling dust particles test, sea sand having particle sizes of 100–300 μm were dropped from a height of ≈ 165 cm onto a microtextured FEP film (10 cm x 10 cm) attached to a planar glass tilted at a 45° angle. Meanwhile for the forced dust impingement, a microtextured FEP film (10 cm x 10 cm) was sand blasted perpendicularly from a ≈ 5 cm distance using fused alumina silica particles

4 Random Microtextured PV Module Cover Film

(particle size of 34–82 μm) with a pressure of ≈ 1 bar and under a single pass of the nozzle. In both tests, the initial and resulting conditions of the microtextured FEP films were observed using an optical microscope for the analysis.

4 Random Microtextured PV Module Cover Film

This chapter presents the development of a self-cleaning microtextured fluoropolymer PV module front cover. At this stage of the research, a random microtextured design was investigated as proof of concept. Partially, the work in this chapter was used as a learning curve to better understand the fabrication limits of fluoropolymers in this context and also as training for the fabrication and characterization techniques that will be used throughout this Ph.D. research. The results in this chapter were partially published in: Solar Energy Materials and Solar Cells, 2019 [44]. The author would like to gratefully acknowledge the contribution of all co-authors for the publication.

The original idea for this chapter was inspired by Dr. Efthymios Klampaftis and Prof. Bryce S. Richards based on a work that the author was partially involved in as published in [43]. Credit goes to Dr. Felix Vüllers and Dr. Maryna N. Kavalenka whose work on nanofur inspired the random microtexture design used in this chapter. The author then developed a random microtextured shim with the kind assistance of Dr. Uwe Köhler, Marco Heiler and Dr. Markus Guttman. The hot-embossing fabrication process was conducted by the author, having received guidance and training from Marc Schneider. SEM images were produced with the assistance of Dr. Stephan Dottermusch. The author conducted all the following characterization, initially receiving training from colleagues: Characterization of wetting properties with the guidance of Richard Thelen (contact angle) and Dr. Nico Keller (roll-off angle); Structural characterization with the guidance of Richard Thelen; Spectral response (reflection and transmission) characterization and IV characterization with the guidance of Dr. Stephan Dottermusch. The self-cleaning tests and related images were conducted and produced by the author. All authors were involved in the discussion and writing for the publication [44].

In addressing the PV soiling problem, a superhydrophobic PV module cover film was developed. Based on a previous bio-inspired work developing PC superhydrophobic nanofur that the author was involved with, it was learnt that random microcavities resulted in reduced front reflectance [43]. This would be suitable for PV applications where it would increase the light that reaches the solar cell. Unfortunately, the superhydrophobic property was a result of the high aspect ratio nanofur, which does not contribute towards the enhancement of the optical properties and in fact can become a hindrance when damaged [43]. Therefore, this work investigates how it would be possible to achieve a superhydrophobic surface without the high aspect ratio nanofur textures such that it would be suitable for PV application.

4.1 Influence of Random Microtextured FEP Film on Properties Relevant for PV Applications

The wetting property of a surface is determined by the material property and the surface contact area [122]. Therefore, to develop a superhydrophobic cover film, a low energy fluoropolymer material was selected and random microcavities were introduced on the surface.

4.1.1 Wetting Properties

The wetting properties of the investigated surfaces in this work are defined by the contact angle and roll-off angle, as previously explained in Chapter 2. The evaluation of the microtextured surfaces were compared to a reference untextured planar FEP film which has a contact angle and roll-off angle of $112\pm 3^\circ$ and $31\pm 1^\circ$, respectively.

Initially, the parameters for the hot-embossing fabrication process in producing the desired random microtextures were unknown. Therefore, combinations of various temperature and force settings were used to produce several random microtextured FEP samples. This step was conducted to understand how these parameters affect the resulting samples and the subsequent wetting property. Here, the measured wetting properties for the different fabrication parameters were reported as shown in Figure 4.1.

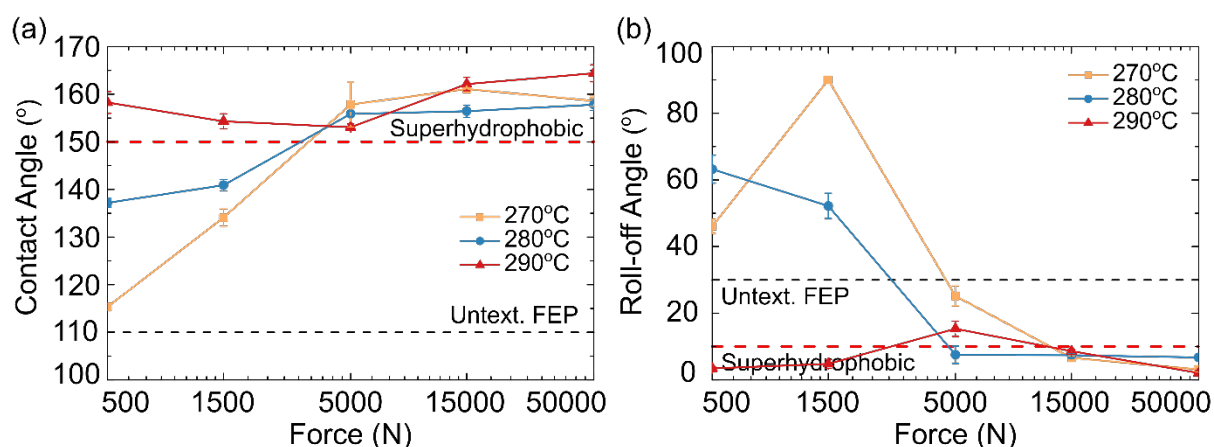


Figure 4.1 Influence of fabrication parameters (temperature and force) on the wetting properties of hot-embossed random microtextured FEP samples. The (a) contact angle and (b) roll-off angle for each sample were plotted together with standard error bars. The values for untextured (---) and those that define superhydrophobicity (---) were also plotted as reference. (Adopted from [44])

Figure 4.1 demonstrates that the enhancement of the wetting property to obtain a superhydrophobic surface was successfully achieved with the introduction of random microtextures. Nevertheless, there is a threshold for fabrication parameters that needs to be considered before superhydrophobicity can be achieved which highly relates to the resulting microtextures morphology for the respective fabrication parameters; this is discussed further in Section 4.3. Figure 4.1a shows that superhydrophobic contact angles were achieved, at all fabrication temperatures, for forces ≥ 5000 N. Meanwhile, superhydrophobic roll-off angles were achieved, at all fabrication temperatures, for forces >15000 N as shown in Figure 4.1b. A higher fabrication force would tend to result in a superhydrophobic microtexture.

It can also be concluded that the fabrication temperature plays a significant role in achieving superhydrophobicity. At 290°C, almost all samples achieved superhydrophobicity even at the lowest investigated force of 500 N. Most likely, this is due to the existence of multiscale texturing for samples fabricated at this temperature since multiscale roughness has been shown to enhance superhydrophobicity [48], [51]. This was contrary to samples fabricated at 270°C and 280°C where there is a minimum threshold force above which the samples' surface achieves superhydrophobicity. Only one sample fabricated at 290°C did not meet the required superhydrophobic roll-off angle – sample fabricated with force of 5 kN which exhibits a roll-off angle of $15 \pm 2^\circ$. However, this roll-off angle was relatively small compared to untextured FEP and would be sufficient for self-cleaning applications at locations with higher PV module tilt angle. For example, the optimum tilt angle of a PV system is between 33° and 36° for Europe [123].

A unique observation was made for the sample fabricated at 270°C with a force of 1.5 kN. In this case, the contact angle increased with the increase in force; however, the roll-off angle was not reduced and in fact, increased greatly to 90° . A roll-off angle of 90° means that the droplet does not roll-off even when the sample is held vertically, an observation of the “rose petal effect” [56]. Traditionally, the increase in contact angle can be explained by the introduction of surface textures, since roughness increases the already prevalent wetting behavior as explained by *Wenzel* [49].

Meanwhile the “rose petal effect” observed in this case is most likely due to insufficient texturing, thus not having a big enough effect on air entrapment within the cavities. This resulted in an increase in the liquid–solid contact area and therefore an increase in the adhesion, which is observed from the higher roll-off angle. The detailed morphology of the random microtextures fabricated with 1.5 kN at 270°C will be presented in Section 4.3. This will enable better understanding of the fabrication parameters required to produce precise microtextures to achieve superhydrophobic surfaces.

The impact of texturing FEP films on the wetting behavior is visually demonstrated in Figure 4.2. The different shape and contact angle of water droplets on untextured and random microtextured FEP (5 kN at 280°C) can be observed in Figures 4.2a and 4.2b, respectively. Initially, the untextured FEP has a hydrophobic surface as seen from the near-hemispherical shape of the water droplet having a contact angle of $\approx 112^\circ$. The subsequent microtexturing of FEP results in a significant increase of the contact angle ($\approx 156^\circ$), seen from the more spherical shape of the water droplet in Figure 4.2b.

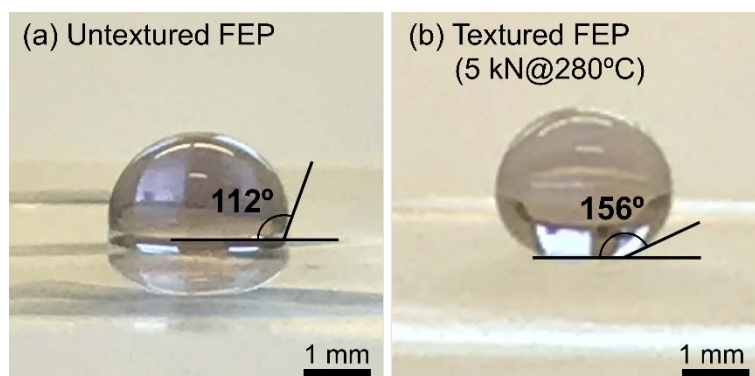


Figure 4.2 Water droplet on (a) untextured FEP and (b) microtextured FEP fabricated with 5 kN at 280°C. The impact of the microtextures is demonstrated by the water droplet keeping its almost spherical shape (contact angle of $156\pm 1^\circ$) on the microtextured FEP. (Adopted from [44])

As discussed in Chapter 2, there were different approaches to define the superhydrophobicity of a surface including the bouncing of a water droplet [55]. This thesis will not use this parameter to quantify the wetting property of the surface considering the intended application of the developed microtextured PV module front cover. Nevertheless, a simplified test of bouncing water droplet was conducted. This would serve as a good demonstration to visually highlight the superhydrophobic effect from the introduction of microtextures on FEP films, as presented in Figure 4.3.

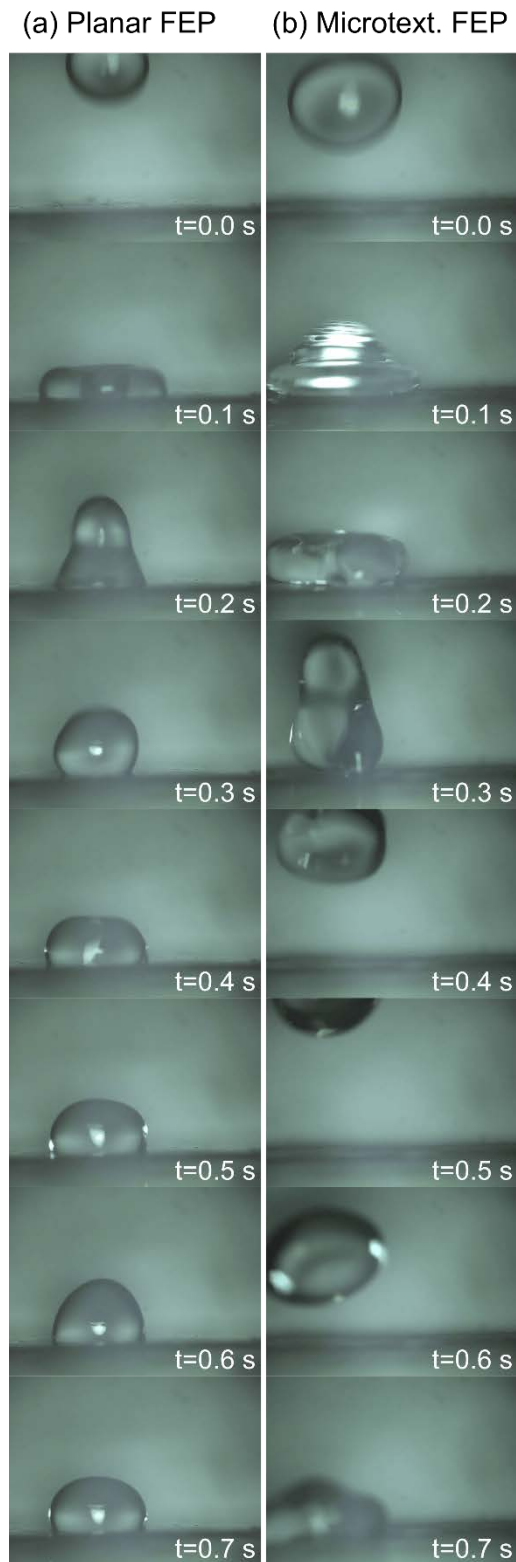


Figure 4.3 Bouncing of water droplets to demonstrate the superhydrophobicity of a surface. Still images taken by a high-speed video camera compare the effect of different wetting properties of (a) a planar FEP surface and (b) a random microtextured FEP surface on the bouncing of the water droplets. Time stamps of each still image are given in the lower right corner.

Figure 4.3 compares the bouncing of water droplets when dropped onto a planar FEP surface and a random microtextured FEP surface. In both cases, the water droplets ($\approx 10 \mu\text{l}$) were manually

dropped from a height of ≈ 5 cm. A high-speed video camera was used to obtain still images at different times to observe the water droplets. In the case of a planar FEP surface, although hydrophobic in nature, it can be observed that the water droplet did not bounce off and still stuck to the surface, as shown in Figure 4.3a. Meanwhile, for the microtextured FEP which was superhydrophobic, the water droplet clearly bounced off the surface as can be observed in Figure 4.3b. These observations clearly demonstrate the impact of microtexturing a surface and thus the different behavior of water droplets when interacting with surfaces of different wetting properties.

4.1.2 Optical Properties

Having proven that superhydrophobic surfaces were successfully achieved through random microtextured FEP, we now have to consider the influence on the optical properties for it to be relevant for PV applications. Reflectance measurements taken at a wavelength of 600 nm were plotted as bar charts in Figure 4.4 with horizontal lines for untextured FEP included for reference. The full reflectance spectra for all samples are shown in Figure 4.5.

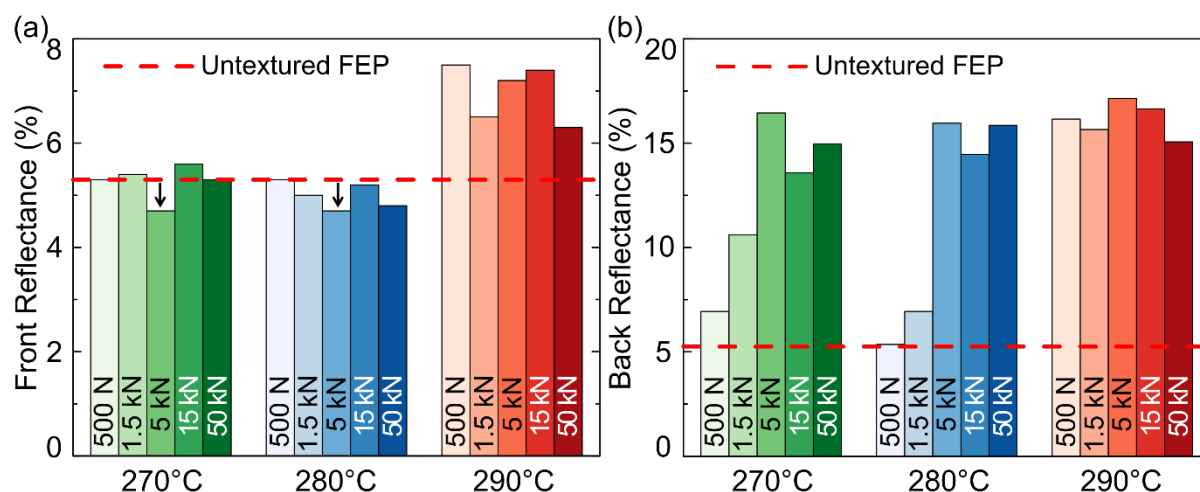


Figure 4.4 Reflectance measurements of various microtextured FEP samples. Reflectance measurements were taken at a wavelength of 600 nm for (a) front side and (b) back side illumination. The results were plotted for the respective samples fabricated with different fabrication force (0.5 kN–50 kN) and different fabrication temperatures (270°C–290°C). An untextured FEP has a reflectance value of 5.3% and was plotted as a red dotted line (---) for reference. (Adopted from [44])

Figure 4.4a shows the reflectance of textured FEP samples taken at a wavelength of 600 nm when illuminated from the front (facing textured interface), while Figure 4.4b shows the reflectance when illuminated from the back (facing planar interface). The random microtextures evidently have an impact on the reflectance depending on which side is illuminated. This is of importance when considering light trapping in a PV module. Ideally, the desired case for PV applications is a reduction in front side reflection while simultaneously increasing the back side reflection.

Several key observations are highlighted here. For fabrication temperatures of 270°C and 280°C, there were no obvious trends observed for the front side reflectance. Nevertheless, a maximum reduction in the front side reflectance was achieved for both temperatures when a force of

5 kN was applied, as highlighted by the black arrows in Figure 4.4a. Meanwhile, the samples fabricated at 290°C exhibit a totally opposite trend where higher reflectance was observed when illuminated from the front for all cases. This increase in front side reflectance is undesirable as it reduces the intensity of incoming light, therefore would not be suitable for PV applications. The increase of reflectance for front side illumination to values higher than those of the untextured FEP was observed in the case of 290°C only. This can be attributed to the existence of multiscale texturing which was not present in the samples fabricated at 270°C and 280°C. These multiscale texturing will be discussed with more detail in Section 4.3.

The back side illumination presented a different trend where an increase in the back side reflectance was desired. For both fabrication temperatures of 270°C and 280°C, the samples enjoyed a high back side reflectance starting from 1.5 kN onwards compared to untextured FEP. Meanwhile, the samples fabricated at 290°C exhibits higher reflectance when illuminated from the back for all investigated forces. It is evident that the reflectance for back side illumination is generally high for the 290°C samples compared to those fabricated at 270°C and 280°C for all hot-embossing forces. This significant improvement in the back side reflectance demonstrates the potential of random microtextured FEP as a top cover for PV modules. The improved back side reflection contributes towards light trapping and is known as the retro-reflection effect [84], [87]. Several samples fabricated at different fabrication parameters demonstrated the desired impact (reduced front side reflection and increased back side reflection, simultaneously).

The full reflectance spectra presented in Figure 4.5 shows that the impact of the microtextures towards the front and back side reflectance was generally consistent throughout the investigated spectrum (300–1100 nm) for all cases. To increase the confidence in the investigation of optical properties of the microtextured surface, the transmittance was also measured and presented in Figure 4.6. In this case, the desired impact would be that there is increased transmittance from front side illumination and reduced transmittance from back side illumination. Eventually, the observations were consistent with what was learnt from the reflectance measurements where there exist microtextured FEP surfaces that had increased front side transmittance and reduced back side transmittance. These observations were also consistent throughout the investigated spectrum for all cases. It must be mentioned that in some of the reflectance and transmittance measurements presented in Figure 4.5 and Figure 4.6, there exist a slight step in the spectra at wavelength ≈ 850 nm. This can be attributed to the detector change during measurements using the UV-Vis-NIR spectrophotometer. It can be considered as a slight error in the results but does not affect comparison between the different measurements that compares readings at wavelength ≈ 600 nm.

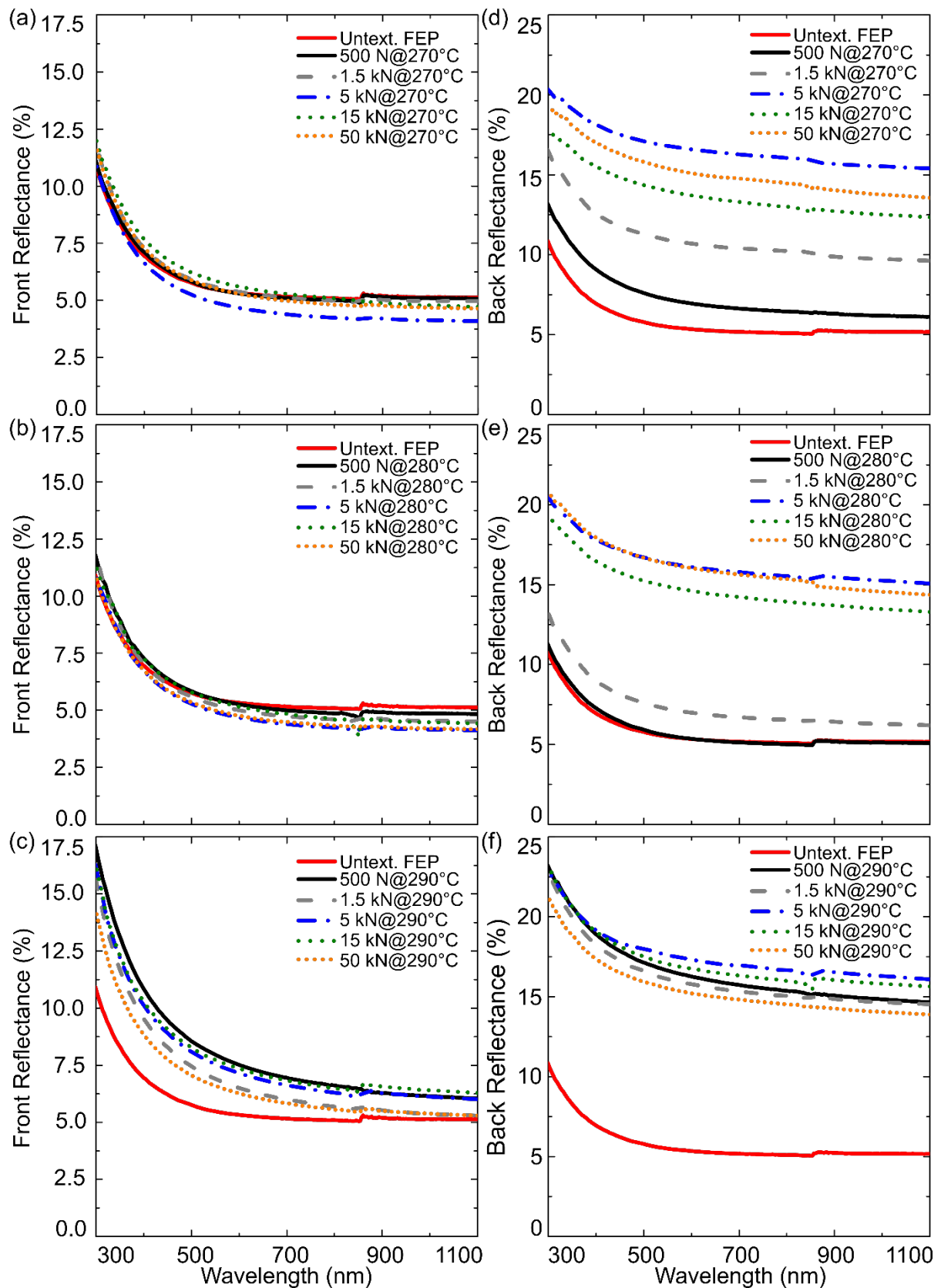


Figure 4.5 Full reflectance spectra for the various fabricated microtextured FEP samples. The reflectance spectra, measured for front-side (a–c) and back-side (d–f) illumination, were plotted in different figures to highlight the influence of fabrication parameters on the reflectance. In all figures, the reflectance of untextured FEP is used as reference and plotted in red (–). (Adapted from [44])

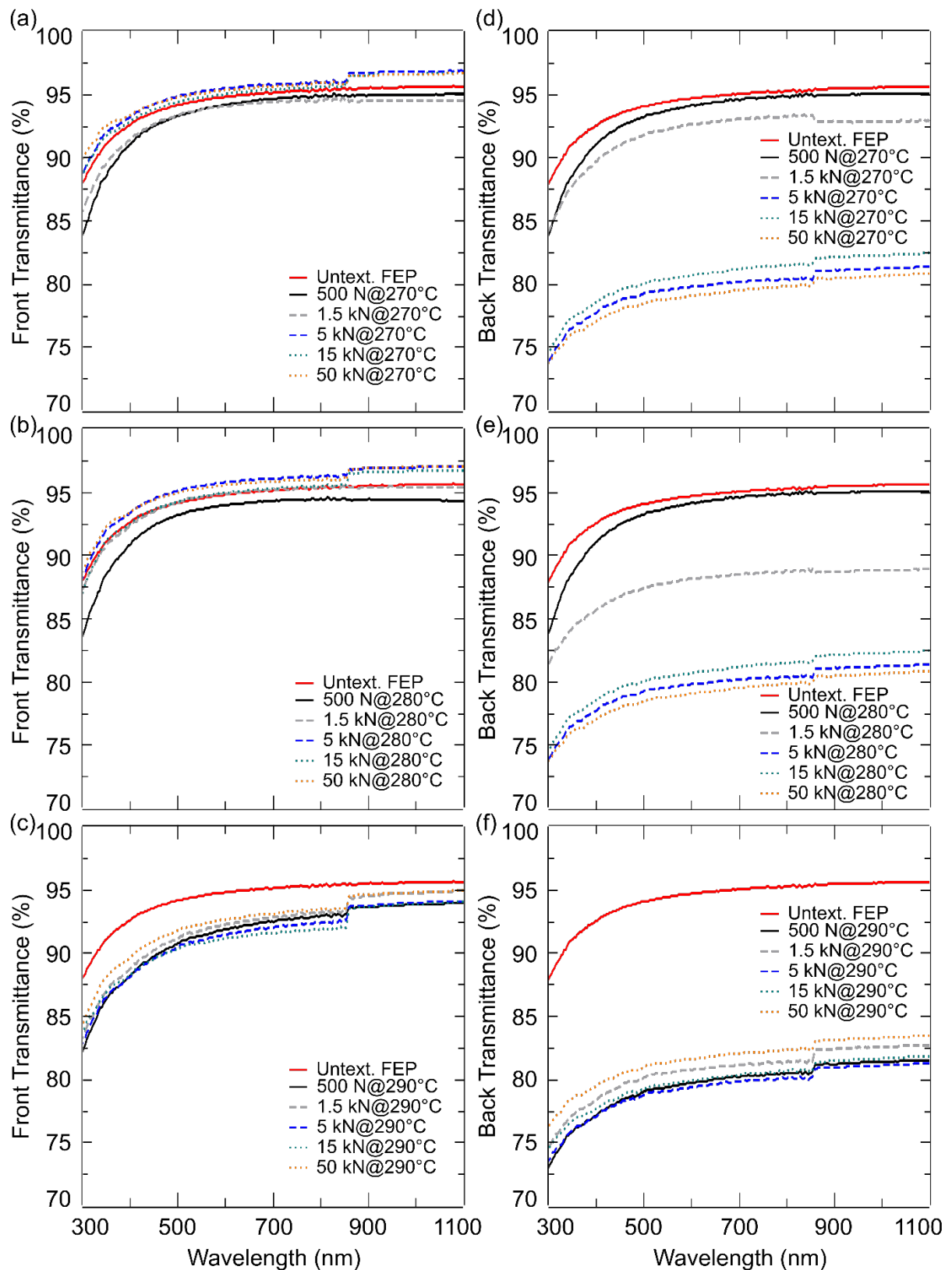


Figure 4.6 Full transmittance spectra for the various fabricated microtextured FEP samples. The transmittance spectra, measured for front-side (a–c) and back-side (d–f) illumination, were plotted in different figures to highlight the influence of fabrication parameters on the transmittance. In all figures, the transmittance of untextured FEP is used as reference and plotted in red (–).

From the results in this section and taking into consideration the wetting properties presented previously in Section 4.2.1, the sample fabricated at 280°C with 5 kN demonstrated both the desired superhydrophobic property and exhibits the highest improvement in front side and back side reflectance; thus, identified as the best random microtextured FEP sample to be used as a PV module front cover and will be used for further investigations in this Chapter.

4.2 Morphological Analysis of the Random Microtextures

To better understand the resulting wetting and optical properties, the fabricated random microtextures were examined. SEM images of the nickel shim morphology used to produce the random microtextures are shown in Figure 4.7a. Meanwhile, Figure 4.7b shows the detailed zoom-in view of the nickel shim surface showing the relatively rough surface of the troughs in between the microtextures.

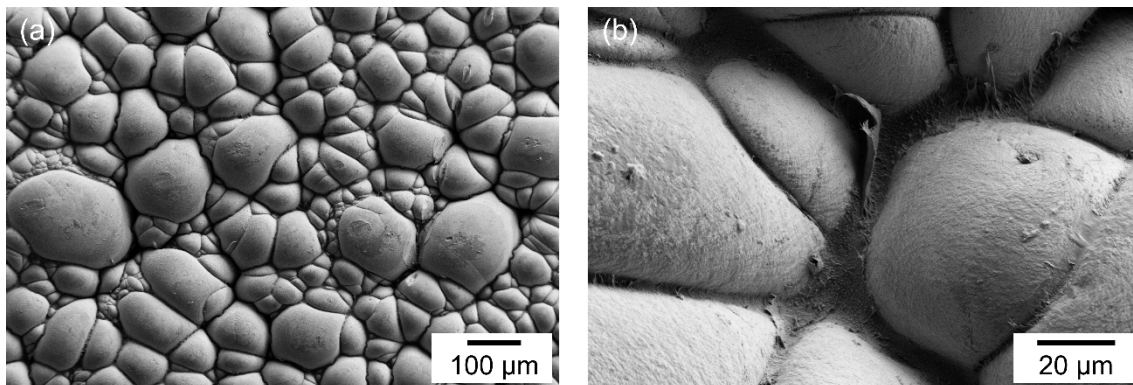


Figure 4.7 SEM images of nickel mold insert for random microtextures showing (a) general view of size and shapes of the random microtextures and (b) enlarged view showing surface details of the nickel shim. (Adapted from [44])

As previously mentioned, to reproduce the best hemispherical cavity random microtextures, the fabrication parameters were varied; Several combinations of temperature (270°C, 280°C and 290°C) and hot-embossing force (500 N, 1500 N, 5000 N, 15 000 N and 50 000 N) were used. SEM images (plane view) of the resulting surface microtextures for the respective fabrication parameters are shown in Figure 4.8.

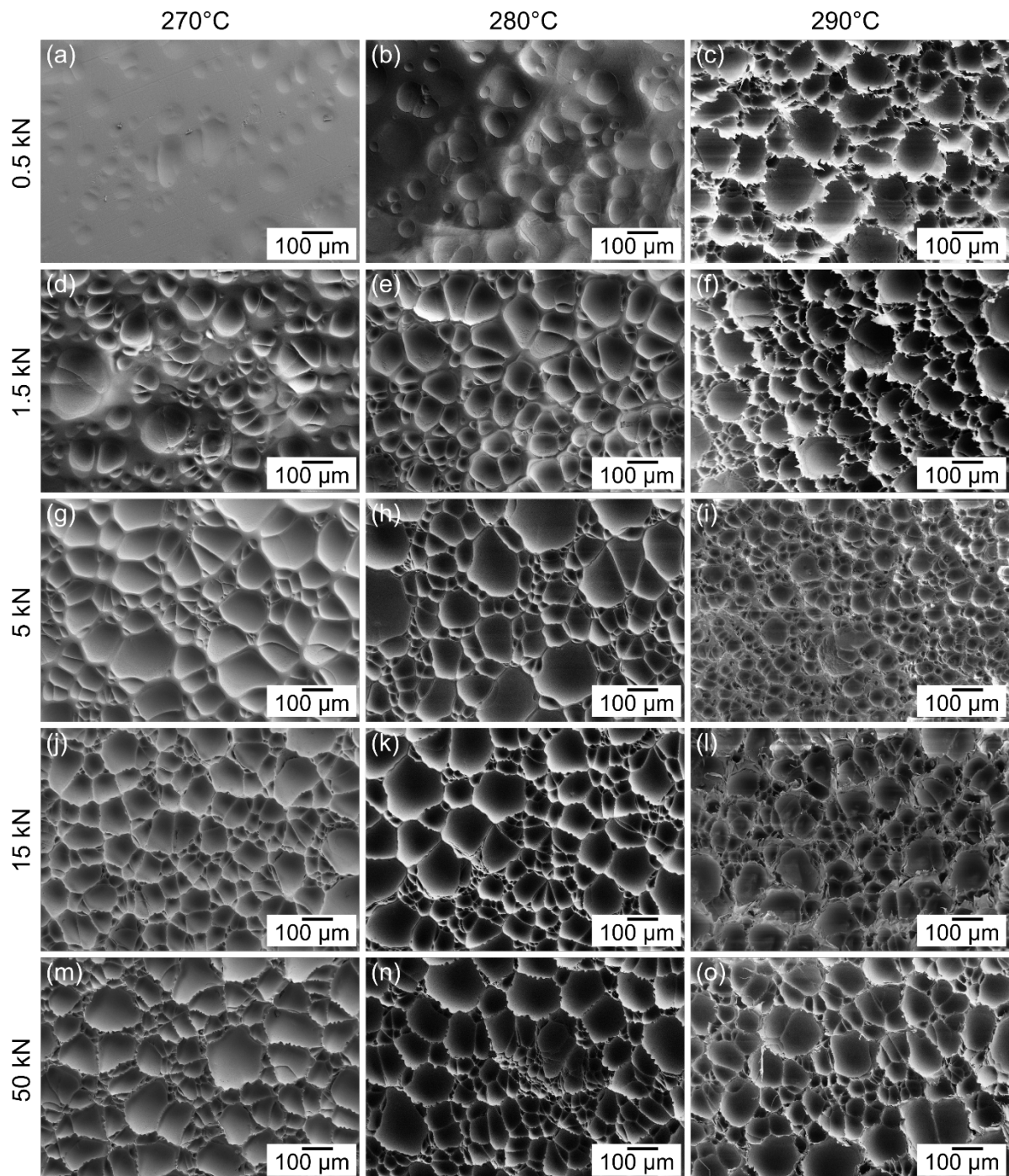


Figure 4.8 Plan view SEM images showing the morphology of all random microtextured FEP samples fabricated at various fabrication forces (0.5 kN, 1.5 kN, 5 kN, 15 kN and 50 kN) and temperatures (270°C, 280°C and 290°C).

From a qualitative point of view, the impact of different fabrication parameters is apparent. Higher fabrication parameter combinations would result in a more prominent pattern being imprinted as observed in Figure 4.8. The initial aim is to fabricate exact replicas of the random microtextures. Retrospectively, since the contributions of the random microtextures design to the wetting property and the optical property was not truly understood, the varying fabrication parameters would produce various microtextures within the same morphological design of the initial master. Furthermore, prior

to conducting the hot-embossing step, the best temperature and force setting to achieve perfect replicas were not known. Most importantly is the evaluation of the resulting wetting and optical properties that are suitable for PV applications as were presented in Section 4.2.

Based on the SEM images, samples hot-embossed at 280°C with a force of 5 kN demonstrated a near-perfect replica where sharp straight ridges were observed on the microcavities as seen in Figure 4.8h. The samples fabricated at 280°C with lower forces (Figure 4.8b and 4.8e) were not so well-defined due to insufficient hot-embossing. Meanwhile, increasing the force causes wrinkles on the ridges (see Figures 4.8k and 4.8n). Figure 4.8 also shows a similar trend for samples fabricated at temperatures 270°C and 290°C.

The qualitative observation of the resulting hot-embossed random microtextures was further investigated through characterization of the surface roughness. The measurements presented were focused on the samples fabricated at 280°C to demonstrate the effect of different fabrication parameters. Figure 4.9 shows that the average roughness (R_a) increases as the hot-embossing force was increased and the sample fabricated with 5 kN achieved the highest average roughness of 20.1 μm . Meanwhile, the existence of flat surfaces on the under-patterned samples contributes towards the lower roughness for samples fabricated with 500 N ($R_a = 7.9 \mu\text{m}$) and 1.5 kN ($R_a = 10.0 \mu\text{m}$). It was expected that the samples fabricated with 15 kN and 50 kN would have similar or higher surface roughness as the sample fabricated with 5 kN because of the same base microcavity shape but with the additional wrinkles. Nevertheless, the average roughness was slightly low for samples fabricated with 15 kN ($R_a = 17.2 \mu\text{m}$) and even much lower for the samples fabricated with 50 kN ($R_a = 10.9 \mu\text{m}$). The most probable explanation is that the existence of secondary features such as wrinkles or tears on the ridges interferes with the interferometry measurements. The presence of these fringe features which affect the roughness value can be observed from Figure 4.8 and also from the interferometry images in Figure 4.9.

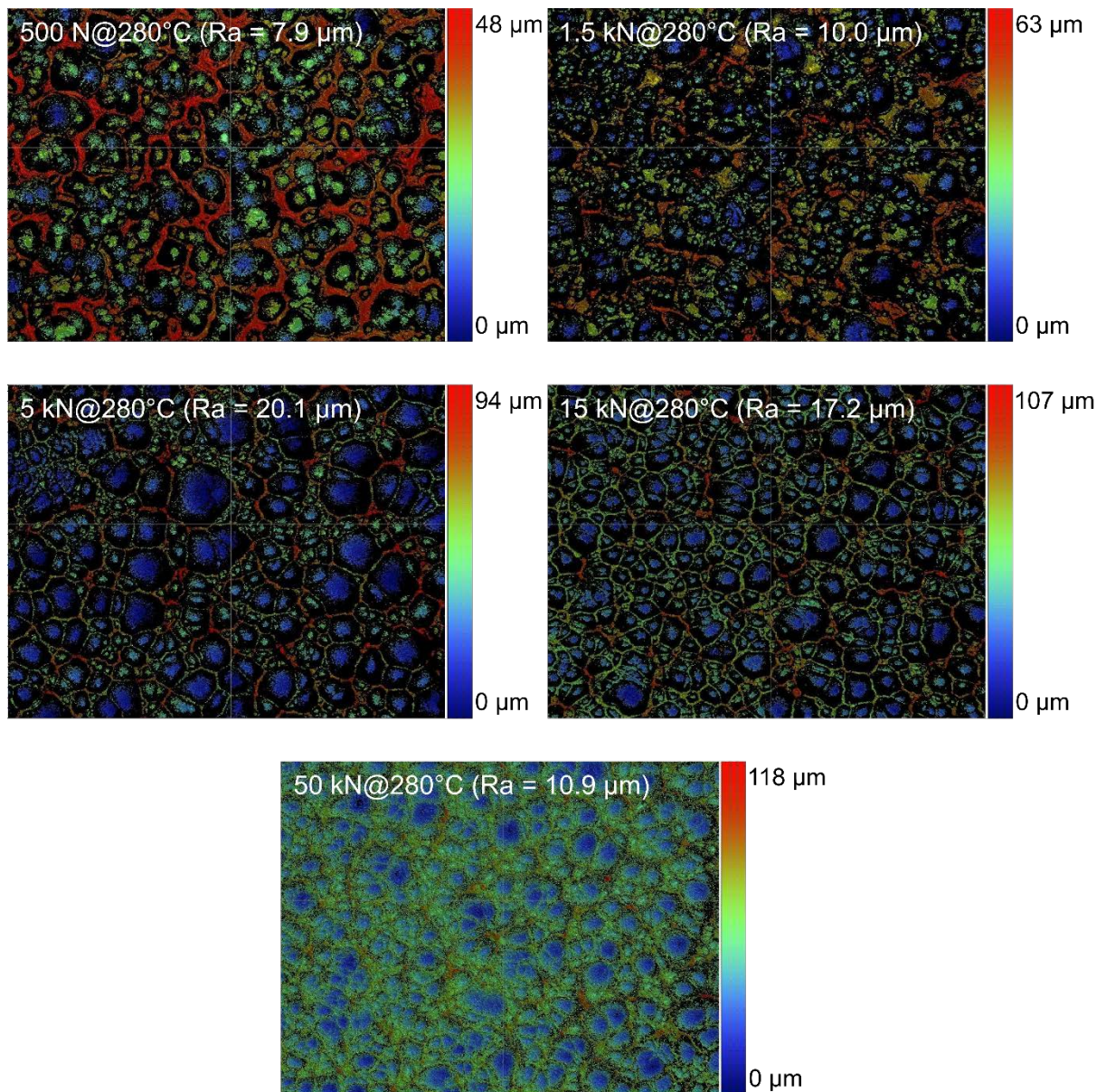


Figure 4.9 Interferometry images for surface roughness (R_a) evaluation. Surface roughness was obtained from vertical spacing interferometry images of textured FEP samples fabricated at 280°C with various fabrication forces. All interferometry images have a scan size of 1.7 mm x 1.3 mm. (Adapted from [44])

For the samples fabricated at 290°C, additional secondary textures were observed which was not present for any of the samples fabricated at 270°C and 280°C (see Figure 4.8). This is of particular interest since multiscale structures was previously shown to play a significant role to induce a superhydrophobic behavior even for polymers with significantly higher surface energy than FEP, such as PC [76]. Therefore, it is reasonable to expect that the additional multiscale textures that were observed for all samples fabricated at 290°C, although vary in sizes as shown in Figure 4.8, will further enhance the wetting property of these FEP samples as well. These secondary textures are thus the main contributor to the superhydrophobicity achieved for all samples fabricated at 290°C as shown previously in Figure 4.1.

From visual inspections, it was evident that all our samples fabricated at 290°C were highly transmissive (comparable to samples fabricated at 270°C and 280°C) and did not suffer from opacity as observed in a recent work [88] when fabricated at higher temperatures. Therefore, it is highly probable that these secondary textures are the main contributors to the high reflectance as presented in Figure 4.4.

Consistent with the findings in Section 4.2, the samples fabricated with 5 kN at 280°C would be used for further investigations since the best replica was obtained with these fabrication parameters. Most importantly, this sample also met the superhydrophobic and anti-reflective requirements making it suitable for PV applications. This chosen random microtextured FEP film has a contact angle = $156\pm 1^\circ$ and a roll-off angle = $8\pm 3^\circ$.

4.3 Application as PV Module Front Covers

So far, a superhydrophobic and anti-reflective random microtextured FEP film was successfully developed. Next, the application of this microtextured FEP film as a top cover was investigated.

4.3.1 Electrical Properties

To demonstrate the impact of a random microtextured FEP film on the photocurrent generation of a PV device, different top surface conditions were compared. A planar untextured FEP film was compared to the random microtextured FEP to understand the contribution of the microtextures by applying the films onto a mc-Si PV mini-module and the J_{SC} compared. Apart from that, the J_{SC} of a bare PV mini-module without any covers was used as a reference. The application of FEP as a top cover improved the output of the PV mini-module in terms of J_{SC} regardless of whether textured FEP (31.6 mA/cm^2) or untextured FEP (31.4 mA/cm^2) was applied compared to the bare PV mini-module – no FEP (31.2 mA/cm^2), as shown in Figure 4.10.

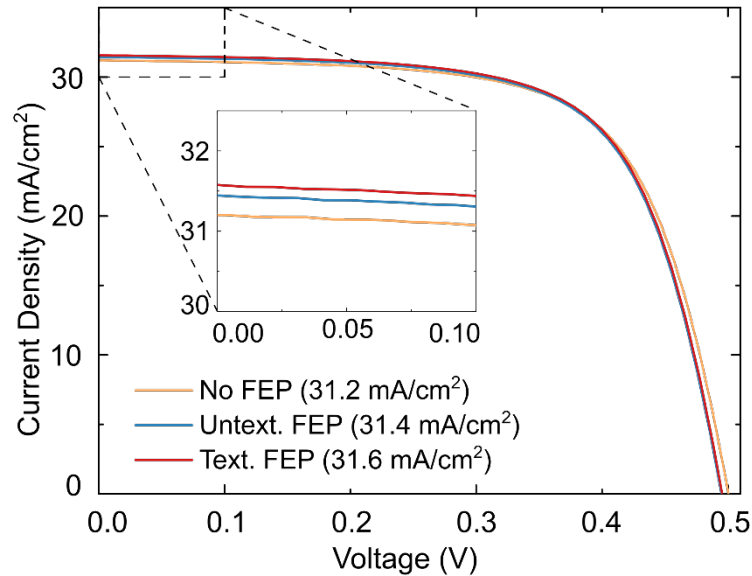


Figure 4.10 J - V characteristic curves of PV mini-module comparing influence of various top covers. The impact of having untextured FEP and textured FEP as top cover were demonstrated compared to the reference device with no top cover, gaining relative J_{SC} improvements of $\approx 0.6\%$ and $\approx 1.2\%$ respectively. The improvements in J_{SC} , which values are given in parentheses, can be clearly seen in the inset. (Adopted from [44])

The improvement in J_{SC} is partially due to the addition of a lower refractive index (compared to glass) top cover layer and partially due to the texturing of the film [43], [76]. The $\approx 0.6\%$ (or 0.2 mA/cm^2) improvement in J_{SC} from the untextured FEP top cover can be attributed to the reduction in Fresnel reflection losses since FEP has a refractive index ($n = 1.34$) in between that of air ($n = 1.0$) and glass ($n = \approx 1.5$). Meanwhile when textured FEP was applied, a further $\approx 0.6\%$ (or 0.2 mA/cm^2) improvement in J_{SC} comes from the impact of the microtexturing on the reflectance. This improvement is expected to be of general relevance to all PV technologies due to the contribution of the microtextured FEP as a top cover that would improve light in-coupling by reducing light reflectance. The usage of a mc-Si PV mini-module in this work serves as an exemplary case to demonstrate the potential of using a textured FEP film as a top cover for PV modules.

Although a reduced reflection (thus improved J_{SC} output) was achieved by applying the FEP layers, this already includes a 0.5% loss in light intensity from absorption by the index matching gel of $\approx 185 \text{ }\mu\text{m}$ thickness used in this work (see Figure 4.11). The index matching gel was only used as a temporary adhesive layer for investigations in this work and would not be part of a permanent PV device architecture. The thickness of the gel used might differ as it was manually applied and the losses could be higher, but the eventual permanent lamination of the FEP on a PV module will eliminate this source of loss and a higher improvement in terms of J_{SC} is expected for actual devices.

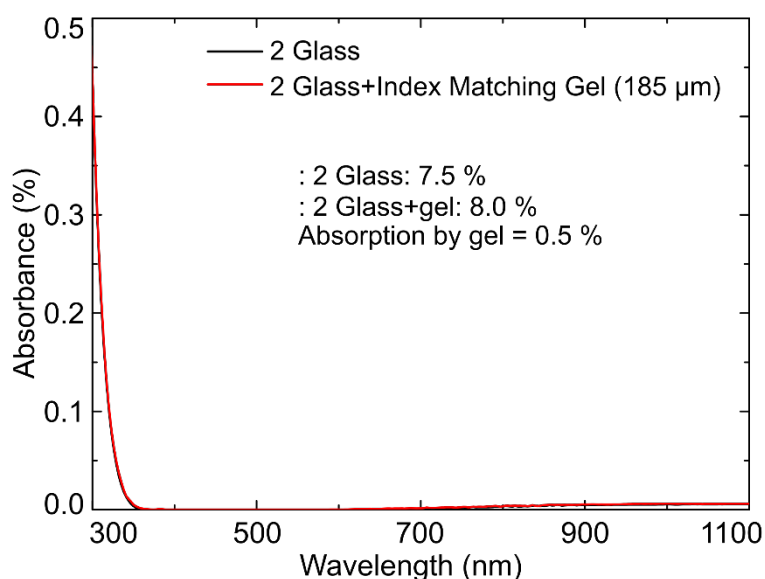


Figure 4.11 Absorbance of index matching gel. The gel was applied in between 2 glass pieces, similar to how the FEP films were coupled to a glass-encapsulated mc-Si PV module, and the absorbance measured. The absorbance of the 2 glass pieces was then subtracted giving us a 0.5% absorption loss from the index matching gel. Absorbance curves were plotted with different colored lines: 2 glass pieces with index matching gel (—) and only 2 glass pieces (—). (Adopted from [44])

The total enhancement in J_{SC} ($\approx 1.2\%$) by the microtextured FEP film in this Chapter is lower compared to previous work using microtextured FEP [43] as well as PC nanofur [76], where a 4.6% and 5.8% enhancement was achieved respectively. Therefore, further work should be conducted to optimize the morphology of the microtextures to improve the photocurrent generation enhancement by the multifunctional self-cleaning top cover.

4.3.2 Self-Cleaning Capability

The applicability of the superhydrophobic random microtextured FEP as a self-cleaning top cover for PV modules is presented in this section. Figure 4.12 exhibits the self-cleaning behavior of a microtextured FEP in comparison to untextured FEP. Both samples were attached to a glass slide tilted at 10° before being soiled with sea sand, as demonstrated in Figure 4.12a. When water droplets were deposited onto the soiled surfaces, the untextured FEP did not exhibit any self-cleaning behavior as the droplets remained on the sample's surface (Figure 4.12b, left). However, in the case of the microtextured FEP (see Figure 4.12b, right), the droplets rolled off removing the particles of the sea sand and resulting in an almost completely cleaned surface. The self-cleaning mechanism demonstrating removal of the sea sand from a tilted surface can be further observed from Figure 4.13. Videos of these self-cleaning behavior can also be observed as part of the published work [44].

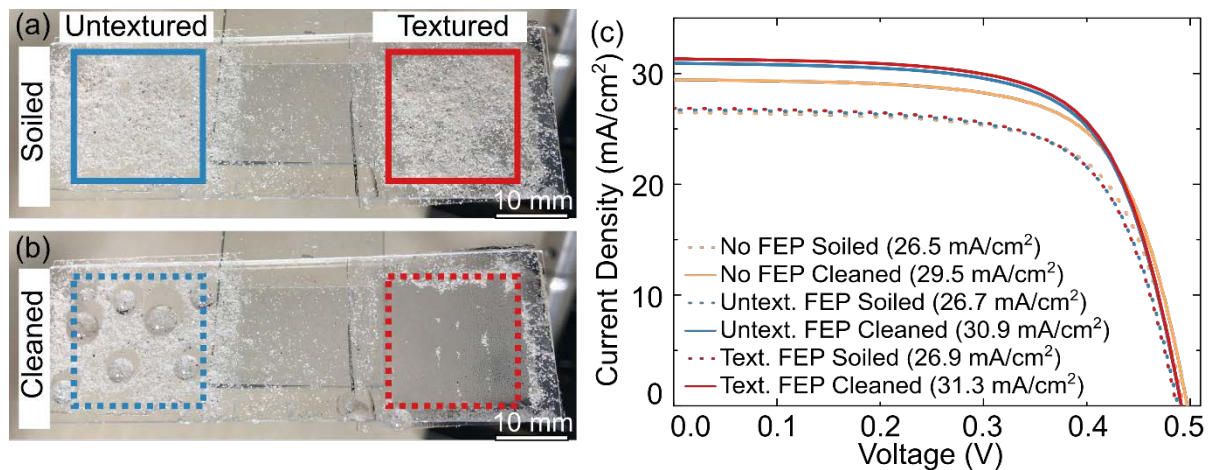


Figure 4.12 Self-cleaning of soiled surface demonstrated visually and quantitatively. Visual demonstration of (a) soiled samples comparing untextured FEP (left side) and textured FEP (right side) held at an angle of 10° ; and (b) the same soiled samples after depositing water droplets to exhibit the self-cleaning function of the microtextured sample. (c) J - V characteristics showing the impact of self-cleaning by the microtextured FEP when applied on a mc-Si PV mini-module. The self-cleaning capability for both untextured and microtextured FEP samples can thus be compared. The J_{sc} of each sample is given in parentheses in the legend. (Adopted from [44])

To further quantify the self-cleaning capability, the impact of self-cleaning a soiled surface at a 10° tilt angle on the electrical output of a PV mini-module was investigated comparing the microtextured FEP, untextured FEP and without any FEP cover as presented by the J - V curves in Figure 4.12c. The soiling of the surface by sea sand was conducted manually and controlled by a reduction in terms of J_{sc} for all cases – suffering a loss of 15.2% (no FEP), 15.0% (untextured FEP) and 14.9% (microtextured FEP). After cleaning the soiled samples with the same amount of water for each case, a recovery ratio of 93.6% was achieved – measured via J - V curves when the microtextured FEP top cover was employed, compared to 61.1% for the reference PV mini-module with no FEP cover and 89.4% for untextured FEP. This is an improvement from a previous self-cleaning surface which applied a microshell textured PDMS film where a 71.8% recovery was achieved [78]. The self-cleaning capability of the microtextured FEP will enable PV modules to reduce the impact of soiling on the electrical output and operate at a higher performance for longer durations of time.

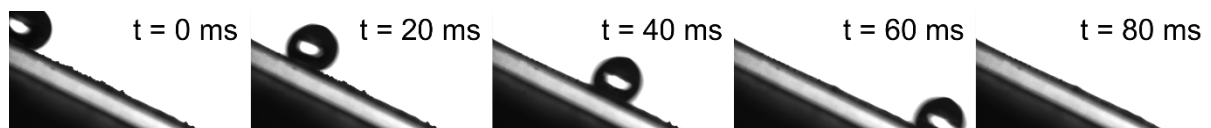


Figure 4.13 Visual demonstration of self-cleaning mechanism on random microtextured FEP at different time-steps demonstrating a rolling water droplet picking up soil particles.

As mentioned in a few paragraphs back, Figure 4.13 demonstrates the removal of dust from a surface. It can be clearly observed that there exist dust particles on the surface prior to the water droplet passing through (at $t = 0$ ms). These particles were picked up by the water droplet even with only a single pass, leaving behind a cleaned surface (at $t = 60$ ms). In actual implementation, the water droplets from rainfall would be more effective in picking up the dust particles due to the multiple passes over a period of time.

4.4 Summary

To this end, a self-cleaning superhydrophobic cover for PV modules was developed by hot-embossing random microtextures on FEP films. It was evident from the SEM images that the degree of texturing increased with higher fabrication parameter combinations. Nevertheless, there exist optimum parameters that were best to be used. Due to the low surface energy of FEP, it was shown that simple random texturing was sufficient to achieve superhydrophobicity. Superhydrophobicity was exhibited for almost all samples fabricated at 290°C regardless of force. Meanwhile for samples fabricated at 270°C and 280°C, superhydrophobicity was achieved as long as a minimum threshold force was applied – leading to a minimum degree of microtexturing. The random microtextures were also shown to significantly impact the reflectance depending on which side was illuminated. The best superhydrophobic sample (fabricated with 5 kN at 280°C) exhibits a water contact angle of $156\pm 1^\circ$, a roll-off angle of $8\pm 3^\circ$ and a significant improvement in the reflectance. The application of the random microtextured FEP as a top cover on a glass-encapsulated mc-Si single-cell PV mini-module afforded a J_{SC} improvement of 1.2%. Apart from the reduction in Fresnel reflection losses by introducing FEP, this improvement in J_{SC} is also attributed to the microtextures introduced. Aside from scattering the light, the random microtextures results in a slightly lower front side reflectance as well as a significantly higher back side reflectance, which contributes to light trapping. The self-cleaning behavior of the random microtextured FEP demonstrated a 93.6% recovery in terms of J_{SC} . Although a multifunctional self-cleaning and anti-reflective PV module cover film was achieved through the random microtextures, the optical contribution can be enhanced further by optimizing the microtextures morphology.

5 Periodic Cone-Shaped Microtextured PV Module Cover Film

This chapter presents the introduction of a periodic cone-shaped microtexture design to further enhance the anti-reflective properties of the developed PV module front cover. The influence of aspect ratio of the cone microtextures was investigated to optimize for both wetting and anti-reflective properties. Potential application issues to implement the microtextured PV module front cover were also investigated and presented in this chapter. The results in this chapter were partially published in: Solar Energy Materials and Solar Cells, 2020 [124]. The author would like to gratefully acknowledge the contribution of all co-authors for the publication.

The initial idea for this chapter was from a brainstorming session with Dr. Raphael Schmager, Dr. Stephan Dottermusch, Dr. Efthymios Klampaftis, Prof. Dr. Ulrich W. Paetzold and Prof. Bryce S. Richards. Further discussions with Dr. Guillaume Gomard and Prof. Hendrik Hölscher also contributed towards development of the work in this chapter. The cone-shaped microtexture design, having different aspect ratio, used in this work was based on a simulation work lead by Dr. Stephan Dottermusch that the author was involved in as presented in a previous publication [85]. Microtextured shims, for each aspect ratio, were developed with the kind assistance of Dr. Uwe Köhler, Marco Heiler and Dr. Markus Guttman. SEM images were produced with the assistance of Dr. Stephan Dottermusch. The author conducted all the fabrication of samples and the remaining characterizations in this work: Wetting properties; Structural; Spectral response; IV characteristics; Mechanical strength; and Self-cleaning tests. All authors were involved in the discussion and writing for the publication [124].

A self-cleaning PV module top cover requires it to not only introduce a self-cleaning function, but also to not hinder the basic photocurrent generation function of the PV module. In Chapter 4, it was shown that this was possible to achieve using random microtextured FEP films. Nevertheless, to add further value to the PV module cover, the anti-reflective functionality of the random microtextured FEP PV module cover can be improved since it was only slightly increased. To this end, introducing periodically designed structures would enable better control of the intended properties.

This chapter will demonstrate how introducing periodic cone-shaped microtextures will not only result in a superhydrophobic self-cleaning surface, but also an enhanced anti-reflective functionality. The aim is to improve photocurrent generation by enhancing light trapping while maintaining the superhydrophobic properties of the microtextured surface.

Hexagonally arranged cones, as depicted in Figure 5.1, were selected as the microtextures design since it can contribute positively to both the wetting and optical properties. It was previously shown that these design of microtextures can enhance light trapping [85]. Furthermore, the sharp tips of the cones would significantly reduce the surface contact area, which is beneficial to achieve superhydrophobicity. Different aspect ratio cones were investigated to understand its influence on the wetting properties and the light trapping. The base diameter of the cones ($30\ \mu\text{m}$) and the center-to-center spacing ($25\ \mu\text{m}$) were kept constant while only changing the height to achieve the different aspect ratios. Any further usage of the term ‘microtextures’ in this chapter would refer to the cone-shaped microtextures, unless specified otherwise.

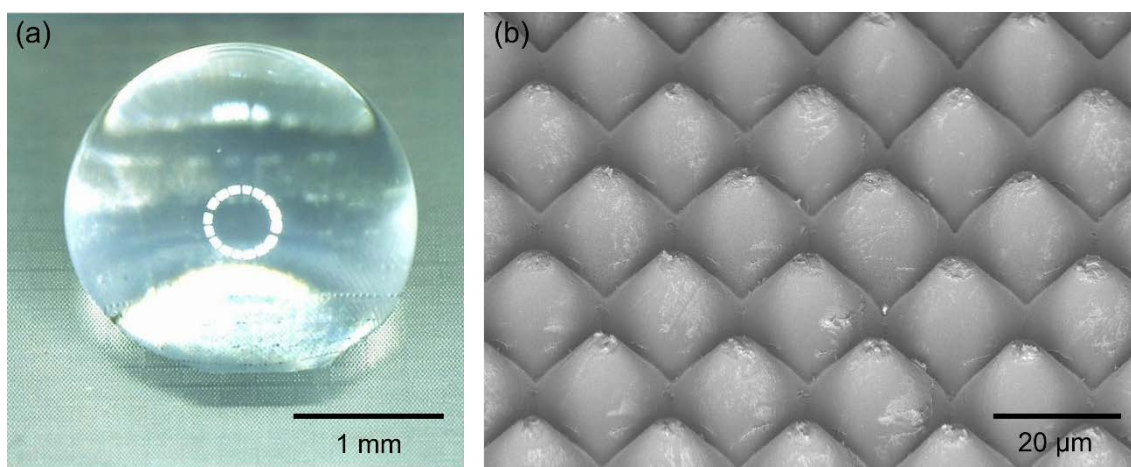


Figure 5.1 Hexagonally arranged cone-shaped microtextures developed in this research. (a) Balled up water droplet resting on the microtextured surface demonstrating the superhydrophobic nature of the surface. (b) Cone-shaped microtextures viewed from a 45° angle.

5.1 Influence of Aspect Ratio on the Wetting Property of Cone-Shaped Microtextured Surfaces

The wetting properties of the newly proposed periodic cone-shaped microtextures were investigated based on the contact angle and roll-off angle to determine whether it would retain the desired superhydrophobicity. The influence of aspect ratio on the wetting properties were also considered to obtain a better understanding and identify the optimum design for the microtextures

as shown in Figure 5.2. Microtextured FEP is the cover film of interest, but to truly understand the relation between aspect ratio and the respective wetting properties, microtextures of different materials (PC and PDMS) were also included for comparison.

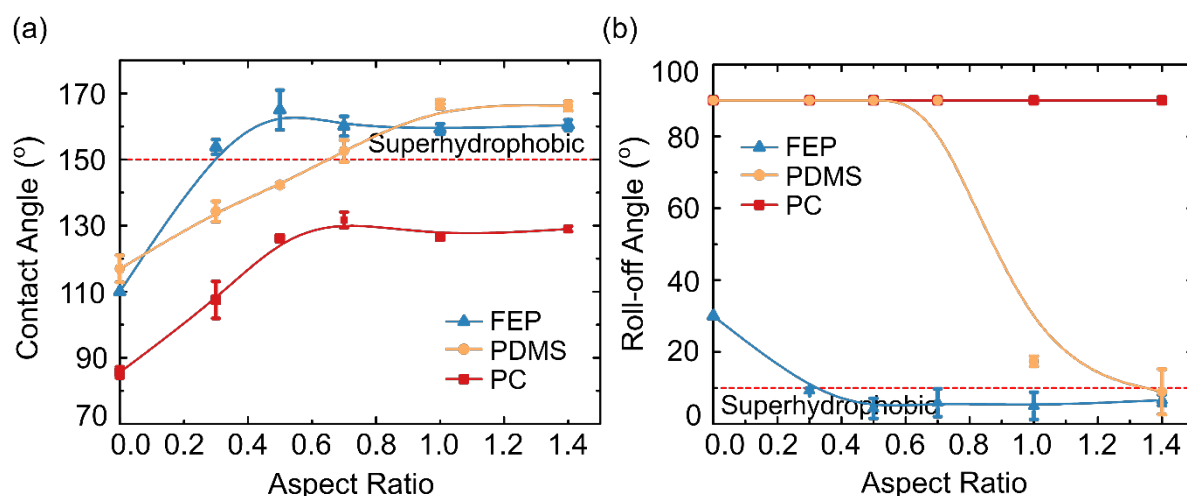


Figure 5.2 Influence of aspect ratio on wetting properties. The impact of the aspect ratio on wetting property is quantified by the (a) contact angle and (b) roll-off angle. Error bars were plotted by averaging over three measurements. Reference angles marking the state of superhydrophobicity are shown in the graphs as dashed lines (---). The solid trend lines are guides for the eye to highlight the trend. (Adapted from [124])

Focusing on the microtextured FEP, superhydrophobicity was achieved for all investigated aspect ratio as shown Figure 5.2a and 5.2b. The measured reference contact angle and roll-off angle of planar untextured FEP were $112\pm 3^\circ$ and $31\pm 1^\circ$, respectively. Superhydrophobicity can be easily achieved with microtextured FEP regardless of the aspect ratio due to the minimized surface contact area from the cone-shaped microtextures. The low surface energy of FEP required only low aspect ratio microtextures to achieve superhydrophobicity, which was in-line with what was observed in Chapter 4 with the random microtextured FEP. Nevertheless, the relation between aspect ratio and wetting properties was not very clear since all samples achieved superhydrophobicity apart from planar FEP.

Therefore, different materials were also investigated to emphasize the influence of the different aspect ratio on the wetting property which should also hold true for the different materials. Microtextured PDMS and PC films were fabricated in order to investigate the relation between aspect ratio, wetting properties and the cover material.

First, the wetting property measurements for PDMS microtextures were presented. For reference, planar PDMS has a measured reference contact angle and roll-off angle of $117\pm 4^\circ$ and $>90^\circ$, respectively. Figure 5.2a demonstrates that the contact angle for PDMS gradually increased with increasing aspect ratio until it reached a superhydrophobic contact angle ($153\pm 3^\circ$) starting from an aspect ratio of 0.7. Meanwhile, the roll-off angle was also reduced to ($17\pm 1^\circ$) for aspect ratio of 1.0 but a superhydrophobic roll-off angle ($9\pm 6^\circ$) was only achieved at the highest aspect ratio of 1.4, as can be observed in Figure 5.2b. This means that it was also possible to achieve superhydrophobicity for microtextured PDMS but would require a higher aspect ratio. This is supported by a previous work

by Tavakoli et al. where superhydrophobic PDMS was only observed at high aspect ratio (>1.0) [70]. In terms of the relation between aspect ratio and wetting property, a trend of enhanced wetting property was observed until it remains around a certain contact angle or roll-off angle with further increase in aspect ratio.

Next, the results for microtextured PC were presented. The measured reference contact angle and roll-off angle for planar untextured PC were $86\pm 2^\circ$ and $>90^\circ$, respectively. For the case of PC, the contact angle increased with the increase in aspect ratio but stabilized at $\approx 130^\circ$ for aspect ratios of 0.7 and greater (see Figure 5.2a). Meanwhile, Figure 5.2b shows that the aspect ratio of the microtextures did not affect the roll-off angle and the water droplet stuck to the surface for all aspect ratios. This was due to the high surface energy which caused the water droplet to adhere to the surface. Although cone-shaped microtextures were implemented, the surface contact area was not sufficiently reduced in order to overcome the adhesion. This does not mean that it was impossible since previous researches has shown that it was in fact possible to achieve superhydrophobicity using PC but would require complex structures such as nanofur having extremely high aspect ratios [76] or hierarchical structures [125]. Putting things into perspective, the superhydrophobic nanofur PC films had an extremely high aspect ratio of ≈ 75 [43]. It can be concluded that PC is not a suitable material to achieve the superhydrophobic self-cleaning surface that was desired, at least not with the present cone-shaped microtextures. Nevertheless, even though that is the case, the trend where an increase in aspect ratio enhanced the hydrophobicity until it stabilized at a certain contact angle still holds for microtextured PC.

From these results, it can be concluded that increasing the aspect ratio of the microtextures enhances the wetting properties of the microtextured surfaces until it stabilizes at a certain contact angle and roll-off angle, where the specific value depends on the selected material. Although the trend holds for all material, it was more demanding to achieve superhydrophobicity with PDMS and PC. It was only possible to achieve superhydrophobicity with PDMS microtextures starting from a high aspect ratio of 1.4. With PC, it was not possible to achieve superhydrophobicity using the investigated microtextures. Meanwhile, microtextured FEP easily achieved superhydrophobicity even at a low aspect ratio of 0.3. FEP was proven to have significantly greater potential to be used as a superhydrophobic self-cleaning microtextured cover for PV module applications.

5.2 Morphological Analysis of Periodic Microtextures and Durability Towards Imperfections

In Chapter 4, it was already shown that texture imperfections and fringe features can influence the wetting property. Therefore, it is essential to also look at the quality of the fabricated periodic microtextures to observe the morphology and ensure that the wetting properties measured were not due to any undesired secondary texturing. For this, investigation was done based on SEM images of the fabricated samples as shown in Figure 5.3

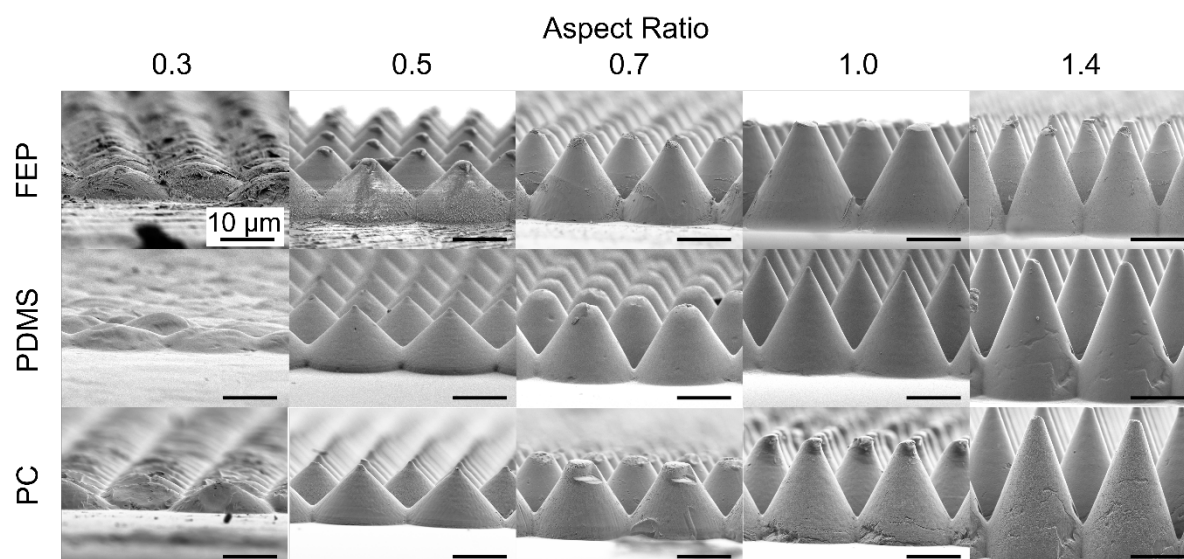


Figure 5.3 SEM images showing periodic cone-shaped microtextured samples having different aspect ratio fabricated from three types of material: FEP, PDMS and PC. The scale is the same for all images. (Adapted from [124])

Figure 5.3 shows that the fabricated samples were periodic cone-shaped microtextures as were designed. Nevertheless, it was observed that there were some imperfections to the fabricated microtextures, mainly in the form of missing cone tips, which can be attributed to defects during the fabrication process. When applied in real-world conditions, these defects might also occur during handling and operation of the PV modules. For potential application as a self-cleaning PV module front cover, what is most important is whether the superhydrophobic properties can still be retained even with the existence of defects in the microtextures.

A simple analytical study was conducted to understand whether the imperfections would affect the wetting properties. Only microtextured FEP was investigated for this purpose since it was the material of interest. The imperfections observed will be called “height loss” throughout this work for simplicity. The height loss, in percentage, was calculated as the height of a missing cone tip compared to the designed cone height. This was measured from side-view SEM images as demonstrated in the Figure 5.4

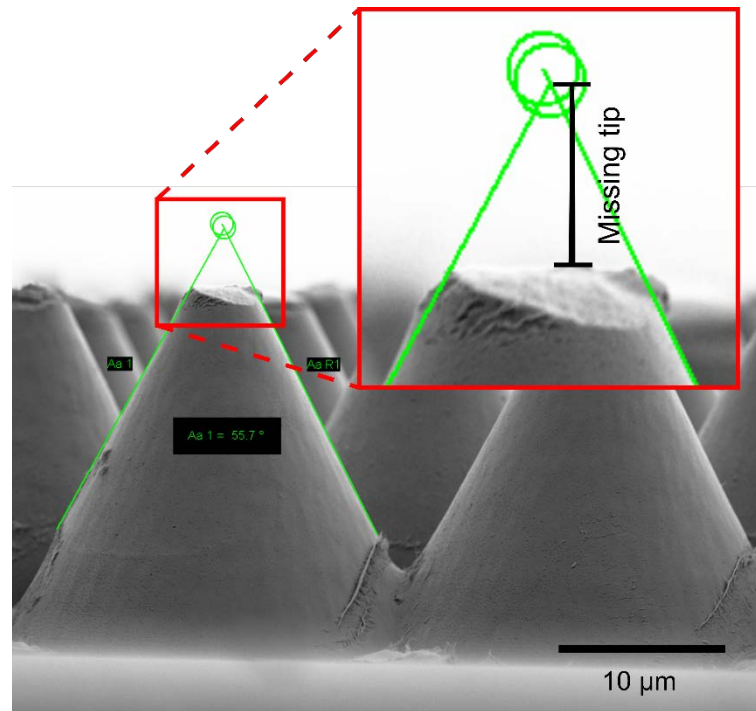


Figure 5.4 SEM image showing defect in fabricated cone-shaped microtextures. Height loss is defined as the percentage of missing cone tip from the designed total cone height. A detailed view of the missing tip is shown in the inset. Microcones with an aspect ratio of 1.0 are demonstrated here as an example of height loss. (Adopted from [124])

By analyzing the height loss of 15 microtextured FEP samples, it was found that superhydrophobicity was still achieved for the majority of samples even with height loss of up to 40% as presented in Figure 5.5. Although all samples still achieved superhydrophobic contact angles, there still exist a few samples that did not achieve superhydrophobic roll-off angles. Even though there were some imperfections in the microtextures, the reduced surface contact area compared to a planar surface was still sufficient to achieve superhydrophobicity. From a wetting perspective, such a blunt tip might actually be an advantage as it can prevent the pinning of water droplets. This was supported by Nosonovsky and Bhushan which suggested that it would be favorable to have rounded tips or edges to enhance superhydrophobicity [126].

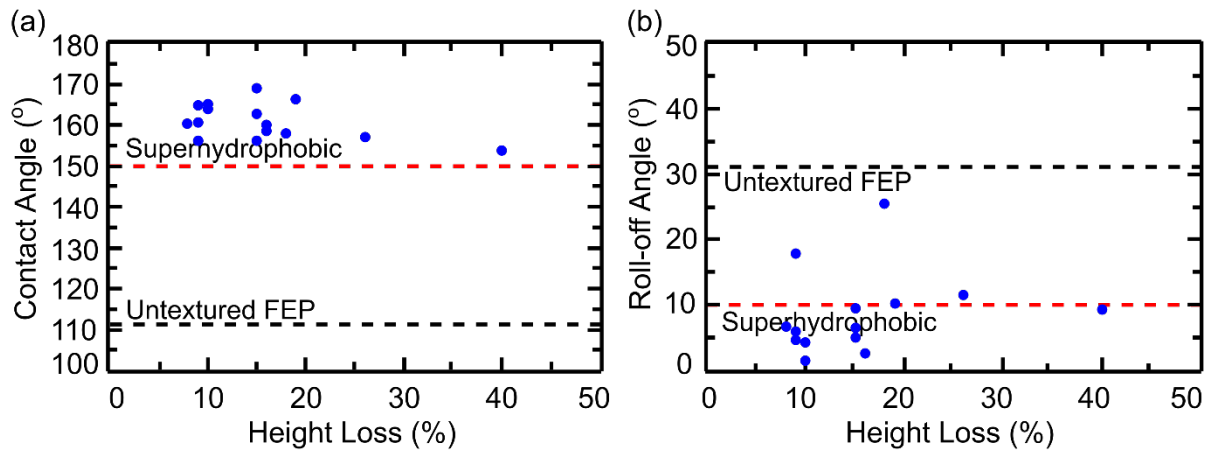


Figure 5.5 Impact of height loss on the wetting properties of microtextured surface. The impact of height loss on both the (a) contact angle and (b) roll-off angle of cone-shaped microtextured FEP samples are presented.

From this simple analytical study, it was shown that there is a tolerable height loss for the microtextured PV module cover such that it still achieves its intended superhydrophobic property. As a basis for this work, the fabricated microtextured covers were still acceptable for further investigations if it exhibits superhydrophobic properties since the self-cleaning function operates when water droplets rolls-off regardless of the microtextures condition.

5.3 Microtextured FEP as Anti-Reflective PV Module Covers

Now that it has been proven that the periodic cone-shaped microtextures were successful to introduce a superhydrophobic property in FEP films, the next focus is whether the periodic microtextures are able to enhance the anti-reflective functionality. The suitability of microtextured FEP as an anti-reflective PV module cover and the influence of aspect ratio were investigated by looking at both the overall reflectance and the actual photocurrent generated when applied to CIGS solar cells, as shown in Figure 5.6.

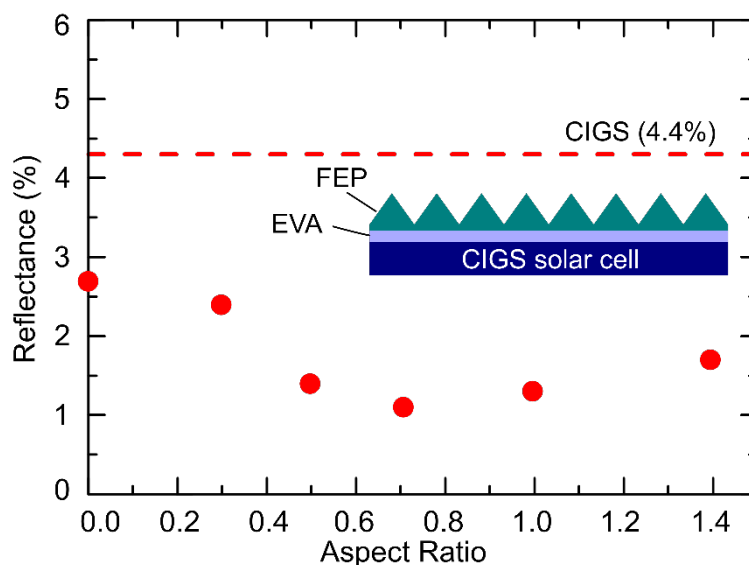


Figure 5.6 Influence of aspect ratio on the reflectance of microtextured FEP top covers when applied to CIGS solar cells. The reflectance (at $\lambda = 600$ nm) of different aspect ratio microtextures were measured from devices having architecture as shown in the inset. The reference reflectance ($4.4 \pm 0.1\%$) for a bare CIGS solar cell (without any cover) is shown as a horizontal dashed line (---) for comparison. (Adapted from [124])

The optoelectronic tests were conducted by applying the microtextured FEP directly onto CIGS solar cells without the usage of a cover glass. This configuration will exhibit a similar impact on the properties as if a conventional cover glass was used, with regards to optics as well as soiling–cleaning process. Since the results were focused on the relative performance improvements by different microtextured FEP covers compared to the bare CIGS solar cells, the relative improvements are expected to be similar if a cover glass was present.

The reference reflectance of a bare CIGS solar cell without a cover layer was measured to be $4.4 \pm 0.1\%$ at $\lambda = 600$ nm. The application of a planar untextured FEP film on a CIGS solar cell, shown as aspect ratio of 0.0 in Figure 5.6, reduced the reflectance to 2.8% due to reduction in Fresnel reflection losses. The intermediary refractive index of FEP ($n = 1.34$ at $\lambda = 589$ nm) makes it suitable for PV module cover usage. The addition of microtextures would serve to further enhance the anti-reflective properties. When the microtextured FEP covers were applied on CIG solar cells, the reflectance reduced further with increasing aspect ratio until it reaches a minimum reflectance of 1.2% at around an aspect ratio of 0.7. A significant 72.7% relative reduction in the reflectance compared to the reference case. The same trend was also observed in a previous work that focused on the optical benefits of cone-shaped microtextures made of a glass-like ultraviolet-curable photoresist NOA88 (Norland Products Inc., Cranbury, NJ) [85]. The reflectance reduction from the application of FEP microtextures can be attributed partially to multiple impinges of light on the optically large microstructures and partially due to a light trapping effect. This light trapping effect – the retro-reflection effect mentioned in Chapter 2 – where out-going light is reflected back onto the active cell material by the microtextures, was also previously observed by Schmager et al. for the Viola flower petal-shaped microtextures [84].

In the evaluation of photocurrent generation, the microtextured FEP was applied permanently to CIGS solar cells and the $J-V$ characteristics were measured. Different CIGS solar cells were used for each aspect ratio, since the microtextured FEP covers were permanently laminated onto the solar cells. The complete $J-V$ characteristic measurements for each CIGS solar cells having different aspect ratio microtextures are shown in Figure 5.7. The initial J_{SC} measurement of the bare (without any front cover) CIGS solar cells were different since they were different samples. Thus, the improvement by the microtextured FEP cover would then be evaluated relative to these respective initial J_{SC} measurements. The results in Figure 5.7 also show enhancement of J_{SC} for all devices with the introduction of planar FEP covers. Further enhancement of J_{SC} was obtained for all devices when the microtextures were introduced, with varying results for the different aspect ratios.

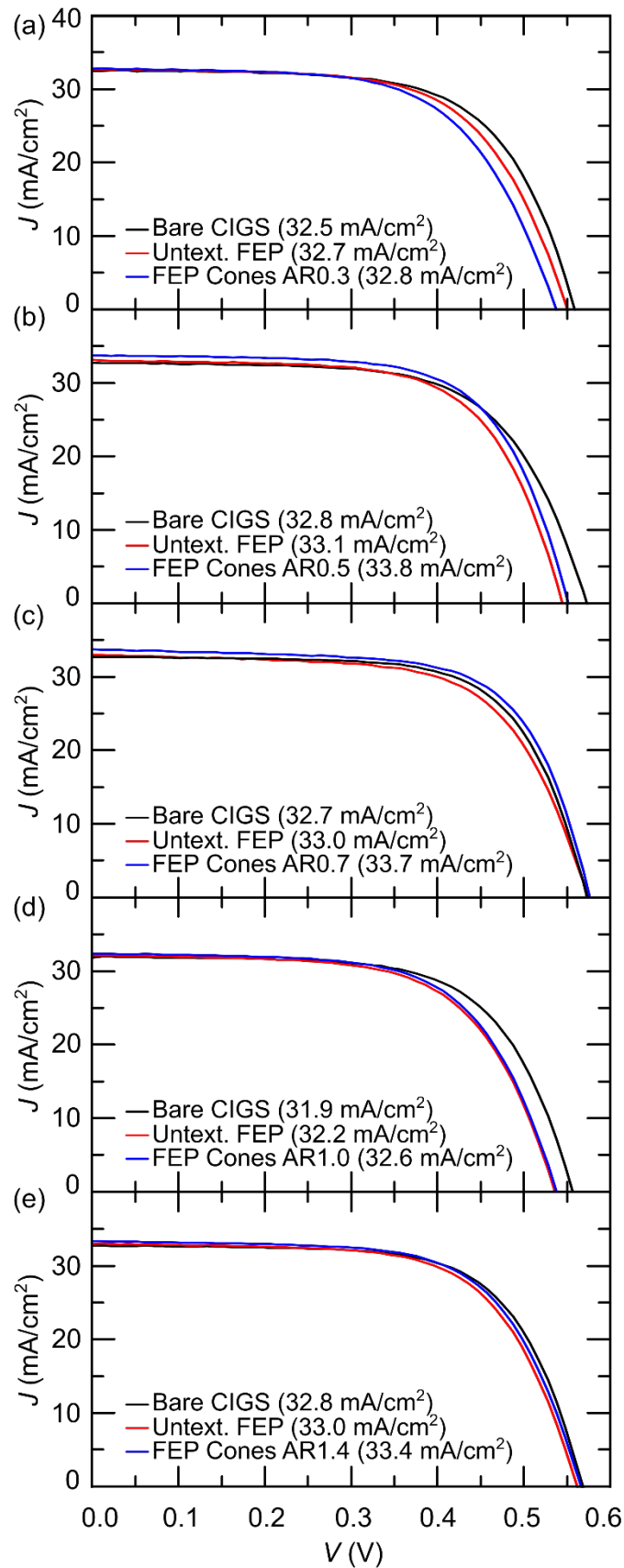


Figure 5.7 J - V characteristic curves of CIGS solar cells with the application of planar untextured FEP and microtextured FEP as front covers. The J - V characteristics are compared to reference bare CIGS solar cell. Different microtextured FEP were investigated having aspect ratios of (a) 0.3, (b) 0.5, (c) 0.7, (d) 1.0 and (e) 1.4. The J_{sc} of the respective device architecture are shown in parentheses.

The relative improvement of the CIGS solar cells in terms of J_{sc} by the microtextured FEP covers (for different aspect ratio) are shown in Figure 5.8. As previously observed, the reflectance reduction due to reduced Fresnel reflection losses from the application of a planar untextured FEP cover resulted in an improved CIGS solar cell J_{sc} by $0.8 \pm 0.2\%$. The introduction of microtextures enhanced the J_{sc} even further for all aspect ratios. The enhanced performance of CIGS solar cells achieved a maximum J_{sc} improvement of $3.1 \pm 0.2\%$ for microtextures having an aspect ratio of 0.7, as shown in Figure 5.8. This will translate into a 2.9% increase in the PCE relative to the reference CIGS solar cell. Emphasizing again, the enhancement is not only attributed to the reduced front reflectance but also attributed to retro-reflection-inspired light trapping by the cone-shaped FEP microtextures [84], [85].

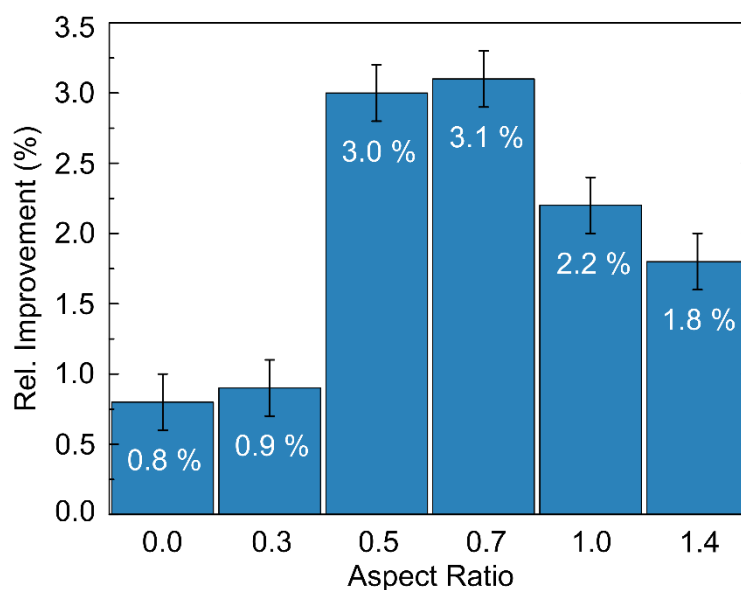


Figure 5.8 Relative improvement of CIGS solar cell by different aspect ratio microtextured FEP covers. As a reference, the relative J_{sc} improvement afforded by untextured FEP is shown as aspect ratio of 0.0. (Adapted from [124])

From these results, it can be concluded that the cone-shaped microtextured FEP introduced significant anti-reflective properties to the front cover films that leads to improved light harvesting. Although positive results were obtained for all aspect ratios, there exists an optimal aspect ratio = 0.7 to maximize the performance enhancement of the CIGS solar cell. Therefore, microtextures having cones with aspect ratio of 0.7 were used in further investigations.

CIGS solar cells were used in this study as an example to demonstrate the influence on solar cell performance enhancement. Nevertheless, the concept is also valid for other PV technologies since the microtextures serve to enhance light in-coupling. This would require specific investigations on the intended device architecture to identify specific performance improvements for different devices.

5.4 Periodic Microtextured FEP as Self-Cleaning Covers

The contact angle and the roll-off angle measurements are good indicators of the potential self-cleaning function that can be induced by the microtextured FEP. Nevertheless, the actual evaluation of the self-cleaning performance would provide a more conclusive indication. To this

extent, the self-cleaning performance of a microtextured FEP cover (aspect ratio of 0.7) was investigated by intentionally soiling the surface and cleaning with water while measuring the PV device photocurrent generation at both those conditions. The J_{sc} , used as the performance indicator, was also compared to the PV device having a bare glass top surface and an untextured FEP cover at both soiled and cleaned conditions. The recovery ratio, as described in Chapter 3, was used as the parameter to compare the self-cleaning performance of the different surfaces. The recovery ratio is reported in percentage for better interpretation of the results.

There exist alternative methods of evaluating the self-cleaning performance such as measuring the transmission of light [127]. Nevertheless, in this work, the photocurrent generation from the solar cell was used since it simulates the intended application (reduced and recovered in-coupling light from soiling and cleaning). Highlighting the impact of soiling and cleaning on device performance, the J_{sc} for each condition was plotted normalized to the initial condition of each PV device configuration (bare glass surface, planar untextured FEP and microtextured FEP covers) as shown in Figure 5.9.

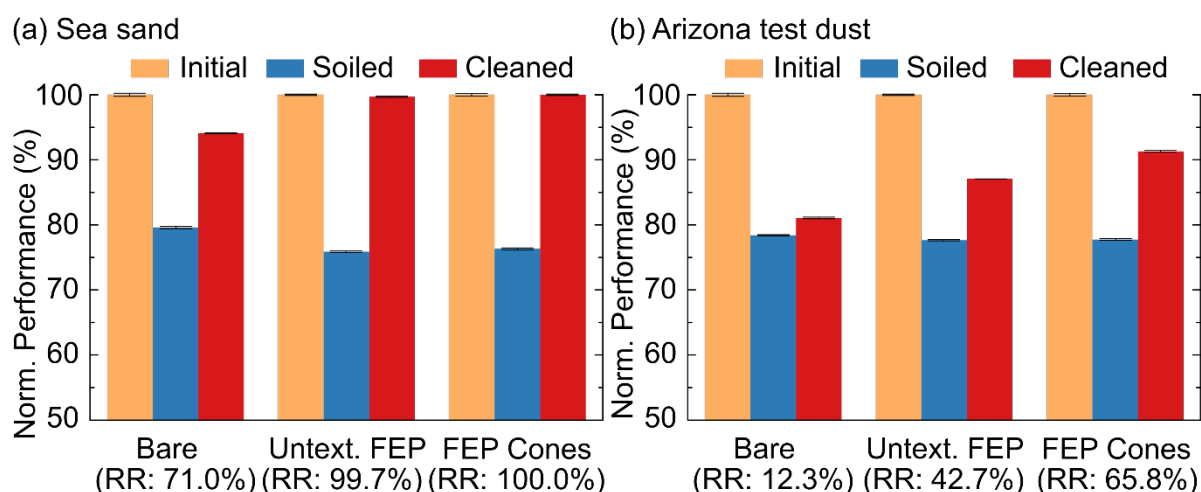


Figure 5.9 Self-cleaning performance of different front covers attached to a glass encapsulated mc-Si solar cell.

The normalized bar chart compares the self-cleaning performance of bare glass (without FEP cover), planar untextured FEP cover and FEP microcone-textured cover (aspect ratio of 0.7). The self-cleaning performance was investigated using two types of soil and presented in different bar charts: (a) Sea sand and (b) Arizona test dust. The recovery ratios (RR) are denoted beneath each respective top surface. (Adopted from [124])

First, the self-cleaning tests were conducted using sea sand as the dust contaminant. A 100% recovery ratio was achieved when a FEP cover was used; for both planar untextured FEP and microtextured FEP covers as shown in Figure 5.9a. This means that sea sand can easily be cleaned from a surface when water droplet rolls-off the surface. In the case of the hydrophobic untextured FEP surface, although singular water droplets did not roll-off initially, but the continuous increase in water droplets build the volume of water resting on the surface until it eventually slides-off; removing the dust at the same time achieving a 99.7% recovery ratio. Figure 5.9a also demonstrates that the conventional bare solar cell only achieved a 71.0% recovery ratio; in which most of the water droplets still remains stuck and rested on the surface.

Next, the self-cleaning test was conducted using the smaller dust particles – Arizona test dust. From initial observations, Arizona test dust was generally harder to clean since it became slurry when wet and thus adhered more to the surface. This observation was already reported in the literature that some dusts, when mixed with water, becomes a mixture that tends to stick to the surface and becomes more difficult to remove [18]. Cleaning Arizona test dust with water from bare glass managed to recover only 12.3% of the loss as can be seen in Figure 5.9b. Meanwhile, a 42.7% recovery ratio was achieved when Arizona test dust was cleaned from planar untextured FEP and a 65.8% recovery ratio from a microtextured FEP cover. Although it was proven harder to remove Arizona test dust compared to sea sand, the introduction of the microtextured FEP cover was shown to significantly improve the self-cleaning performance of the surface.

The self-cleaning performance investigations were conducted using two size categories of dust particles. The large sea sand particles (100–300 μm) and finer Arizona test dust particles (0–22 μm) are demonstrated in Figure 5.10. The sea sand particles were significantly larger than the microtextures spacing and had a generally random rectangular shape with blunt edges as shown in Figure 5.10a. The sea sand particles behaved as individual particles and were not sticking to each other when deposited onto the investigated surface. Meanwhile, Arizona test dust are fine dust particles having random shapes but also without any sharp edges. It was observed that Arizona test dust tends to adhere to each other to form clumps and islands of dust accumulations as can be observed in Figure 5.10b. Particles smaller than the microtextures were observed to rest within the cavities, as shown in Figure 5.10c, which could eventually trap the particles and would be harder to remove during the cleaning process.

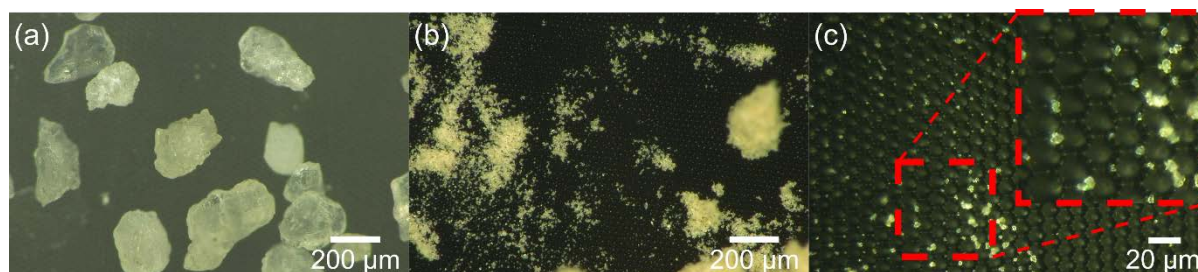


Figure 5.10 Dust particles used for self-cleaning investigations. Microscopy images of the dust particles used in this chapter: (a) Sea sand and (b) Arizona test dust. (c) Fine Arizona test dust particles trapped inside microcavities even after cleaning. An enlarged view of the trapped dust particles shown in the inset. (Adopted from [124])

From closer inspection, the loss in PV performance could have originated partially from some fine dust particles that were trapped within the microtexture cavities as shown in Figure 5.11. If we consider a Cassie-Baxter wetting model, water droplets are suspended above the microtextures with air trapped underneath to create cavities [90]. If this was the case, the water droplets would not interact with the trapped fine dust particles, thus would not be able to clean them from the microtextured surface. This would explain the residual dust particles trapped within the cavities. Based on microscopy image analysis, it was estimated that around $18 \pm 7\%$ of the observed area was still covered in dust particles (partially trapped within the cavities) after cleaning. This corresponds to a potential 5–10% reduction in PV performance in terms of J_{sc} .

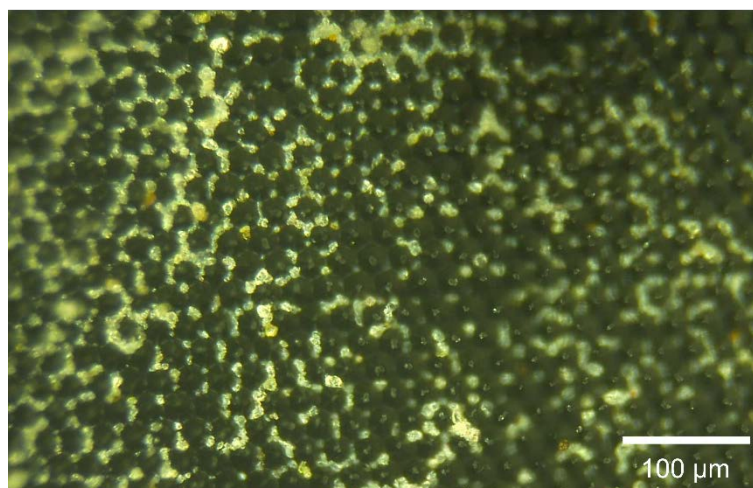


Figure 5.11 Microscopy images of fine dust particles that still remain on the microtextured surfaces after self-cleaning by way of rolling water droplets. Fine dust particles shown are trapped within the microcavity areas. (Adopted from [124])

Using a simple analysis, it was possible to gain some insights of the conditions relating the size of the dust particles and the potential for it being trapped in the microcavities. Assuming that the dust particles were perfectly spherical, particles having a diameter $<13 \mu\text{m}$ can be trapped within the microcavities in between the cone-shaped microtextures (aspect ratio = 0.7), as shown by the diagram in Figure 5.12. In this regard, to prevent trapping of dust particles inside the microcavities, the surface texture asperities should be significantly smaller than the particle diameter [15]. The aim of the work in this Chapter was to achieve a balanced enhancement in both the anti-reflective and self-cleaning properties from the introduction of microtextures that was already proven to be beneficial from an optics point of view [85]. Further optimization of the microtextures dimensions can be conducted in the future to reduce the trapping of fine dust particles within the microcavities. The result in this section indicates that microtextured FEP cover has a superior self-cleaning capability compared to a planar untextured FEP cover since it was able to clean significantly better the two different types of soil when introduced.

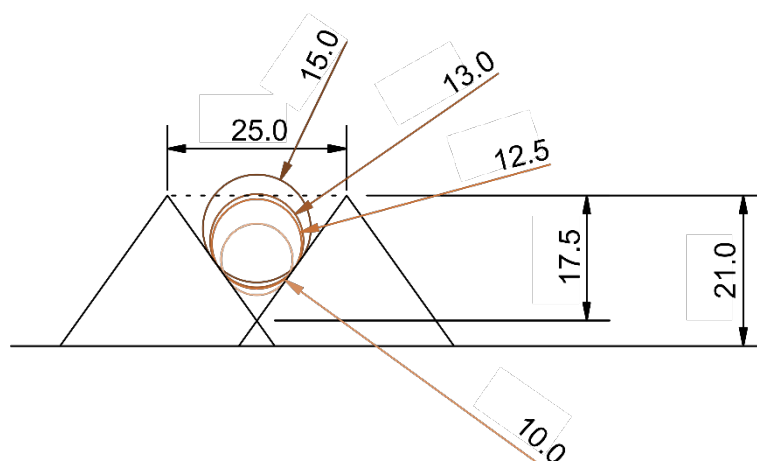


Figure 5.12 Illustration of microcones with aspect ratio of 0.7 (base structure of the microtextures developed in this chapter) and dust particles that could potentially be trapped within the cavities.

(Adopted from [124])

In the environment, dust deposition and cleaning cycle would occur repeatedly throughout the lifetime of the PV modules. Therefore, the effect of multiple soiling-cleaning cycles on the self-cleaning capability was investigated by repeating the self-cleaning test 3 times. The soiled area, by Arizona test dust, after a soiling-cleaning cycle was quantified (in percentage, %) by analyzing the planar images of 5 different areas of the same sample that still had dust deposits. There was an increase in soiled area from $12 \pm 4\%$ to $23 \pm 6\%$ observed after 3 cycles (see Figure 5.13a), which in turn reduced the J_{SC} (Figure 5.13b, full $J-V$ characteristics in Figure 5.14). The reducing trend of photocurrent generated after each soiling-cleaning cycle was due to the reduced light reaching the solar cell active area, which corresponds to the area still being covered with dust particles. Although the J_{SC} of the soiled conditions were kept similar for each soiling cycle, the self-cleaning capability (based on the recovery ratio) was observed to have a slight deteriorating trend (see Figure 5.13c). After 3 soiling-cleaning cycles, only a 47.2% recovery ratio was achieved. This might be due to more dust particles trapped within the microcavities or the residual dust particles from the previous cleaning cycle getting wet thus adhering more to the surface. Nevertheless, the initial 65.8% recovery ratio achieved with the application of microtextured FEP covers was already a significant improvement compared to the 12.3% of a bare glass top surface. This is already an enhancement of the multifunctional features since we are able to reduce the severity of soiling with the application of a microtextured FEP cover, apart from enhancing the anti-reflective properties.

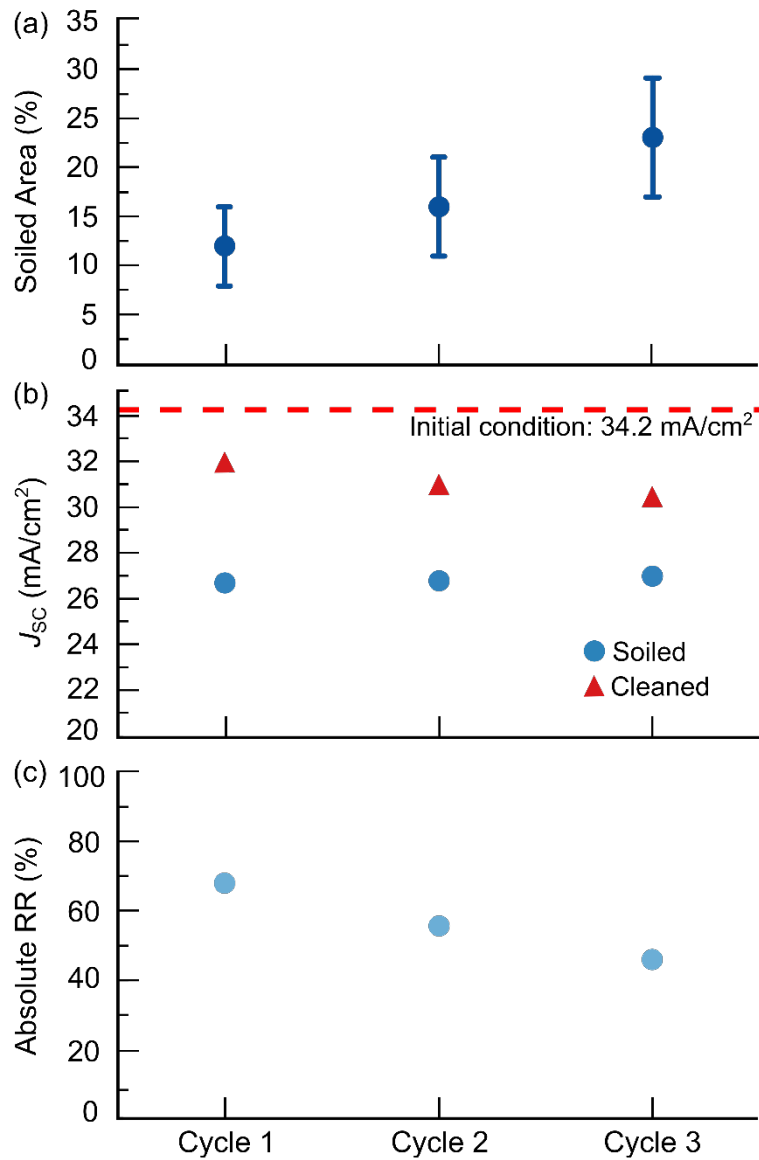


Figure 5.13 Impact of multiple soiling-cleaning cycles on self-cleaning performance. Several key parameters were evaluated: (a) Soiled area after each cleaning cycle, (b) J_{sc} of the soiled and cleaned state for each cycle and (c) the recovery ratio with respect to the initial condition of the PV mini-modules with microtextured FEP covers. (Adopted from [124])

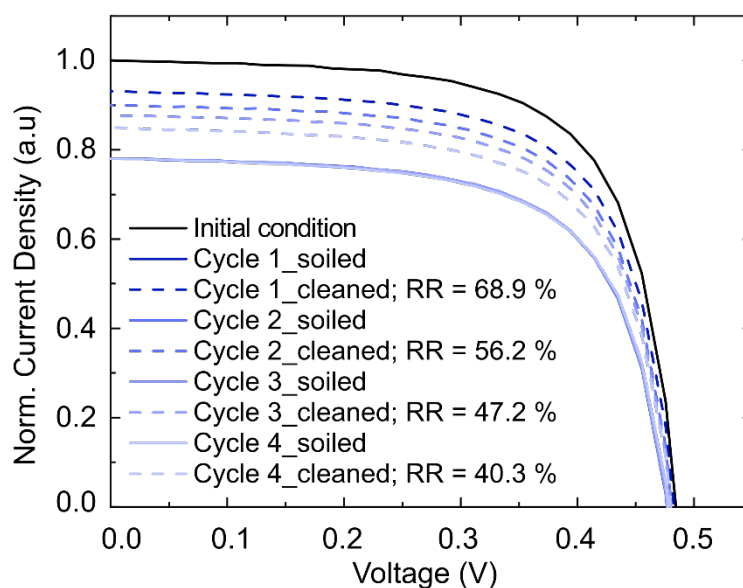


Figure 5.14 J - V characteristic of PV mini-module with microtextured FEP covers showing the result of multiple soiling-cleaning cycles. Soiled conditions of each cycle are represented by the solid lines (—) while the recovered clean conditions are represented by the corresponding dashed lines (---). The absolute recovery ratio (RR) was calculated with the initial condition as the reference.

Previously, several standardized test methods were adapted to investigate laboratory-based soiling of surfaces such as ASTM D7897-18 [128], DIN EN 1096-5 [129] and IEC 60068-2-68 [6]. These standards were developed for various specific purposes (e.g., aging of surfaces, sand abrasion or dust penetration into electronic devices) and for various application scenarios (e.g., dry/wet application in moderate/harsh climates). For a laboratory demonstration and simple comparison of different top surfaces, a manual soiling-cleaning method was used to highlight the self-cleaning capability while additionally considering soiling agent particle size as the only soiling variable. It should be noted that the manual soiling approach used in this work does have its limitations, even if it clearly highlights the self-cleaning capability of different surfaces. A few considerations were made to ensure the quality of the chosen method. First, any strong movement to the investigated sample during the soiling study can lead to removal of soil that was already deposited. Thus, an approach taken to eliminate or reduce movement during the soiling and measurement process, thus minimizing errors, was by conducting an *in-situ* deposition of the dust particles. Next, by controlling the soiling amount via the reduction in J_{SC} , a comparable soiling condition was obtained regardless of manual deposition technique used. Further considerations can also be taken to improve the soiling and cleaning investigations. One limitation in our experiments was the rather small microtextured area. Larger areas would offer improved comparability in the self-cleaning investigation by averaging out any inconsistencies in the soil deposition. The type of soiling agent and their sizes, reflecting realistic conditions, can also be expanded and investigated since a simplification was made by selecting only two sizes of dust particles for this current work.

Evaluating the potential application of the microtextured FEP as a self-cleaning PV module cover, the result in this work was compared with other mitigation methods reported in the literature. Natural cleaning due to rain events was shown to restore the power output of a PV panel to within

1% of the power of a clean panel [130]. An active cleaning method such as manual cleaning using surfactants and alcohol prevents 14.4% loss of energy over a 70-day experiment duration compared to a PV module that was left to accumulate dust [131]. Meanwhile, Al Shehri et. al. used a silicon rubber brush and enhanced power output by 1% compared to an unbrushed PV module [127]. Patil and Malladharaya obtained a 1.6–2.2% increase in power output using an automatic wiper system [132]. A recent work proposed an automated brush cleaning system that achieved an efficiency increase of 6.3% compared to an uncleaned PV panel [133]. Self-cleaning due to surface modification to achieve superhydrophobic and superhydrophilic surfaces by applying chemical coatings have been shown to improve PV module performance by 2.6% [103] and 5–6% [134]. In this current work on microtextured FEP PV modules covers, a recovery ratio of 65.8% was achieved to remove Arizona test dust particles and 100% recovery ratio to remove the larger sea sand particles. This translates into a performance recovery of between 4.7 and 7.8 mA/cm² in terms of J_{sc} (or 2.4–3.4% in terms of PCE). This is a comparable achievement to the other mitigation methods as what has been reported. Apart from that, the approach of implementing microtextured FEP did not suffer from the transmission losses that was previously reported when using chemical coatings [135]. Moreover, the developed microtextured FEP cover managed to enhance the light in-coupling due to the anti-reflective properties of the cone-shaped microtextures.

5.5 Multifunctional Integrity Under Fabrication and Abrasion Defects

The investigations in this current work were laboratory based, raising the question of practicality when applied in real-world conditions. Conducting a complete in-depth evaluation on actual implementation in real-world applications is beyond the scope of this research work. Nevertheless, an investigation was conducted to evaluate the robustness of the multifunctional FEP microtextures. This would give us an initial indicator on the practicality of the microtextured FEP PV module covers. Abrasion tests based on relevant standards were used [121]; 1) falling dust particles (particle size of 100–300 μm) which imitates common low-velocity impact events and 2) forced dust impingement (particle size of 34–82 μm) that simulates intense dust storm occurrences.

The morphology of both dust particles used for the abrasion tests is shown in Figure 5.15. The sea sand particles were significantly larger than the microtextures and had random but generally rectangular shapes with blunt edges. Meanwhile, the fused alumina particles have elongated, irregular shape with sharp edges. For the falling sand particles, 400 ml of sea sand particles was dropped from a height of ≈ 165 cm through a ≈ 2 cm diameter guiding tube onto the microtextured FEP sample that was placed directly under the tube at a 45° inclination angle. For the forced sand impingement, the microtextured FEP film was sand blasted using fused alumina particles from a distance of ≈ 5 cm with a pressure of 1 bar and with one pass of the nozzle.

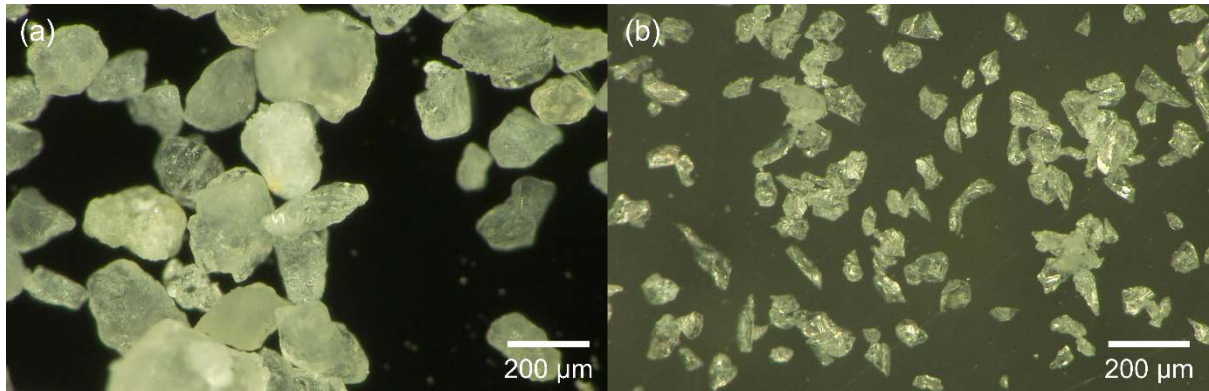


Figure 5.15 Microscopy images of dust particles used in abrasion tests. For the abrasion tests (a) sea sand particles (100–300 μm) were used for the falling sand abrasion test and (b) fused alumina particles (34–82 μm) was used for the forced impingement abrasion. (Adapted from [124])

The structural condition of the microtextured surfaces were investigated and observed as shown in Figure 5.16 with the initial condition being periodically arranged microtextures showing well-defined cones. A slight abrasion was apparent from the falling sand where the conical form of the structures remains intact and only the sharp tips were damaged as can be observed in Figure 5.16b. Meanwhile, the harsher forced sand impingement abrasion test damaged the microtextures and removed a significant amount of FEP material since the conical microtextured can no longer be recognized and only random bumps remained (see Figure 5.16c).

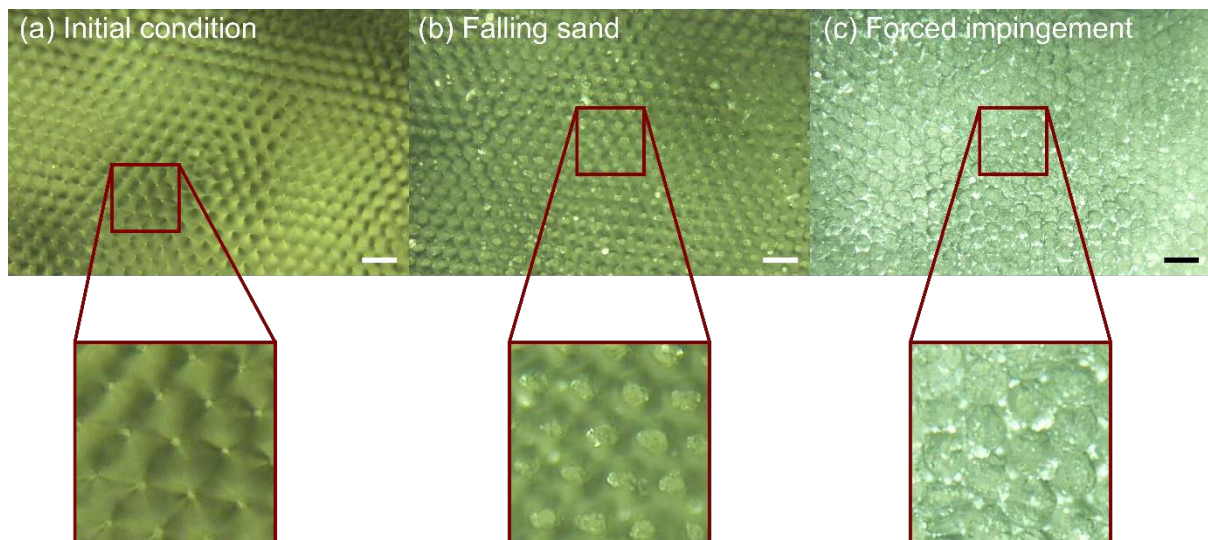


Figure 5.16 Impact of abrasion on cone-shaped microtextured FEP films. Microscopy images of FEP microtextures are shown in: (a) initial condition showing homogenous hexagonally arranged periodic cone-shaped microtextures, (b) after abrasion by falling sand showing damaged tips and (c) after abrasion by forced sand impingement showing irregular bumps which were leftovers from the base of the microcones. The corresponding microtextures are also enlarged and shown in the insets. Scale bars represent 50 μm. (Adapted from [124])

Nevertheless, how this affects the previously demonstrated superhydrophobic properties (aspect ratio = 0.7) is the question. The contact angle of all three conditions is visually shown in Figure 5.17. In terms of superhydrophobicity, the slight abrasion of the microtextures would still result in a superhydrophobic surface ($155\pm 2^\circ$) and the harsher abrasion would cause a reduction in the hydrophobicity, observed from the decreased contact angle ($146\pm 3^\circ$). It was shown that the contact angle was not significantly affected by abrasion and still had contact angles $\approx 150^\circ$. Nevertheless, when the roll-off angle was evaluated, the falling sand abrasion resulted in a superhydrophobic roll-off angle ($<10^\circ$) while the forced sand impingement significantly increased the roll-off angle ($>45^\circ$). One possible explanation for the harsher force impingement abrasion is that there were insufficient air cavities, due to the damaged microtextures, to overcome the adhesion of water to the surface. This highlights the importance of the cone-shaped microtextures to achieve superhydrophobic FEP surfaces.

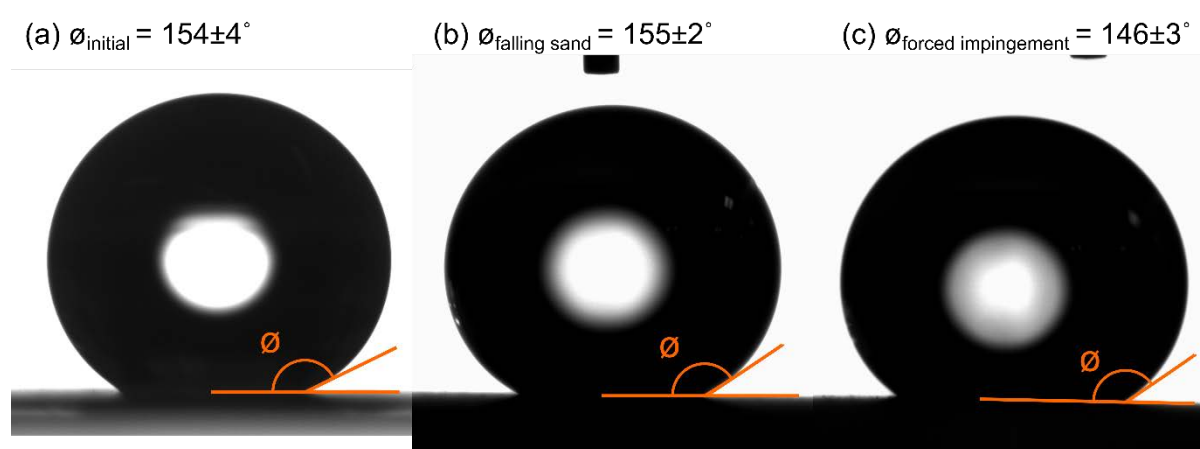


Figure 5.17 Impact of abrasion on contact angle of microtextured FEP films. Contact angle measurements were observed from resting water droplets ($5\ \mu\text{l}$) on (a) reference microtextures, (b) microtextures after abrasion by falling sand and (c) microtextures after abrasion by forced sand impingement. (Adopted from [124])

Furthermore, the impact of the abrasions on reflectance, which is also a key parameter in this work, was investigated and presented in Figure 5.18. The slight abrasion due to falling sand did not result in a significant change in the reflectance ($<1\%$ difference). Meanwhile, the harsh abrasion due to forced sand impingement almost doubled the reflectance ($11.7\pm 0.4\%$ at $\lambda=600\ \text{nm}$) compared to the initial reflectance of the microtextures. This increase in reflectance can be attributed to the random roughness and possible tears on the surface after the harsh abrasion. A similar observation where the reflectance increased due to some tears and stretches on the microtextures was also observed in Chapter 4 with the work on random microtextured FEP [44].

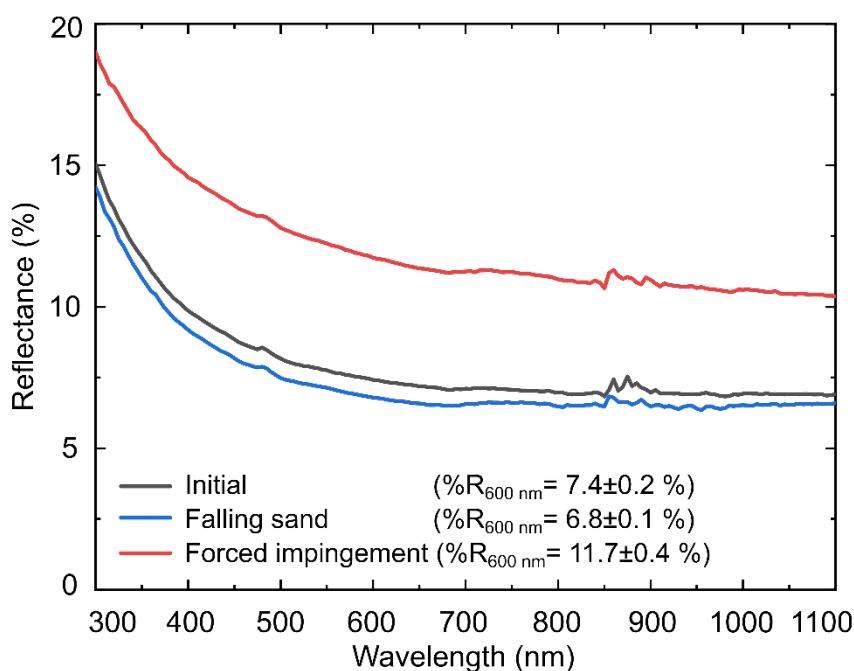


Figure 5.18 Impact of abrasion on reflectance of microtextured FEP films (aspect ratio of 0.7). The reflectance measurements were taken at $\lambda = 600$ nm for the initial microtextured condition, after abrasion by falling sand and forced sand impingement and are shown in the parentheses. (Adopted from [124])

These results, although still preliminary investigations, hint at the robustness of the microtextured FEP cover under different external damages. The initial benefits of the microtextures, in terms of superhydrophobicity and anti-reflectivity, can still be achieved with slight abrasion of the microtextures, but a severe abrasion would have a significant effect on the optical benefits of the microcone-textured FEP. Compared to superhydrophobic properties, the influence of abrasion on the optical response was more sensitive since the light trapping benefit is highly related to the microtextures morphology. The results from the abrasion test, and the fabrication imperfections discussed in Section 5.3, provides confidence that the microtextured FEP covers would be able to retain its multifunctional properties with typical processing or handling either during manufacturing, installation or operation and typical environmental exposure but would suffer greatly from harsh desert storm occurrences.

5.6 Comparing Random and Cone-Shaped Microtextured FEP

The objective of the research work reported in this Chapter was to improve the microtexture design to enhance the anti-reflective properties and thus the photocurrent generation of the PV device. So far in this Chapter, the cone-shaped microtextures were applied to CIGS solar cells as presented in Section 5.4. For a fair comparison with the work in Chapter 4 (random microtextured FEP), the cone-shaped microtextures was also applied on a mc-Si PV mini-module and the $J-V$ characteristics and self-cleaning performance measured; as shown in Figure 5.19 and Figure 5.20, respectively.

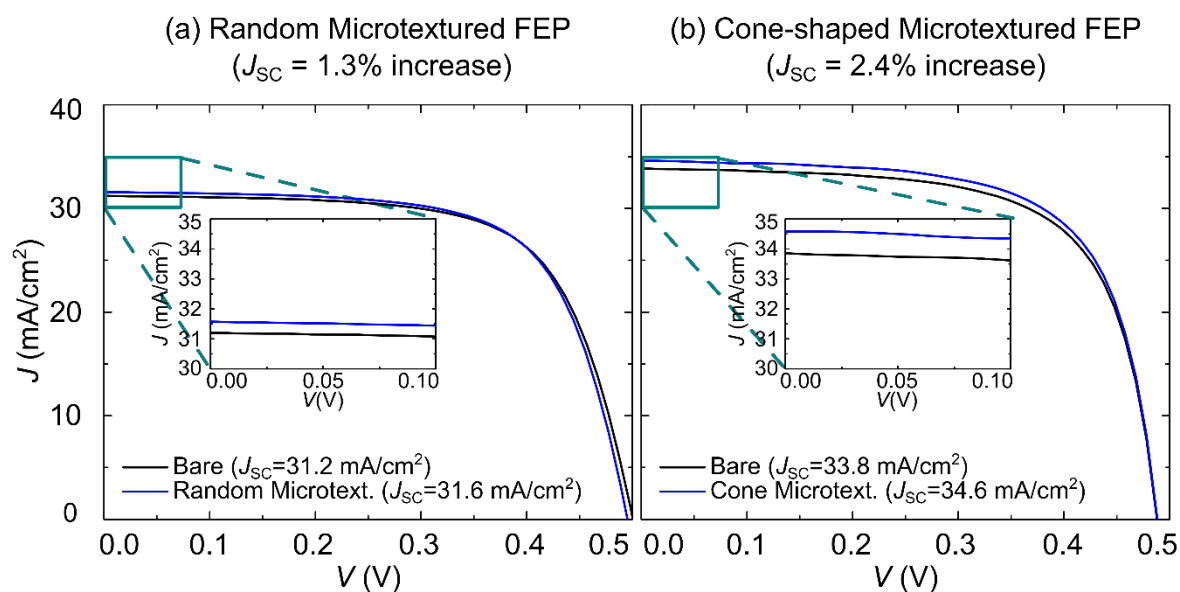


Figure 5.19 Impact of different microtextured front covers on J – V characteristic when attached to a mc-Si PV mini-module. The results compare (a) a random microtextured FEP and (b) a cone-shaped microtextured FEP as PV mini-module front covers. A glass encapsulated mc-Si PV mini-module having no front cover (bare glass surface) was used as a reference. The J_{SC} for each case is given in parentheses.

Figure 5.19a shows that there was an increase of 1.3% in the J_{SC} from the random microtextured FEP cover compared to the 2.4% increase in J_{SC} (Figure 5.19b) when the cone-shaped microtextured FEP was applied. This significant improvement in the anti-reflective function of the microtextured top cover was from the introduction of a periodically arranged cone-shaped microtexture design. This proves that it was possible to introduce different functions by carefully selecting the design of the microtextures; in this case, improved light in-coupling to enhance the anti-reflective function.

It has to be noted that the 2.4% increase in J_{SC} when applied to a mc-Si PV mini-module is lower compared to the 3.1% increase in J_{SC} when applied to a CIGS solar cell (refer Section 5.4). This means that improvement achieved by the anti-reflective cover is also influenced by the PV device used. A more specific study should be conducted to determine the actual improvement for the various PV device types and device architecture. At this point of time, this research work only focuses on improving the self-cleaning and anti-reflective functions of the microtextured cover film.

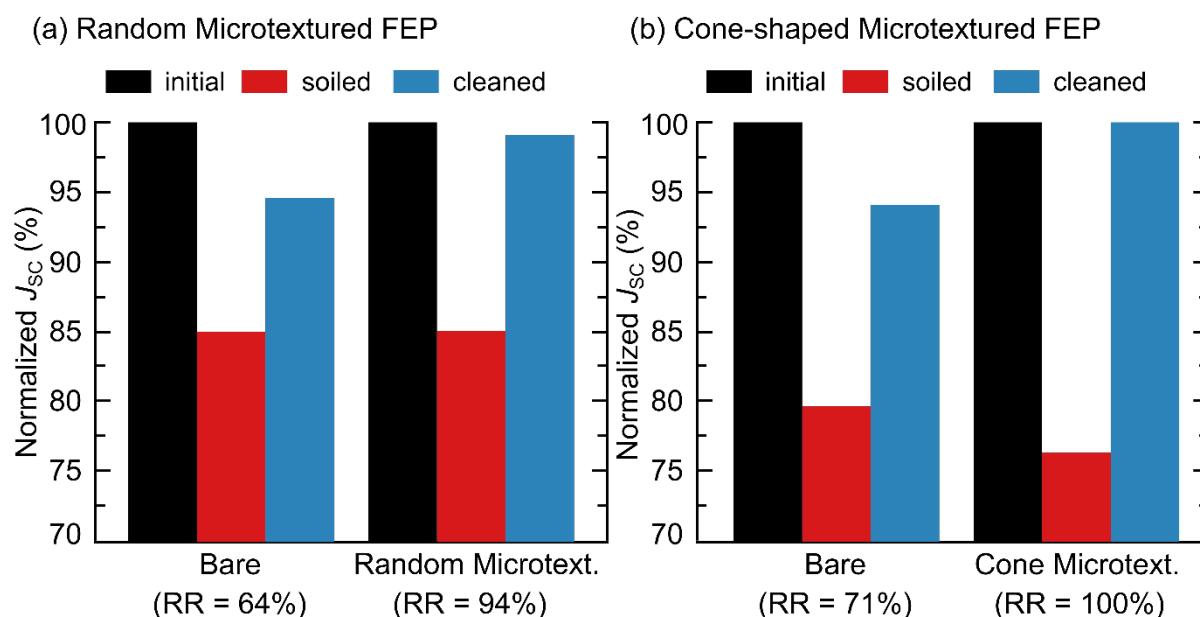


Figure 5.20 Self-cleaning performance of different front surfaces comparing (a) random microtextured FEP and (b) cone-shaped microtextured FEP as PV module front covers. The performance evaluation is based on normalized J_{sc} . A glass encapsulated mc-Si PV mini module having no front cover (bare glass surface) was used as a reference. Recovery ratios of the respective top surfaces are given in parentheses.

A similar procedure was used for the self-cleaning investigation in both Chapter 4 and Chapter 5. Sea sand was used as the investigated dust contaminant. Comparing the results from both Chapters, the self-cleaning performance of a mc-Si PV mini-module having a bare glass top surface were slightly different, where a recovery ratio of 64% (Figure 5.20a) and 71% (Figure 5.20b) were achieved, respectively. This difference can be attributed to the slightly different procedure used for the cleaning process where a larger amount of water droplets was used for the work in this Chapter. Using a larger amount of water would affect the self-cleaning performance measurement since more dust can eventually be removed. Nevertheless, by keeping the amount of water used constant for each cleaning step within a specific investigation, the influence of the different covers on the self-cleaning can be compared with confidence.

Both the random microtextures and cone-shaped microtextures achieved a high recovery ratio; 94% and 100%, respectively. This was expected since both surfaces were superhydrophobic and water droplets would easily roll-off from the surface – thus removing the dust contaminants. The slightly lower recovery ratio by the random microtextured FEP surface can also be attributed to the slightly different procedure as explained in the previous paragraph. At the end, the main objective of the work reported in this Chapter was achieved i.e., to enhance the anti-reflective function while retaining the anti-soiling function.

5.7 Summary

The application of PV module covers that can introduce either a self-cleaning or anti-reflection functionalities is highly desirable. This chapter demonstrates a significant enhancement of both self-cleaning and light harvesting that was successfully realized via application of periodic cone-shaped microtextured FEP covers. Varying the aspect ratio demonstrates that there is an optimum aspect ratio (aspect ratio = 0.7) that would enhance the role of microtextured FEP as PV module covers when considering both the anti-reflection and superhydrophobic properties. Reflectance measurements provide good indications of the performance enhancement of solar cells that the application of microtextured FEP can bring. The microtextured FEP covers demonstrated a significant reduction in reflectance (72.7% reduction compared to the reference), achieving a minimum reflectance of 1.2% for aspect ratio of 0.7. When applied to a CIGS solar cell, these microtextures achieved a significant 3.1% relative improvement in J_{sc} . Meanwhile, the wetting property based on contact angle and roll-off angle measurements is a good indicator for the self-cleaning potential. The evaluation of actual self-cleaning capability, quantified based on the recovery ratio when microtextured FEP was applied to a glass encapsulated mc-Si solar cell, demonstrated significant self-cleaning when soiled with sea sand (recovery ratio = 100%) and Arizona test dust (recovery ratio = 65.8%). The microtextured FEP used in this work achieved superhydrophobicity for all investigated aspect ratios, highlighting the superior potential of FEP as a self-cleaning cover material. Moreover, microtextured FEP is robust to defects where it still achieved superhydrophobicity even with height losses of up to 40%. This chapter successfully demonstrates the great potential of using a cone-shaped microtextured FEP film as a self-cleaning multi-functional cover for PV modules.

6 Wind as an Alternative Force for Self-cleaning Soiled PV Modules

This chapter highlights the potential of using wind as an alternative force for self-cleaning and the influence of microtextured covers on dust removal by wind. The main results in this chapter were partially published in: IEEE Journal of Photovoltaic, 2021 [119]. The author would like to gratefully acknowledge the contribution of all co-authors for the publication. Some parts of the experimental work in this chapter were conducted at the INGV in Rome, Italy.

The idea for this chapter was initially from a discussion with Dr. Jacopo Taddeucci that the author met at a conference. Further discussions with Prof. Dr. Ulrich W. Paetzold, Prof. Dr. Hendrik Hölscher and Prof. Dr. Bryce S. Richards developed the idea further. The author enlarged the previously developed microtextured design into a 10 cm x 10 cm area. It was then developed into a shim with the kind assistance of Dr. Uwe Köhler, Marco Heiler and Dr. Markus Guttman. Different samples (planar and microtextured) were prepared by the author by laminating the different films onto glass pieces for testing. Dr. Jacopo Taddeucci prepared the volcanic dust and wind tunnel at the INGV. The author then conducted the dust-removal tests with the help of Dr. Jacopo Taddeucci. All authors were involved in the discussion and writing for the publication [119].

The self-cleaning mechanism of the microtextured FEP PV module front cover developed in this research work relies on the presence of water droplets, mainly from rainfall. Deposited soil on the surface will be picked up by the rolling water droplets and thus cleans the surface from any soiling.

Nevertheless, the existence of rainfall highly depends on the location. For example, arid or semi-arid areas which has high PV potential would have very little to almost no rainfall [136], [137]. Thus, in cases where rainfall was scarce or non-existent, the self-cleaning mechanism from before would be deemed non-functional.

The question was thus asked whether there exist alternative natural forces that could be relied on to accomplish the passive self-cleaning objective of the developed self-cleaning microtextured cover films. Thus, this chapter explores wind as a natural force that could potentially remove dust from PV module surfaces. Wind is ever present at almost all locations around the globe but differs greatly in terms of magnitude, frequency, and direction. It would be highly beneficial if we were able to utilize the wind flows for cleaning soiled PV modules.

The samples investigated compare the microtextured FEP surface with a planar glass surface, as shown in Figure 6.1. While familiarizing with the settings of the camera used, some high-speed videos were taken to visually observe the different wetting properties of the samples. Figure 6.1 shows still images from the video taken at different time intervals to demonstrate the effect of the surface wetting property on the bouncing of a water droplet.

A planar glass surface generally has a hydrophilic wetting property. Thus, it can be observed in Figure 6.1a that the water droplet immediately sticks to the surface and does not bounce off. Meanwhile for the microtextured FEP surface, the falling water droplet eventually bounced off from the superhydrophobic surface, as shown in Figure 6.1b at $t = 25$ ms. These observations were consistent with what was observed in Chapter 4 and highlight the effect of microtextures on the wetting properties.

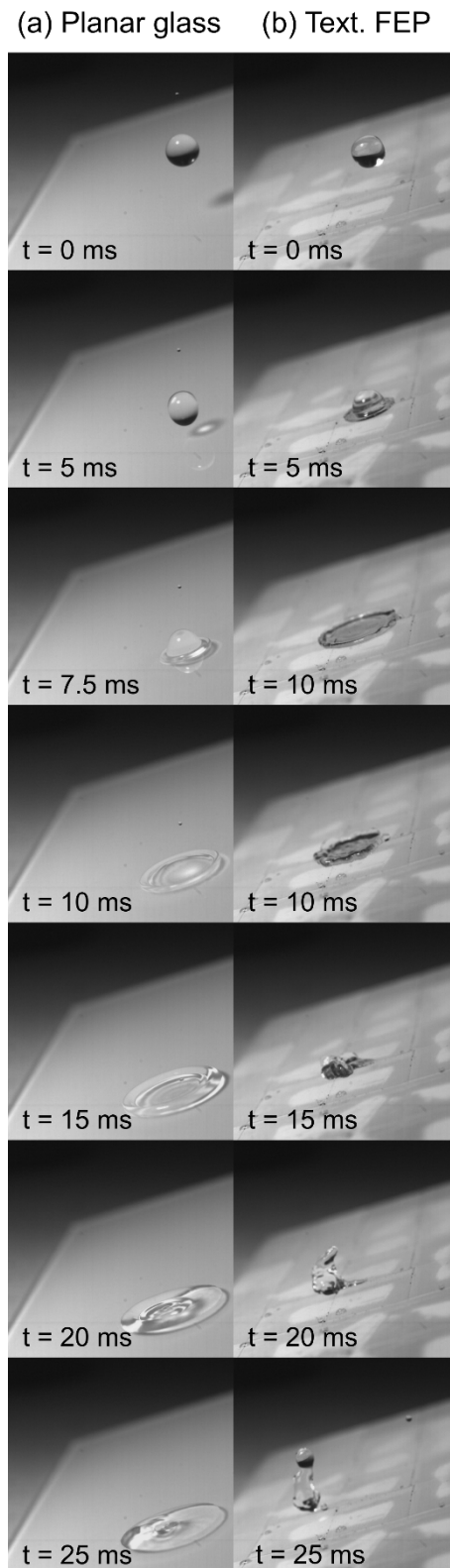


Figure 6.1 Bouncing of falling water droplets on different surfaces; (a) planar glass surface and (b) microtextured FEP surface. The investigated surfaces were placed at an angle. Time stamps are shown in the lower right corner.

The scope of this chapter was limited to the investigation of dust removal from microtextured FEP PV module covers that was previously developed and reported in Chapter 5. In the following

sections, removal of different dust particles based on their size categories will be presented first before discussing the influence of the microtextured FEP cover film on dust removal and finally correlating the dust removal with PV output recovery in terms of J_{SC} . In any case, this was compared to the removal of dust from a planar glass surface, which was used as the reference case since a conventional commercial PV module would have such a surface.

Another motivation behind this collaborative work was the observation of volcano ash deposition on PV modules after volcano eruptions. Engagement and networking during a conference brought about this possible collaboration with Dr. Jacopo Taddeucci from the Istituto Nazionale di Geofisica e Vulcanologia, INGV (National Institute of Geophysics and Volcanology) in Rome, Italy who has previously worked on volcano ash resuspension from a surface. Hence, volcano ash was used as one of the dust contaminants of interest in this Chapter.

6.1 Self-Cleaning of Dust Under the Influence of Wind

This section focuses on the removal of different sized dust particles from different surfaces. In both Chapter 4 and 5, it was already shown that the size of dust particles could affect its removal from the microtextured FEP due to some small particles being trapped inside the cavities. In the environment, there exists a wide range of dust particle sizes and types depending on the location [14]. Nevertheless, for the purpose of investigating the potential of wind as a driving force for self-cleaning of soiled PV modules, a simplification by selecting two size categories of dust – one relatively small and one relatively large – relative to the microtextures spacing was sufficient.

6.1.1 Removal of Large Dust Particles

The removal of large dust particles at different wind velocities were presented as shown in Figure 6.2. For dust particles larger than the spacing between the microtextures, coarse volcano ash and sea sand were selected as the dust contaminants. The graphs in Figure 6.2 demonstrates that wind can effectively remove the majority of deposited large dust particles, achieving removal between $\approx 70\text{--}94\%$ relative to the initial soiling for the different cases investigated in this Chapter. This was in agreement with theory and previously reported experimental work, where the majority of large dust particles ($>100\ \mu\text{m}$) were removed from the surface [138]. This significant removal of large dust particles in this chapter hints at the potential of wind as a driving force for dust removal and can eventually be translated into the recovery of PV module performance after suffering from soiling losses.

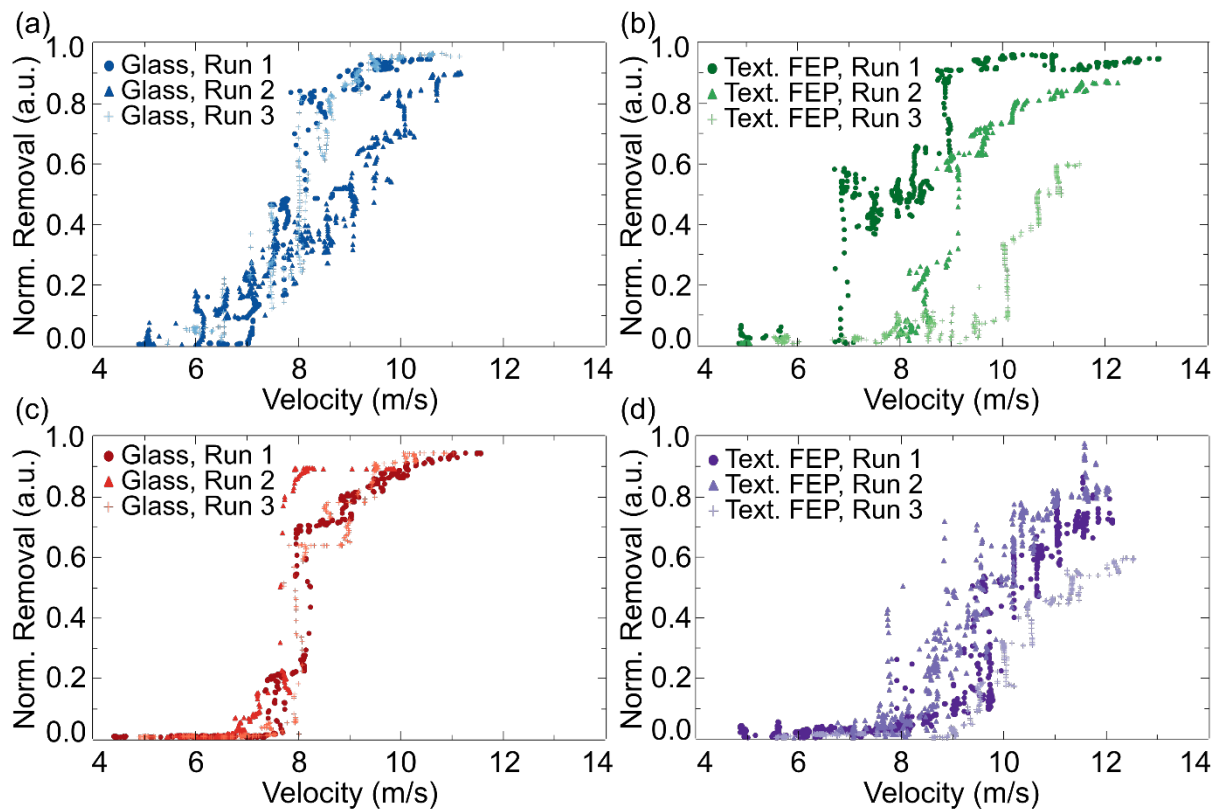


Figure 6.2 Influence of wind velocity on the removal of large dust particles. The normalized graphs present several cases for removal of different types of large dust particles from different top surfaces: (a) Coarse volcano ash on planar glass, (b) coarse volcano ash on microtextured FEP, (c) sea sand on planar glass and (d) sea sand on microtextured FEP. The test for each case was repeated 3 times. (Adapted from [119])

Another key parameter to evaluate the potential of wind to remove dust is the initial removal velocity. The initial removal velocity can be understood as the wind speed sufficient to displace dust particles – in this case, defined as removal of 5% of deposited dust. At that moment when the initial removal velocity is reached, the force exerted on the dust particles by the wind flow was sufficient to overcome the adhesion from the particle–particle or particle–surface interactions. The results from this work demonstrate that removal of large dust particles began at different initial removal velocities for the different cases, but all occurring within the range of 6.4–8.3 m/s (at 5% dust removal) as shown in Figure 6.2.

From a more qualitative point of view, the observation on the spread of data points would also provide some insights towards the dust removal behavior. It was demonstrated in Figure 6.2 that the dust removal from the microtextured FEP surface was more dispersed compared to dust removal from planar glass. This can be related to both the wind flow profile (turbulent versus laminar) and the adhesion between the particles and the surface. The microtextured surface results in a more turbulent wind flow due to the higher surface roughness, resulting in a more sporadic dust removal pattern due to the irregular forces acting on the individual dust particles. This is consistent with previous reported works on surface roughness which produced turbulent flows that would then influence dust particle removal [139]–[141]. Apart from that, the reduced surface contact area from a microtextured surface would influence the adhesion with each dust particle that needs to be overcome by the external force

from the wind [142]. It should also be noted that the dust particles, having irregular rough surfaces, would also influence the adhesion to the surface. The main purpose of the work in this Chapter was not to fully understand the influence of different dust particles and surface roughness on the adhesion – thus those factors were not focused on thoroughly. Nevertheless, due to the relatively high quantity of dust particles and the experiment repetitions, it is safe to assume that the variations in particle–surface interactions will be averaged out for all the different cases. What is most important, clear trends for the dust removal can be observed for each case from the plots in Figure 6.2 and will also be discussed further in the following sections.

6.1.2 Removal of Small Dust Particles

For the small dust particles, fine volcano ash and Arizona test dust were used as the dust contaminants. The resulting normalized dust removal in relation to the wind velocities were plotted for each investigated case as shown in Figure 6.3. One setback related to the measurements of the fine volcano ash removal from microtextured FEP surface occurred, where only one repetition was successfully obtained due to some technical difficulties – which was only realized later during the data analysis stage. While this might result in a less accurate analysis, the removal trend should still be a good approximation of the general dust removal behavior in the investigated cases.

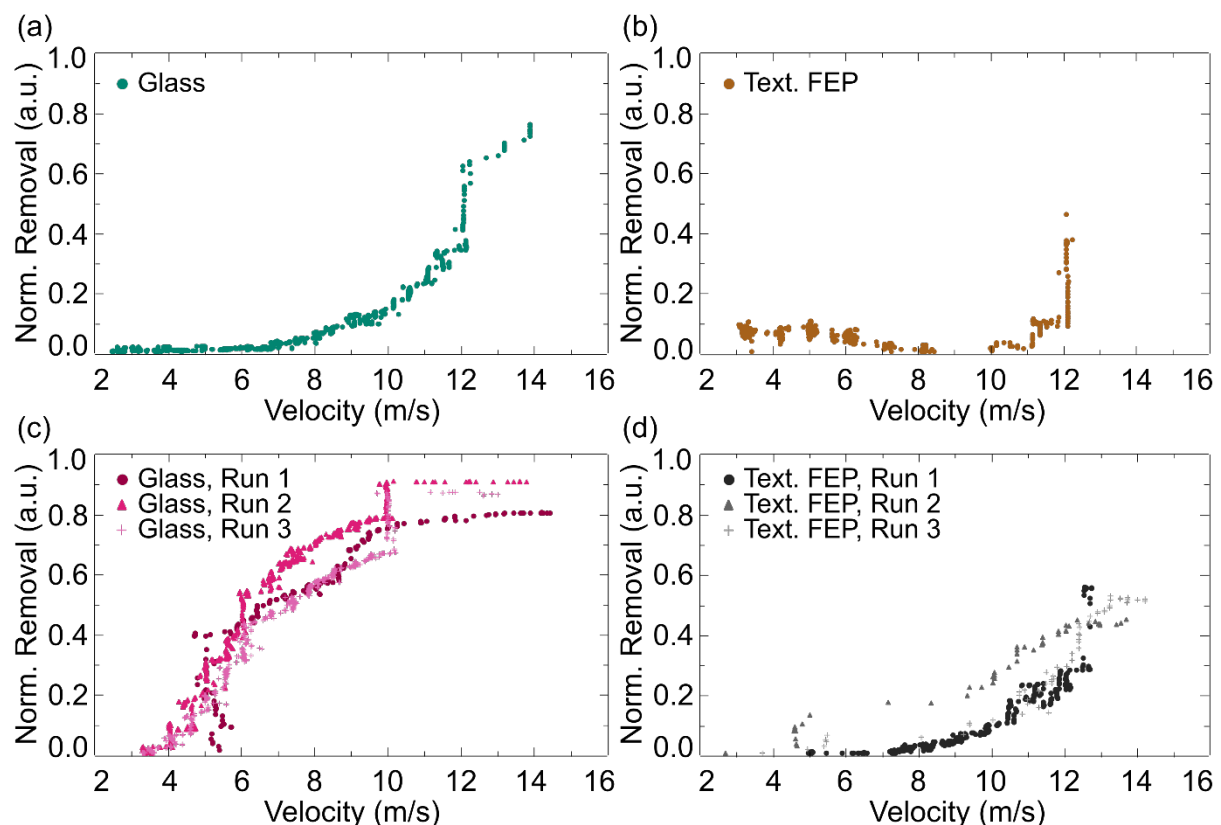


Figure 6.3 Influence of wind velocity on the removal of small dust particles. The normalized graphs present several cases for removal of different types of small dust particles from different top surfaces: (a) Fine volcano ash on planar glass, (b) fine volcano ash on microtextured FEP, (c) Arizona test dust on the planar glass and (d) Arizona test dust on microtextured FEP. (Adapted from [119])

Figure 6.3 demonstrates that removal of dust particles smaller than the microtextured spacing was also possible, achieving dust removal between 34 and 83%. From a qualitative point of view, the removal of small dust particles exhibited a wider normalized removal range compared to the large dust particles (see Figure 6.2). One reason being that some small dust particles can get trapped in between the microtexture cavities even after dust removal under the influence of wind. This observation was similar to what was discussed in Chapter 5 where small dust particles were trapped within the cavities even after cleaning with water. Meanwhile, the initial removal velocity was observed to begin between 4.0 and 11.2 m/s, again taken at 5% dust removal, as shown in Figure 6.3. In most cases, a higher wind velocity is required to initiate dust removal of the smaller dust particles compared to the larger dust particles.

Although the purpose of this study was not to investigate the relation between dust size and the physics behind the dust removal process, the results does concur with previously reported observations where it was more challenging to remove the smaller dust compared to the larger dust particles [143]–[147]. Commonly, small dust particles of sizes $<100\ \mu\text{m}$ would be situated within the viscous sublayer (boundary layer close to surface) of the wind flow where turbulence was significantly reduced [143]. Thus, in the case of smaller dust particles, it would be probable that force, if any, exerted on the particles by the wind would not be sufficient to overcome the adhesion with the surface. Furthermore, Figure 3.8c and 3.8d as shown in Chapter 3 demonstrates that the relatively small dust particles do not deposit individually but are attracted to each other and form clusters of dust particles. Higher cohesion between the small dust particles compared to the adhesion with the surface would also contribute to the higher wind requirement for small dust particle removal [148].

From the results presented, it would be safe to conclude that it is harder to remove smaller dust particles compared to the larger particles since higher wind velocities were required to initiate and achieve maximum dust removal. Nevertheless, the dust removal for both small and large dust particles showed similar trends where a certain wind velocity for each case has to be reached before dust removal was initiated and continued until it reaches a maximum removal level which varies for the different cases.

6.1.3 Dust Particle Removal Behavior

It would also be interesting to get some insights on how the dust particles were removed. Towards this end, the video of the dust removal process was further analyzed. Figure 6.4 presents the different soiled surfaces when exposed to wind flow at different time intervals. Several different cases – removal of (a) sea sand from planar glass, (b) volcano ash from planar glass and (c) sea sand from microtextured FEP – were compared to determine the validity of the observations. The wind velocity is also shown in the figure indicating an increased velocity over time.

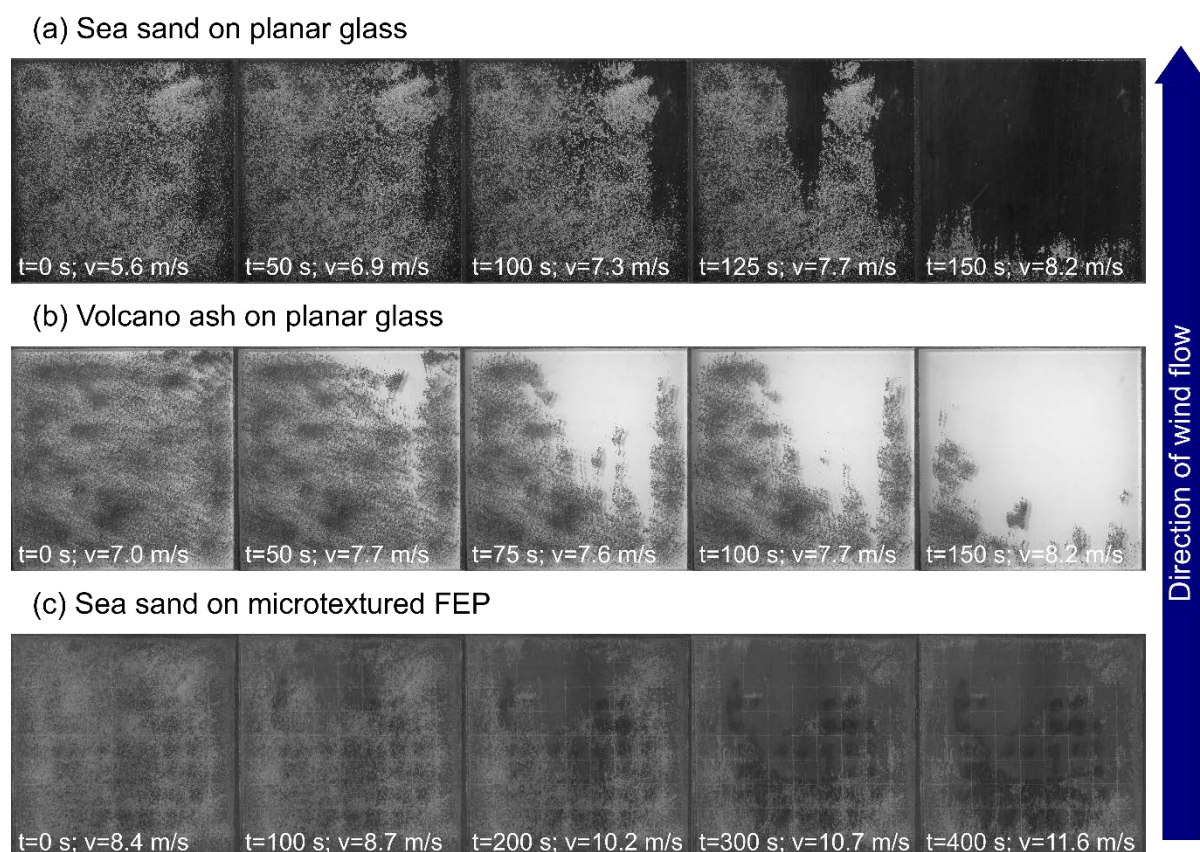


Figure 6.4 Visual observation of dust removal behavior throughout the test. Plan view microscopy images of several investigated test cases are shown as examples; (a) Sea sand on planar glass, (b) Volcano ash on planar glass and (c) Sea sand on microtextured FEP. The direction of the wind flow is shown by the arrow on the right. Time stamps and velocity of wind are included for each image.

It can be observed that the dust particles were removed, after a minimum wind velocity was reached, beginning from the tail end of the sample – farthest from the wind flow. This was true for all the cases analyzed. As the time interval and velocity increased, more dust particles were removed as demonstrated in Figure 6.4. This observation can be partially explained by either (i) a turbulent wind flow when the wind interacts with the rough microtextured surface or the dust particles that causes a higher force acting on the dust at the tail end of the sample or by (ii) a splashing phenomenon where dust particles that were displaced at the front hits dust particles at the back and causes an increase in dust removal [149], [150].

6.2 Comparing Dust Particle Removal from Microtextured PV Module Cover Films

At this juncture, it would be good to remember that one of the objectives of the work in this Chapter is to investigate the potential of using wind as an alternative natural force for self-cleaning of soiled PV modules. Therefore, this section compares dust removal from the previously developed superhydrophobic microtextured FEP PV module cover film (as reported in Chapter 5) with dust removal from a planar glass surface of conventional PV modules.

For the purpose of a better discussion and comparison, trendlines were extracted from Figure 6.2 and Figure 6.3 for the different cases as described in the previous section. The trendlines were then plotted as shown in Figure 6.5 and Figure 6.6 for the large and small dust particles, respectively. A Boltzmann fit was used to generate the trendlines due to the sigmoidal (S-shaped) curve observed in the dust removal trend (see Figure 6.2 and Figure 6.3). Thus, it should also be noted that the quantitative values used in the following discussions are approximations based on mathematical fits and not absolute values but would enable better comparison of the results.

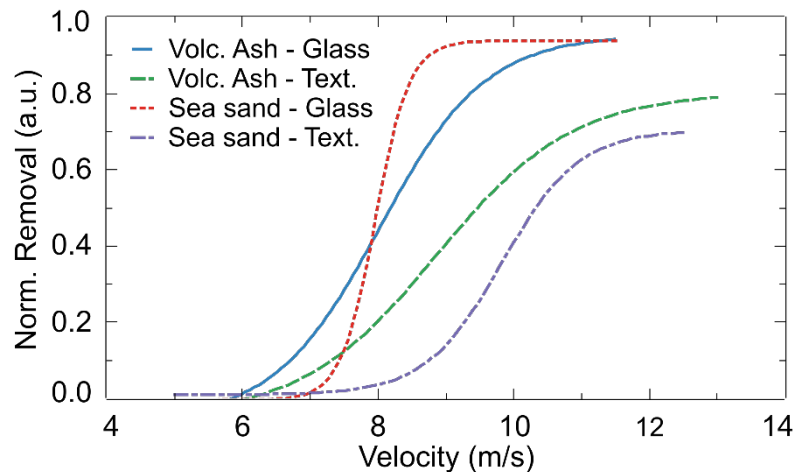


Figure 6.5 Trendlines of large dust particle removal behavior. The plotted graphs compare removal trends of coarse volcano ash and sea sand from planar glass and microtextured FEP. (Adapted from [119])

The dust removal from the microtextured FEP surface was first analyzed with respect to the large dust particles. The maximum dust removal of both coarse volcano ash (79%) and sea sand (70%) from the microtextured FEP surface was significantly lower compared to removal from a planar glass surface, which achieved removal of 94% and 94%, respectively as demonstrated in Figure 6.5. In terms of initial removal velocity, the removal of dust from the microtextured FEP surface required a slightly higher wind velocity before dust resuspension was initiated. The wind velocity at 5% dust removal began at 6.4 m/s (planar glass) compared to 6.8 m/s (microtextured FEP) for the coarse volcano ash and 7.3 m/s (planar glass) compared to 8.3 m/s (microtextured FEP) for the sea sand as also shown in Figure 6.5. The observation of both the amount of dust removed and the initial dust removal velocity in this work implies that removal of dust particles was harder from microtextured FEP surface compared to planar glass. This was contrary to popular belief whereby an increase in surface roughness will result in a decreased adhesion, thus expecting easier dust removal [145], [151].

In general, an increased surface roughness will result in both: (i) a reduced surface contact area, thus lower adhesion; and (ii) a turbulent flow, therefore an increased force acting on the dust particles. The near-wall turbulent flow will have a profound effect on the dust particle removal process. The turbulent unstable wind flow will destroy the viscous sublayer and increase the force acting on the dust particles [152]. Moreover, any turbulence ‘burst’ will result in an increased lift force to displace a dust particle from the surface [153]. This view contradicts the observations in the present

work, where it was harder to remove dust particles from a microtextured surface, and points towards a more complex understanding relating the surface roughness and dust resuspension.

A previous literature by Ilse et al. reported that for dust resuspension, the surface roughness at the microscale was not decisive, but rather the properties at the nanoscale dominates dust particle adhesion and also removal [154]. This indicates that the scale of the surface roughness plays a huge role in determining the resuspension behavior of the dust particles. Another research focusing on the particle–wall interaction provides a clearer explanation of this relation. Jiang et al. reported that for surface roughness in the nano-scale and submicron-scale, the particle resuspension shifts towards lower air velocity requirements with increasing surface roughness [139]. Meanwhile, for micron-scale surface roughness, the particle resuspension shifts towards higher velocities [139]. This explains the observation in the present work where the microtextures, being in the micron-scale, resulted in an increase in the initial removal wind velocity requirement as observed in Figure 6.5. Furthermore, a large surface roughness could even become a hindrance towards the displacement mechanism of dust particles by providing more shielding and resistance to the displacement motions (rolling or sliding) [155]. Therefore, this validates the results reported in this Chapter and becomes a basis for further potential research on microtextured surface designs to utilize wind for dust removal.

For confidence, it is important to compare whether the large dust removal behavior from the microtextured FEP surface also holds for relatively small dust particles. In the case of small dust particles, removal of dust was also higher for planar glass compared to the microtextured FEP as plotted in Figure 6.6. Figure 6.6 shows that the normalized removal of fine volcano ash and Arizona test dust from the planar glass achieved a maximum removal of 69% and 83% respectively. Meanwhile for the microtextured FEP, the maximum removal was 34% for fine volcano ash and 60% for Arizona test dust. In terms of initial removal velocity, similar to the observation with large dust particle removal, higher wind velocities were required for dust removal from the microtextured FEP surface (fine volcano ash = 11.2 m/s; Arizona test dust = 9.1 m/s) compared to planar glass (fine volcano ash = 8.9 m/s; Arizona test dust = 4.0 m/s). The maximum dust removal and initial dust removal velocity trend was consistent with the observation for large dust particle removal where the application of microtextured FEP resulted in higher wind speed requirements for dust removal. Moreover, it could be potentially worse for the small dust particles since they have the possibility to be trapped in between the microcavities as previously explained.

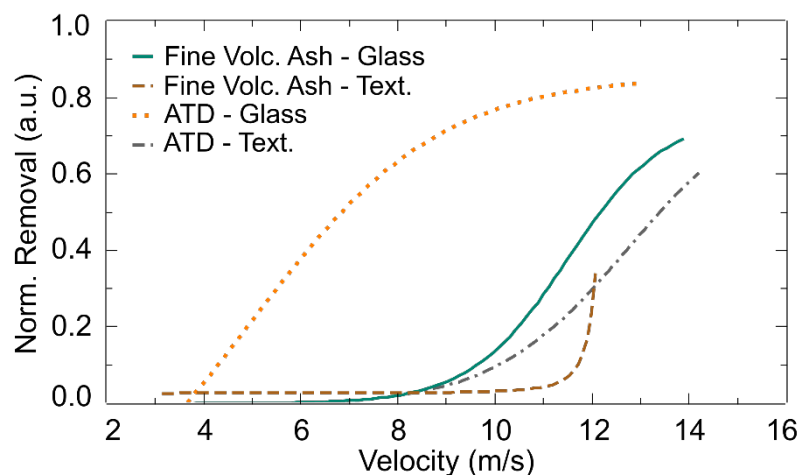


Figure 6.6 Trendlines of small dust particle removal behavior. The plotted graphs compare removal trends of fine volcano ash and Arizona test dust from planar glass and microtextured FEP. (Adapted from [119])

From the analysis of the removal behavior for both small and large dust particles, it can be understood that the application of the previously developed cone-shaped microtextured FEP as PV module front covers would lessen the reliability of wind as a natural cleaning force. Although it was shown to be possible, but the wind speed requirements would be greater to clean dust deposits from the microtextured FEP surface compared to the conventional planar glass PV module surface.

6.3 Wind for Self-Cleaning PV Module Applications

In order for the utilization of wind for cleaning soiled PV modules to be relevant, several aspects related to the intended application should be considered. Among key aspects are the impact on the PV module output and the available wind conditions at PV relevant locations. Apart from that, some insights regarding further research necessary before actual application are also discussed briefly in this section.

6.3.1 PV Module Performance Recovery

Most importantly, since the main motivation behind this research is to investigate self-cleaning of soiled PV modules, it would be necessary to understand how the removal of dust by wind impacts a PV module's performance. The experiments conducted in this study focused on the investigation of wind as an alternative dust removal force and thus the direct impact of dust removal by wind on a PV module output was not directly measured. Nevertheless, it was possible to conduct an analytical investigation based on the self-cleaning study from Chapter 4 and Chapter 5 where the J_{SC} of both the soiled and cleaned conditions were measured. The same initial and soiled outputs, in terms of J_{SC} , of the glass-encapsulated mc-Si PV mini-module were used as reference for this analysis. In Chapter 5, both sea sand and Arizona test dust were removed using water droplets that simulate self-cleaning by rainfall. The regained photocurrent, relative to the soiled PV mini-module, can be extrapolated for the analysis in this Chapter by replacing the amount of dust removed by water with

the amount of dust removed by wind for the different cases, thus identifying the regained J_{SC} as shown in Figure 6.7. The dust removal by wind in this work (33.8–94.0%) will result in a regained J_{SC} between 2.6 and 6.5 mA/cm². This can be translated to a 9.7–24.1% PV output recovery in terms of J_{SC} , relative to the soiled condition of the PV mini-module.

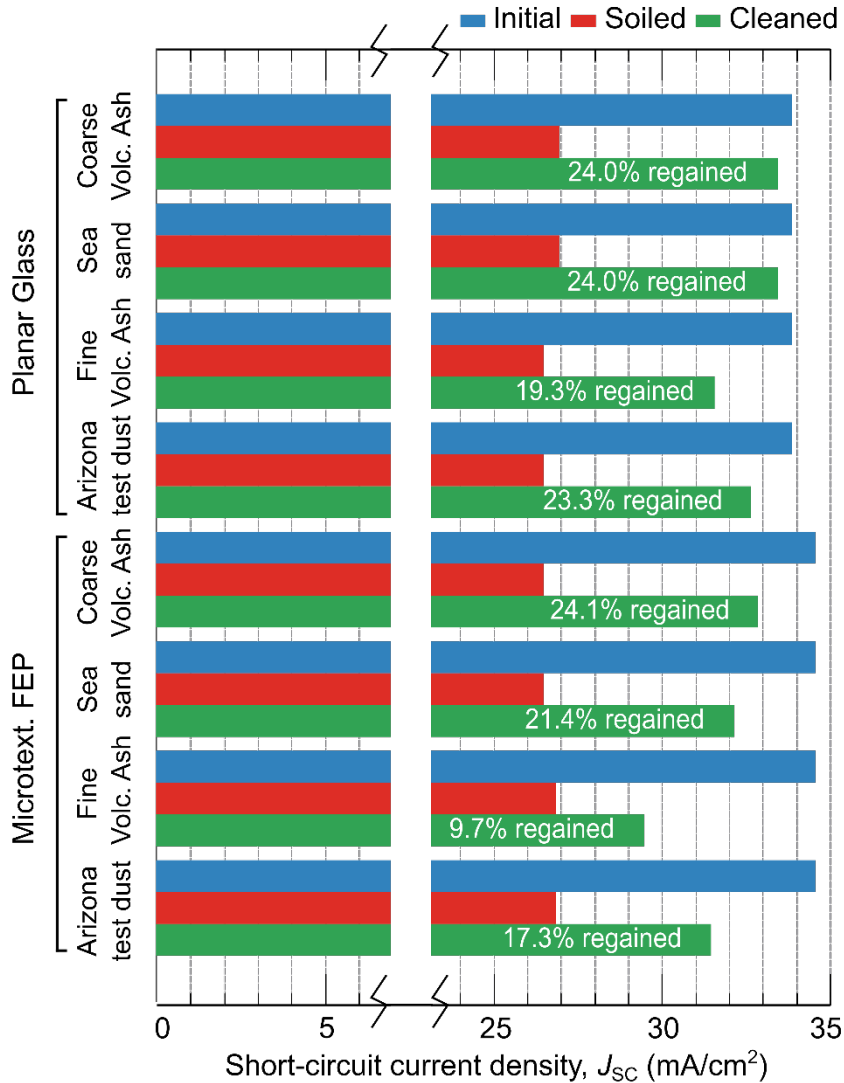


Figure 6.7 Impact of dust removal on PV output in terms of J_{SC} . The groups (on the y-axis) represent the different dust contaminants cleaned from the respective surfaces (planar glass or microtextured FEP). The J_{SC} regained after dust removal from the soiled condition of a mc-Si PV mini-module are highlighted in percentage. (Adopted from [119])

The findings from this analytical investigation demonstrate that self-cleaning of soiled PV modules by wind can achieve potentially significant improvements in the PV module output. Considering the effect of long term performance degradation of PV systems due to soiling, this performance recovery would be more significant and results in higher PV device output over a longer period of time [156]. Furthermore, the potential PV output recovery presented in this work can be further enhanced through optimization of the microtextured cover film if designed to fully utilize wind for dust removal since the cone-shaped microtextures negatively affects dust removal. Although

promising utilization of wind for PV output recovery was shown in this section, the actual application for self-cleaning soiled PV modules would highly depend on the location and requires consideration of real-world conditions.

6.3.2 Wind Speed Requirements in Real-World Conditions

Evaluating whether wind can be utilized for self-cleaning in real world applications, the minimum wind speeds required to initiate dust removal was compared with wind speeds that were reported in the literature for heights relevant to installed PV systems.

The wind speeds to initiate removal of dust particles were shown in this Chapter to have a wide range (4.0–11.2 m/s) and depended heavily on dust size and surface roughness. Whether wind can be utilized in real world self-cleaning applications would then depend on the available wind speeds at ground level (<3 m) which are more relevant for dust resuspension and ground-mounted PV systems [157]. It was difficult to find any reports of locations having consistent wind speeds that exceeded the wind velocities required for dust removal in this work. From literature, a study on volcanic ash resuspension reported an annual average wind speed of up to 8.3 m/s in the Patagonian steppe of Argentina, but studies that report similar observations were almost non-existent [158]. Wind speeds reaching >10 m/s were also reported for some locations, but these were maximum wind speeds which might occur in the form of sudden gusts of wind or during the occasion of a desert storm, albeit rarely [159], [160]. Although these few reported wind speeds were within the range to initiate dust removal, it bodes the question of how many locations would enjoy these winds and how consistent would they be throughout the year since the maximum speeds were towards the upper half of the range.

Before we can fully utilize wind for self-cleaning PV applications, further research and assessments should be conducted. Better understanding of wind conditions at various locations would help provide better evaluation of the potential usage of wind as a cleaning force. Furthermore, a more localized and specific measurement that better defines the balance between adhesion and lift acting on the dust particles would be the threshold friction velocity [147]. This would be a more exact measurement of the required wind velocity near the surface boundary layer for dust removal that would enable us to better evaluate the utilization of wind for self-cleaning in relation to the specific locations around the world. From another angle, a different strategy would be to reduce the wind speed requirements to initiate dust removal. This can be achieved through modification of the microtexture design to optimize dust removal by wind. The ideal case would be to add the enhanced self-cleaning by wind to the superhydrophobic and anti-reflection functions that was already achieved by the periodic cone-shaped microtextures in Chapter 5.

6.3.3 Limitations of Investigation

Some of the observations made were not fully understood due to limitations in the scope of the investigation conducted in this Chapter. For example, it should be noted that the removal trend of fine volcano ash and Arizona test dust from planar glass exhibited completely different removal

behaviors. Since both are within similar size categories, it would have been expected that a similar removal trend would have been observed, as demonstrated by the large dust particles in Figure 6.5. From only the results of this work, it was not possible to completely understand the different removal behaviors and further work is required. The focus of this research work is on the superhydrophobic microtextured PV module front covers and the investigation on wind was to identify the viability of considering an alternative force for self-cleaning, apart from rainfall, when applied in real-world environments. Therefore, the work in this Chapter can be considered as a simple preliminary study and further research is required to fully utilize wind for self-cleaning.

As discussed throughout this Chapter, the dust removal behavior was influenced by multiple factors: wind velocity, surface roughness, particle size and scale of surface roughness (micron or sub-micron). Apart from that, there are other factors that were not considered for simplification purposes such as, among others: (i) wind direction; (ii) particle geometry; (iii) humidity; (iv) deposition behavior; or (v) particle–particle interaction. Furthermore, there are also occurrences during the displacement of the dust particles that would influence the dust removal behavior such as: (i) the splash phenomena, whereby resting particles become loose and are then resuspended due to the impact of displaced particles [149], [150]; or (ii) the rebound effect due to bouncing of dust particles during deposition and removal, which adds uncertainty in the interpretation apart from resuspension [154]. Thus, further investigations are suggested to fully understand the dust removal behavior while taking into consideration the aforementioned factors. Future researchers might also consider modifying the current experimental design in order to investigate the minimum exposure time at certain wind speeds before initial dust removal occurs. Nevertheless, the macroscopic observation from the work reported in this Chapter was sufficient to demonstrate the influence of wind on dust removal, especially volcano ash, from a microtextured PV module cover films.

6.4 Summary

The work in this Chapter investigates the influence of wind to remove dust contaminants from a self-cleaning PV module front cover film. The viability of using wind as an additional self-cleaning force was explored, since the superhydrophobic microtextured cover film (as presented in Chapters 4 & 5) were developed relying on water droplets or rainfall for the self-cleaning mechanism. Having in mind arid/semi-arid locations where rainfall is scarce, wind was investigated as an alternative driving force for self-cleaning. Two particle size categories were investigated with respect to the microtexture spacing, volcano ash being the dust contaminant of interest due to the threat of volcano ash deposition on the performance of PV installations. For each dust size category, reference dusts used in Chapter 4 and 5 were also investigated for comparison. The results in this Chapter demonstrate that the self-cleaning of dust utilizing wind was indeed possible, achieving dust removal >60% in all cases except for one. The wind speeds for initial dust removal required for the investigated cases (4.0–11.2 m/s) were almost never met by any location in terms of annual average wind speed at ground level. This means that although wind can potentially be used as an additional force for self-cleaning of soiled PV modules, further research is required before it can be considered as a practical solution. Moreover, the addition of the superhydrophobic cone-shaped microtextured FEP PV module cover films does not improve the removal of dust by wind. In fact, the microtextured FEP cover film made it

harder to remove dust, although possible. The wind speed requirements were higher to remove dust from the microtextured surface compared to the conventional planar glass surface of a PV module. Nevertheless, there are possible strategies to further develop the microtextured FEP cover films to make it more viable. Since the surface roughness was proven to influence dust removal, a further optimization of the microtextures design and dimensions should be conducted to be able to utilize wind as an additional self-cleaning force and thus produce a more robust self-cleaning PV module cover film.

7 Summary and Outlook

The research work presented in this thesis addresses the issue of PV soiling which can severely reduce the performance of PV modules. Among the various mitigation options available, the chosen approach of a passive mitigation solution is an attractive one since it reduces the need for frequent maintenance and reduces the negative impact of PV soiling. To achieve this, a superhydrophobic microtextured front cover was developed that has the potential to introduce a self-cleaning function to the PV modules. Moreover, by optimizing the microtextures design, an anti-reflective function was also introduced to enhance the photocurrent generation output of PV modules.

As proof-of-concept, a random microtextured front cover was first investigated and is presented in Chapter 4. Chapter 4 also reviews the potential of using FEP as a front cover material. Even though it meets the basic requirements of transmittance and low surface energy, whether it would be applicable for the intended objective has still to be tested. At the same time, the fabrication process was investigated to get a better understanding of the fabrication parameters to produce the microtextured films. The best fabricated sample resulted in a superhydrophobic front cover having a contact angle of $156\pm 1^\circ$ and a roll-off angle of $8\pm 3^\circ$. The microtextured FEP front cover also resulted in a significant reduction in the front reflectance, leading to an improved J_{SC} by 1.3% compared to a reference PV mini-module. The self-cleaning performance of the random microtextured FEP front cover demonstrated a 93.6% recovery in terms of J_{SC} .

After it was proven that random microtextured FEP can be applied as a self-cleaning superhydrophobic PV module front cover, there was the question of whether the anti-reflective properties can be enhanced. It was improved by the microtextured cover, but only slightly. Chapter 5 presented the introduction of a periodically patterned microtextures – a cone-shaped microtexture design – that improved the light in-coupling while retaining the superhydrophobic property of the surface. A more controlled design would enable the intentional introduction of certain features or functions. The sharp tips significantly minimized the surface contact area achieving superhydrophobic surfaces for all investigated cone-shaped microtexture designs, regardless of their aspect ratio.

The periodic cone-shaped microtextured FEP covers (aspect ratio = 0.7) demonstrated a significant enhancement of both self-cleaning and anti-reflective properties. It successfully retains the superhydrophobicity previously achieved (contact angle = $161\pm 3^\circ$ and roll-off angle = $6\pm 4^\circ$). The microtextured FEP covers also resulted in a significant reduction in reflectance, achieving a minimum reflectance of 1.2% compared to 4.4% of the reference CIGS solar cell. This effect contributed to a significant 3.1% relative improvement in J_{SC} . Compared with the random microtextures (J_{SC} improvement = 1.3%), when applied on a mc-Si PV mini-module, the cone-shaped microtextures enhanced the performance by almost double (J_{SC} improvement = 2.4%). The self-cleaning performance was also enhanced where a recovery ratio of 100% and 65.8% were achieved when soiled with sea sand and Arizona test dust, respectively. Thus, the potential of using a cone-shaped microtextured FEP film as a self-cleaning cover for PV modules was successfully demonstrated.

Another question that frequently came up was whether the self-cleaning function can still operate without rainfall. The superhydrophobic microtextured front cover was designed such that the self-cleaning function relies on water droplets, from rainfall or auxiliary systems. Chapter 6 presented the investigation of using wind as the alternative dust removal force, instead of the water droplets. In any case, how the developed cone-shaped microtextured FEP front cover affects dust removal by wind was investigated.

It was shown that it was indeed possible to utilize wind and remove >60% of deposited dust in most cases studied in this work. The wind speeds required for initial dust removal/displacement in the investigated cases were between 4.0 and 11.2 m/s. In reality, there was almost no location which has annual average wind speeds with those requirements. Thus, although it is possible to utilize wind for dust removal in general, to become a viable option it still requires further research. In fact, the current cone-shaped microtextured FEP front cover made it harder to remove the dust and required higher wind speeds compared to dust removal from a planar glass surface. Nevertheless, since it was shown that microtexturing does influence dust removal by wind, there might be a viable microtexture design that can enhance dust removal by wind, either by reducing the wind speed requirements or by reducing the adhesion of dust to the surface. This would eventually further enhance the multifunctional PV module front cover developed in this work.

To conclude, this work demonstrated significant promising results in the development of a passive mitigation solution for the problem of PV soiling. Nevertheless, the development of the multifunctional PV module front cover was an achievement in proof-of-concept. Therefore, there are further research opportunities that could be of interest for future work.

The issue of PV soiling highly depends on the location – depending on the geographical, environmental conditions and the human activities in that area. In this work, only four different dust types were used to investigate the self-cleaning capability. It would be interesting to expand this investigation to include different soiling contaminants ranging from different dust types and sizes, biological matters, and artificial contaminants from human activities. A mixture of the soiling contaminants, reflecting actual PV soiling of specific locations imitating urban, sub-urban or rural areas, could be used to reflect actual real-world soiling. More in-depth studies could also include the understanding of the soiling deposition mechanism of different contaminants. The current work focuses only on the cleaning or removal of dust from PV module surfaces.

So far, the self-cleaning performance evaluation has been conducted in a laboratory. A further improvement would be to investigate the self-cleaning covers in real-world conditions, which would entail enlarging the covers to an acceptable size and conducting outdoor testing over a significant period of time. Better still would be to conduct the tests in different locations around the world to include the influence of the different environmental conditions on the soiling and self-cleaning of the PV modules. It would be interesting to then also investigate the self-cleaning of soiled PV modules by other natural phenomena such as dew or ice that might be predominantly unique characteristics of different locations. Understanding the observations from these tests in real-world conditions would help the selection of material for the self-cleaning covers or the microtextures to be re-designed to what is more suitable to the dust particles and weather conditions at specific locations. Since there is yet to exist a standard testing method for self-cleaning performance of PV modules, the development

of a standardized testing system or guideline is also an opportunity that will enable better evaluation of the self-cleaning capability of various surfaces.

The self-cleaning PV module cover would enhance PV output but comes at additional cost and processes. There is an opportunity to conduct a techno-economic analysis to evaluate the cost benefits of this approach to address the PV soiling issue that would enable identification of suitable conditions that would make it beneficial. Having a deeper understanding of conditions suitable for application would provide insights of directions to take for further research to improve the microtextured self-cleaning covers or where and how best to implement it.

For actual applications, the developed microtextures FEP covers would need to be enlarged and applied on PV modules. The initial microtextured FEP samples produced were used for laboratory testing, with the largest having a size of ≈ 2 cm x 2 cm. For the work in Chapter 6, it was enlarged into a ≈ 10 cm x 10 cm microtextured area by stitching a large number of samples to produce the large area mold. This manual process did come with some defects and limitations, thus still needs to be improved. Up-scaling to a size suitable for PV module would require some further research. A roll-to-roll hot-embossing is a promising option for upscaling since it has been widely used to fabricate microtextured polymer films surfaces. Compared to conventional hot-embossing, this continuous fabrication process has the advantage of being fast, cost efficient, suitable for large area and large-scale replication, thus is suitable for commercialization. Moreover, the roll-to-roll texturing technique can also improve the fabrication process by reducing the required hot-embossing force since only a small area (line) is in contact at one time. Further application can include other processes where it is also possible to utilize a roll-to-roll lamination process to attach the microtextured polymer films onto flexible PV modules. In fact, there might be a possibility to simply add an additional step in the fabrication line of glass encapsulated PV modules in order to attach the microtextured polymer films since laminating the glass layers using EVA as the encapsulant is already a commonly used method in the PV industry.

In Chapter 4, random microtextures were hot-embossed on FEP films to introduce superhydrophobic properties in PV module front cover. Further work in Chapter 5 improved the front covers by using cone-shaped periodic microtextures that enhanced the anti-reflective properties, on top of maintaining the previously achieved superhydrophobicity. It would be interesting to investigate potential microtexture designs that could introduce further beneficial functions such as superoleophobicity, to utilize wind or dew for self-cleaning or to enhance the mechanical strength of the microtextures.

In this work, FEP was chosen from the material family fluoropolymers due to its suitable properties to achieve the desired outcome. It might be interesting to explore other materials, either from the same fluoropolymer family or others, that can achieve the same superhydrophobic and anti-reflective properties. Understanding the compensation in properties or what additional modifications are required will enable the selection of the most suitable material for different applications. Furthermore, the cost of fluoropolymers is relatively higher compared to other polymers, the benefits might just outweigh the cost and can be identified from an in-depth cost-benefit analysis.

A question that was asked constantly was whether the microtextures would be intact when exposed to the environment over a long period of time. In Chapter 5, it was demonstrated that the

cone-shaped microtextures could still maintain the superhydrophobic functions even with some defects. The mechanical strength and rigidity of the microtextures can still be investigated which will give more confidence for long term outdoor applications. A subsequent investigation from the outdoor testing of PV modules having the microtextured front covers would be to observe if they still retain the microtextures and function as intended. Other stability tests could also be conducted through an accelerated weather chamber or other important parameters.

The developed microtextured front cover was applied and investigated on mc-Si PV and CIGS PV modules. Further investigation can be conducted by applying the microtextured covers on different PV module technologies to understand the suitability of adding a multifunctional front cover for different technologies. Furthermore, for certain PV module technologies, it might be possible to develop new PV device architectures if the microtextured front cover can supplement characteristics of conventional layers of the PV devices.

The results and discussion presented in this thesis gives confidence that there is huge potential for the microtextured FEP covers to be applied in real-world applications since the material and process involved has been used and is still being developed further in the industry. To completely evaluate the value of the microtextured FEP cover, one must also consider the overall system cost, the maintenance cost, and the loss of energy due to soiling over a period of time apart from the potential energy gain.

This work proves that there are significant multifunctional benefits from the application of a microtextured fluoropolymer PV module front cover. Most importantly, it addresses the issue of PV soiling that reduces the performance of the PV modules. As we move towards higher efficiency devices and approach the theoretical limit, improvement in optical transmittance of the cover glass and encapsulation materials becomes more critical and any research that contributes towards this improvement becomes worthwhile.

References

- [1] International Energy Agency, "World Energy Outlook 2021 : Part of the World Energy Outlook," 2021. Accessed: Sep. 13, 2023. [Online]. Available: <https://www.iea.org/reports/world-energy-outlook-2021>
- [2] International Energy Agency, "Snapshot of Global PV Markets 2023 Task 1 Strategic PV Analysis and Outreach PVPS," 2023. Accessed: May 01, 2024. [Online]. Available: <https://iea-pvps.org/snapshot-reports/>
- [3] M. Aghaei *et al.*, "Review of degradation and failure phenomena in photovoltaic modules," *Renew. Sustain. Energy Rev.*, vol. 159, no. January, p. 112160, 2022, doi: 10.1016/j.rser.2022.112160.
- [4] W. Luo *et al.*, "Photovoltaic module failures after 10 years of operation in the tropics," *Renew. Energy*, vol. 177, pp. 327–335, 2021, doi: 10.1016/j.renene.2021.05.145.
- [5] M. A. Hamdan and B. A. Kakish, "Solar radiation attenuation caused by atmospheric pollution," *Energy Convers. Manag.*, vol. 36, no. 2, pp. 121–124, 1995, doi: 10.1016/0196-8904(94)00052-2.
- [6] T. Sarver, A. Al-Qaraghuli, and L. L. Kazmerski, "A comprehensive review of the impact of dust on the use of solar energy: History, investigations, results, literature, and mitigation approaches," *Renew. Sustain. Energy Rev.*, vol. 22, pp. 698–733, 2013, doi: 10.1016/j.rser.2012.12.065.
- [7] F. Ju and X. Fu, "Research on impact of dust on solar photovoltaic(PV) performance," *2011 Int. Conf. Electr. Control Eng. ICECE 2011 - Proc.*, pp. 3601–3606, 2011, doi: 10.1109/ICECENG.2011.6058487.
- [8] M. A. M. L. de Jesus, J. T. da S. Neto, G. Timò, P. R. P. Paiva, M. S. S. Dantas, and A. de M. Ferreira, "Superhydrophilic self-cleaning surfaces based on TiO₂ and TiO₂/SiO₂ composite films for photovoltaic module cover glass," *Appl. Adhes. Sci.*, vol. 3, no. 1, pp. 1–9, 2015, doi: 10.1186/s40563-015-0034-4.
- [9] W. J. Jamil, H. Abdul Rahman, S. Shaari, and Z. Salam, "Performance degradation of photovoltaic power system: Review on mitigation methods," *Renew. Sustain. Energy Rev.*, vol. 67, pp. 876–891, 2017, doi: 10.1016/j.rser.2016.09.072.
- [10] R. Siddiqui and U. Bajpai, "Correlation between thicknesses of dust collected on photovoltaic module and difference in efficiencies in composite climate," *Int. J. Energy Environ. Eng.*, vol. 3, no. 1, pp. 1–7, 2012, doi: 10.1186/2251-6832-3-26.
- [11] F. M. Zaihidee, S. Mekhilef, M. Seyedmahmoudian, and B. Horan, "Dust as an unalterable deteriorative factor affecting PV panel's efficiency: Why and how," *Renew. Sustain. Energy Rev.*, vol. 65, pp. 1267–1278, 2016, doi: 10.1016/j.rser.2016.06.068.
- [12] A. Y. Al-Hasan, "A new correlation for direct beam solar radiation received by photovoltaic panel with sand dust accumulated on its surface," *Sol. Energy*, vol. 63, no. 5, pp. 323–333, 1998, doi: 10.1016/S0038-092X(98)00060-7.
- [13] M. R. Maghami, H. Hizam, C. Gomes, M. A. Radzi, M. I. Rezadad, and S. Hajighorbani, "Power loss due to soiling on solar panel: A review," *Renew. Sustain. Energy Rev.*, vol. 59, pp. 1307–

- 1316, 2016, doi: 10.1016/j.rser.2016.01.044.
- [14] J. J. John, S. Warade, G. Tamizhmani, and A. Kottantharayil, "Study of soiling loss on photovoltaic modules with artificially deposited dust of different gravimetric densities and compositions collected from different locations in India," *IEEE J. Photovoltaics*, vol. 6, no. 1, pp. 236–243, 2016, doi: 10.1109/JPHOTOV.2015.2495208.
- [15] K. K. Ilse, B. W. Figgis, V. Naumann, C. Hagendorf, and J. Bagdahn, "Fundamentals of soiling processes on photovoltaic modules," *Renew. Sustain. Energy Rev.*, vol. 98, pp. 239–254, 2018, doi: 10.1016/j.rser.2018.09.015.
- [16] D. Rieger *et al.*, "Impact of the 4 April 2014 Saharan dust outbreak on the photovoltaic power generation in Germany," *Atmos. Chem. Phys.*, vol. 17, no. 21, pp. 13391–13415, 2017, doi: 10.5194/acp-17-13391-2017.
- [17] L. L. Kazmerski *et al.*, "Fundamental studies of adhesion of dust to PV module surfaces: Chemical and physical relationships at the microscale," *IEEE J. Photovoltaics*, vol. 6, no. 3, pp. 719–729, 2016, doi: 10.1109/JPHOTOV.2016.2528409.
- [18] S. Ghazi, A. Sayigh, and K. Ip, "Dust effect on flat surfaces - A review paper," *Renew. Sustain. Energy Rev.*, vol. 33, pp. 742–751, 2014, doi: 10.1016/j.rser.2014.02.016.
- [19] E. Zorn and T. R. Walter, "Influence of volcanic tephra on photovoltaic (PV)-modules: An experimental study with application to the 2010 Eyjafjallajökull eruption, Iceland," *J. Appl. Volcanol.*, vol. 5, no. 2, 2016, doi: 10.1186/s13617-015-0041-y.
- [20] V. Schlosser, M. Drapalik, and G. Klinger, "About the usability of a photovoltaic module to monitor air pollution," *3rd Int. Conf. Clean Electr. Power Renew. Energy Resour. Impact, ICCEP 2011*, pp. 434–438, 2011, doi: 10.1109/ICCEP.2011.6036378.
- [21] M. K. Butwin, S. Von Löwis, M. A. Pfeffer, P. Dagsson-Waldhauserova, J. Thorsson, and T. Thorsteinsson, "Influence of weather conditions on particulate matter suspension following the 2010 Eyjafjallajökull volcanic eruption," *Earth Interact.*, vol. 24, no. 6, pp. 1–16, 2020, doi: 10.1175/EI-D-20-0006.1.
- [22] M. Jaszczur *et al.*, "The field experiments and model of the natural dust deposition effects on photovoltaic module efficiency," *Environ. Sci. Pollut. Res.*, vol. 26, no. 9, pp. 8402–8417, 2019, doi: 10.1007/s11356-018-1970-x.
- [23] Y. Jiang, L. Lu, and H. Lu, "A novel model to estimate the cleaning frequency for dirty solar photovoltaic (PV) modules in desert environment," *Sol. Energy*, vol. 140, pp. 236–240, 2016, doi: 10.1016/j.solener.2016.11.016.
- [24] D. Olivares *et al.*, "Characterization of soiling on PV modules in the Atacama Desert," *Energy Procedia*, vol. 124, pp. 547–553, 2017, doi: 10.1016/j.egypro.2017.09.263.
- [25] W. Javed, Y. Wubulikasimu, B. Figgis, and B. Guo, "Characterization of dust accumulated on photovoltaic panels in Doha , Qatar," *Sol. Energy*, vol. 142, pp. 123–135, 2017, doi: 10.1016/j.solener.2016.11.053.
- [26] H. A. Kazem and M. T. Chaichan, "Experimental analysis of the effect of dust's physical properties on photovoltaic modules in Northern Oman," *Sol. Energy*, vol. 139, pp. 68–80, 2016, doi: 10.1016/j.solener.2016.09.019.
- [27] U. Mehmood, F. A. Al-sulaiman, and B. S. Yilbas, "Characterization of dust collected from PV modules in the area of Dhahran , Kingdom of Saudi Arabia , and its impact on protective transparent covers for photovoltaic applications," *Sol. Energy*, vol. 141, pp. 203–209, 2017,

- doi: 10.1016/j.solener.2016.11.051.
- [28] F. Mani, S. Pulipaka, and R. Kumar, "Characterization of power losses of a soiled PV panel in Shekhawati region of India," *Sol. Energy*, vol. 131, pp. 96–106, 2016, doi: 10.1016/j.solener.2016.02.033.
- [29] R. E. Cabanillas and H. Munguía, "Dust accumulation effect on efficiency of Si photovoltaic modules," *J. Renew. Sustain. Energy*, vol. 3, no. 4, 2011, doi: 10.1063/1.3622609.
- [30] P. D. Burton and B. H. King, "Spectral Sensitivity of Simulated Photovoltaic Module Soiling for a Variety of Synthesized Soil Types," vol. 4, no. 3, pp. 890–898, 2014.
- [31] S. C. S. Costa, A. S. A. C. Diniz, and L. L. Kazmerski, "Dust and soiling issues and impacts relating to solar energy systems: Literature review update for 2012–2015," *Renew. Sustain. Energy Rev.*, vol. 63, pp. 33–61, 2016, doi: 10.1016/j.rser.2016.04.059.
- [32] Y. Ota, K. Araki, and K. Nishioka, "Impact of volcanic ash on CPV system in Miyazaki Japan," *AIP Conf. Proc.*, vol. 1477, pp. 340–343, 2012, doi: 10.1063/1.4753900.
- [33] G. Masson *et al.*, "Trends in Photovoltaic Applications," 2019. Accessed: May 29, 2023. [Online]. Available: <https://iea-pvps.org/wp-content/uploads/2020/02/5319-iea-pvps-report-2019-08-lr.pdf>
- [34] Y. N. Chanchangi, A. Ghosh, S. Sundaram, and T. K. Mallick, "Dust and PV Performance in Nigeria: A review," *Renew. Sustain. Energy Rev.*, vol. 121, p. 109704, 2020, doi: 10.1016/j.rser.2020.109704.
- [35] A. Sayyah, M. N. Horenstein, and M. K. Mazumder, "Energy yield loss caused by dust deposition on photovoltaic panels," *Sol. Energy*, vol. 107, pp. 576–604, 2014, doi: 10.1016/j.solener.2014.05.030.
- [36] M. K. Mazumder *et al.*, "Mitigation of Dust Impact on Solar Collectors by Water-Free Cleaning with Transparent Electrodynamic Films: Progress and Challenges," *IEEE J. Photovoltaics*, vol. 7, no. 5, pp. 1342–1353, 2017, doi: 10.1109/JPHOTOV.2017.2721462.
- [37] R. Sharma, C. A. Wyatt, J. Zhang, C. I. Calle, N. Mardesich, and M. K. Mazumder, "Experimental evaluation and analysis of electrodynamic screen as dust mitigation technology for future Mars missions," *IEEE Trans. Ind. Appl.*, vol. 45, no. 2, pp. 591–596, 2009, doi: 10.1109/TIA.2009.2013542.
- [38] J. Son *et al.*, "A practical superhydrophilic self cleaning and antireflective surface for outdoor photovoltaic applications," *Sol. Energy Mater. Sol. Cells*, vol. 98, pp. 46–51, 2012, doi: 10.1016/j.solmat.2011.10.011.
- [39] Alchemie, "Solar Panel Manual Cleaning," Webpage. Accessed: Nov. 20, 2023. [Online]. Available: <https://www.solar-facts-and-advice.com/solar-panel-cleaning.html>
- [40] M. N. Horenstein *et al.*, "Modeling of Trajectories in an Electrodynamic Screen for Obtaining Maximum Particle Removal Efficiency," *IEEE Trans. Ind. Appl.*, vol. 49, no. 2, pp. 707–713, 2013, doi: 10.1109/TIA.2013.2244192.
- [41] SERBOT, "Robot Gekko Solar," Webpage. Accessed: Nov. 20, 2023. [Online]. Available: <https://www.serbot.ch/en/gallery/photos-gallery>
- [42] K. A. Moharram, M. S. Abd-Elhady, H. A. Kandil, and H. El-Sherif, "Influence of cleaning using water and surfactants on the performance of photovoltaic panels," *Energy Convers. Manag.*, vol. 68, pp. 266–272, 2013, doi: 10.1016/j.enconman.2013.01.022.

- [43] F. Vüllers *et al.*, “Self-Cleaning Microcavity Array for Photovoltaic Modules,” *ACS Appl. Mater. Interfaces*, vol. 10, no. 3, pp. 2929–2936, 2018, doi: 10.1021/acsami.7b15579.
- [44] A. Roslizar *et al.*, “Self-cleaning performance of superhydrophobic hot-embossed fluoropolymer films for photovoltaic modules,” *Sol. Energy Mater. Sol. Cells*, vol. 189, pp. 188–196, 2019, doi: 10.1016/j.solmat.2018.09.017.
- [45] M. T. Chaichan, B. A. Mohammed, and H. A. Kazem, “Effect of pollution and cleaning on photovoltaic performance based on experimental study,” *Int. J. Sci. Eng. Res.*, vol. 6, no. 4, pp. 594–601, 2015, doi: 10.13140/RG.2.1.2928.2725.
- [46] A. Sayyah, R. S. Eriksen, M. N. Horenstein, L. Fellow, M. K. Mazumder, and L. Fellow, “Performance Analysis of Electrodynamical Screens Based on Residual Particle Size Distribution,” *IEEE J. Photovoltaics*, vol. 7, no. 1, pp. 221–229, 2017, doi: 10.1109/JPHOTOV.2016.2617088.
- [47] M. Mani and R. Pillai, “Impact of dust on solar photovoltaic (PV) performance: Research status, challenges and recommendations,” *Renew. Sustain. Energy Rev.*, vol. 14, no. 9, pp. 3124–3131, 2010, doi: 10.1016/j.rser.2010.07.065.
- [48] P. Roach, N. J. Shirtcliffe, and M. I. Newton, “Progress in superhydrophobic surface development,” *Soft Matter*, vol. 4, no. 2, pp. 224–240, 2008, doi: 10.1039/B712575P.
- [49] R. N. Wenzel, “Resistance of solid surfaces to wetting by water,” *Ind. Eng. Chem.*, vol. 28, no. 8, pp. 988–994, 1936, doi: 10.1021/ie50320a024.
- [50] D. Quéré, A. Lafuma, and J. Bico, “Slippy and sticky microtextured solids,” *Nanotechnology*, vol. 14, no. 10, pp. 1109–1112, 2003, doi: 10.1088/0957-4484/14/10/307.
- [51] W. Barthlott and C. Neinhuis, “Purity of the sacred lotus, or escape from contamination in biological surfaces,” *Planta*, vol. 202, no. 1, pp. 1–8, 1997, doi: 10.1007/s004250050096.
- [52] A. B. D. Cassie and S. Baxter, “Wettability of porous surfaces,” *Trans. Faraday Soc.*, vol. 40, no. 5, pp. 546–551, 1944, doi: 10.1039/TF9444000546.
- [53] J. W. Drelich *et al.*, “Contact angles: History of over 200 years of open questions,” *Surf. Innov.*, vol. 8, no. 1–2, pp. 3–27, 2020, doi: 10.1680/jsuin.19.00007.
- [54] S. Wang and L. Jiang, “Definition of superhydrophobic states,” *Adv. Mater.*, vol. 19, no. 21, pp. 3423–3424, 2007, doi: 10.1002/adma.200700934.
- [55] M. Nosonovsky and B. Bhushan, “Energy transitions in superhydrophobicity: Low adhesion, easy flow and bouncing,” *J. Phys. Condens. Matter*, vol. 20, no. 39, 2008, doi: 10.1088/0953-8984/20/39/395005.
- [56] L. Feng *et al.*, “Petal effect: A superhydrophobic state with high adhesive force,” *Langmuir*, vol. 24, no. 8, pp. 4114–4119, 2008, doi: 10.1021/la703821h.
- [57] C. R. Crick and I. P. Parkin, “Water droplet bouncing—a definition for superhydrophobic surfaces,” *Chem. Commun.*, vol. 47, no. 44, p. 12059, 2011, doi: 10.1039/c1cc14749h.
- [58] Y. Lu, S. Sathasivam, J. Song, W. Xu, C. J. Carmalt, and I. P. Parkin, “Water droplets bouncing on superhydrophobic soft porous materials,” *J. Mater. Chem. A*, vol. 2, no. 31, pp. 12177–12184, 2014, doi: 10.1039/C4TA02391A.
- [59] M. Jin *et al.*, “Super-hydrophobic PDMS surface with ultra-low adhesive force,” *Macromol. Rapid Commun.*, vol. 26, no. 22, pp. 1805–1809, 2005, doi: 10.1002/marc.200500458.

- [60] M. Z. Jacobson and V. Jadhav, "World estimates of PV optimal tilt angles and ratios of sunlight incident upon tilted and tracked PV panels relative to horizontal panels," *Sol. Energy*, vol. 169, pp. 55–66, 2018, doi: 10.1016/j.solener.2018.04.030.
- [61] C. Antonini, M. Innocenti, T. Horn, M. Marengo, and A. Amirfazli, "Understanding the effect of superhydrophobic coatings on energy reduction in anti-icing systems," *Cold Reg. Sci. Technol.*, vol. 67, no. 1–2, pp. 58–67, 2011, doi: 10.1016/j.coldregions.2011.02.006.
- [62] B. Bhushan and M. Nosonovsky, "The rose petal effect and the modes of superhydrophobicity," *Philos. Trans. R. Soc. A Math. Phys. Eng. Sci.*, vol. 368, pp. 4713–4728, 2010, doi: 10.1098/rsta.2010.0203.
- [63] D. Helmer *et al.*, "Transparent, abrasion-insensitive superhydrophobic coatings for real-world applications," *Sci. Rep.*, vol. 7, pp. 1–6, 2017, doi: 10.1038/s41598-017-15287-8.
- [64] T. Aytug *et al.*, "Monolithic graded-refractive-index glass-based antireflective coatings: Broadband/omnidirectional light harvesting and self-cleaning characteristics," *J. Mater. Chem. C*, vol. 3, no. 21, pp. 5440–5449, 2015, doi: 10.1039/c5tc00499c.
- [65] K. H. Tsui *et al.*, "Low-cost, flexible, and self-cleaning 3D nanocone anti-reflection films for high-efficiency photovoltaics," *Adv. Mater.*, vol. 26, no. 18, pp. 2805–2811, 2014, doi: 10.1002/adma.201304938.
- [66] J. W. Leem, S. Kim, S. H. Lee, J. A. Rogers, E. Kim, and J. S. Yu, "Efficiency enhancement of organic solar cells using hydrophobic antireflective inverted moth-eye nanopatterned PDMS films," *Adv. Energy Mater.*, vol. 4, no. 8, pp. 1–7, 2014, doi: 10.1002/aenm.201301315.
- [67] J. De Chen *et al.*, "Enhanced light harvesting in organic solar cells featuring a biomimetic active layer and a self-cleaning antireflective coating," *Adv. Energy Mater.*, vol. 4, no. 9, pp. 1–8, 2014, doi: 10.1002/aenm.201301777.
- [68] R. J. Vrancken *et al.*, "Fully reversible transition from Wenzel to Cassie-Baxter states on corrugated superhydrophobic surfaces," *Langmuir*, vol. 26, no. 5, pp. 3335–3341, 2010, doi: 10.1021/la903091s.
- [69] C. Credi, D. Pintossi, C. L. Bianchi, M. Levi, G. Griffini, and S. Turri, "Combining stereolithography and replica molding: On the way to superhydrophobic polymeric devices for photovoltaics," *Mater. Des.*, vol. 133, pp. 143–153, 2017, doi: 10.1016/j.matdes.2017.07.068.
- [70] M. M. Tavakoli *et al.*, "Highly Efficient Flexible Perovskite Solar Cells with Antireflection and Self-Cleaning Nanostructures," *ACS Nano*, vol. 9, no. 10, pp. 10287–10295, 2015, doi: 10.1021/acsnano.5b04284.
- [71] B. Bhushan, K. Koch, and Y. C. Jung, "Fabrication and characterization of the hierarchical structure for superhydrophobicity and self-cleaning," *Ultramicroscopy*, vol. 109, no. 8, pp. 1029–1034, 2009, doi: 10.1016/j.ultramic.2009.03.030.
- [72] K. Koch, H. F. Bohn, and W. Barthlott, "Hierarchically sculptured plant surfaces and superhydrophobicity," *Langmuir*, vol. 25, no. 24, pp. 14116–14120, 2009, doi: 10.1021/la9017322.
- [73] A. Fernández *et al.*, "Design of Hierarchical Surfaces for Tuning Wetting Characteristics," *ACS Appl. Mater. Interfaces*, vol. 9, no. 8, pp. 7701–7709, 2017, doi: 10.1021/acsam.6b13615.
- [74] A. Fernández *et al.*, "Hierarchical surfaces for enhanced self-cleaning applications," *J. Micromechanics Microengineering*, vol. 27, no. 4, p. 045020, 2017, doi: 10.1088/1361-

6439/aa62bb.

- [75] E. Huovinen, J. Hirvi, M. Suvanto, and T. A. Pakkanen, "Micro-micro hierarchy replacing micro-nano hierarchy: A precisely controlled way to produce wear-resistant superhydrophobic polymer surfaces," *Langmuir*, vol. 28, no. 41, pp. 14747–14755, 2012, doi: 10.1021/la303358h.
- [76] F. Vüllers *et al.*, "Bioinspired Superhydrophobic Highly Transmissive Films for Optical Applications," *Small*, vol. 12, no. 44, pp. 6144–6152, 2016, doi: 10.1002/smll.201601443.
- [77] B. Fritz *et al.*, "Towards mass fabrication of hot embossed plant surface texture replicas as photovoltaic cover layers," in *Proceedings of SPIE 10730, Nanoengineering: Fabrication, Properties, Optics, and Devices XV*, 2018, pp. 49–58. doi: 10.1117/12.2320555.
- [78] Y.-B. Park, H. Im, M. Im, and Y.-K. Choi, "Self-cleaning effect of highly water-repellent microshell structures for solar cell applications," *J. Mater. Chem.*, vol. 21, no. 3, pp. 633–636, 2011, doi: 10.1039/C0JM02463E.
- [79] B. Dudem, J. H. Heo, J. W. Leem, J. S. Yu, and S. H. Im, "CH₃NH₃PbI₃ planar perovskite solar cells with antireflection and self-cleaning function layers," *J. Mater. Chem. A*, vol. 4, no. 20, pp. 7573–7579, 2016, doi: 10.1039/c6ta01800a.
- [80] D. H. Macdonald *et al.*, "Texturing industrial multicrystalline silicon solar cells," *Sol. Energy*, vol. 76, no. 1–3, pp. 277–283, 2004, doi: 10.1016/j.solener.2003.08.019.
- [81] M. Abbott and J. Cotter, "Optical and electrical properties of laser texturing for high-efficiency solar cells," *Prog. Photovoltaics Res. Appl.*, vol. 14, no. 3, pp. 225–235, 2006, doi: <https://doi.org/10.1002/pip.667>.
- [82] P. Campbell and M. A. Green, "High performance light trapping textures for monocrystalline silicon solar cells," *Sol. Energy Mater. Sol. Cells*, vol. 65, pp. 369–375, 2001, doi: 10.1016/S0927-0248(00)00115-X.
- [83] K.-C. Park, H. J. Choi, C.-H. Chang, R. E. Cohen, G. H. McKinley, and G. Barbastathis, "Nanotextured Silica Surfaces with Robust Superhydrophobicity and Omnidirectional Broadband Supertransmissivity," *ACS Nano*, vol. 6, no. 5, pp. 3789–3799, 2012, doi: 10.1021/nn301112t.
- [84] R. Schmager *et al.*, "Texture of the Viola Flower for Light Harvesting in Photovoltaics," *ACS Photonics*, vol. 4, no. 11, pp. 2687–2692, 2017, doi: 10.1021/acsp Photonics.7b01153.
- [85] S. Dottermusch *et al.*, "Micro - cone textures for improved light in - coupling and retroreflection - inspired light trapping at the front surface of solar modules," *Prog. Photovoltaics Res. Appl.*, vol. 27, no. 7, pp. 593–602, 2019, doi: 10.1002/pip.3133.
- [86] S. J. Cho, T. An, and G. Lim, "Three-dimensionally designed anti-reflective silicon surfaces for perfect absorption of light," *Chem. Commun.*, vol. 50, no. 99, pp. 15710–15713, 2014, doi: 10.1039/c4cc07341j.
- [87] M. Jaysankar *et al.*, "Perovskite-silicon tandem solar modules with optimised light harvesting," *Energy Environ. Sci.*, vol. 11, no. 6, pp. 1489–1498, 2018, doi: 10.1039/C8EE00237A.
- [88] Y. H. Yeong and M. C. Gupta, "Hot embossed micro-textured thin superhydrophobic Teflon FEP sheets for low ice adhesion," *Surf. Coatings Technol.*, vol. 313, pp. 17–23, 2017, doi: 10.1016/j.surfcoat.2017.01.026.
- [89] S. Yu, Z. Guo, and W. Liu, "Biomimetic transparent and superhydrophobic coatings: from

- nature and beyond nature," *Chem. Commun.*, vol. 51, no. 10, pp. 1775–1794, 2015, doi: 10.1039/C4CC06868H.
- [90] N. Valipour M., F. C. Birjandi, and J. Sargolzaei, "Super-non-wettable surfaces: A review," *Colloids Surfaces A Physicochem. Eng. Asp.*, vol. 448, no. 1, pp. 93–106, 2014, doi: 10.1016/j.colsurfa.2014.02.016.
- [91] T. Gorter and A. H. M. E. Reinders, "A comparison of 15 polymers for application in photovoltaic modules in PV-powered boats," *Appl. Energy*, vol. 92, pp. 286–297, 2012, doi: 10.1016/j.apenergy.2011.10.042.
- [92] M. DeBergalis, "Fluoropolymer films in the photovoltaic industry," *J. Fluor. Chem.*, vol. 125, no. 8, pp. 1255–1257, 2004, doi: 10.1016/j.jfluchem.2004.05.013.
- [93] N. J. Glassmaker, R. S. McLean, M. H. Reilly, K. R. Warrington, and L. Zhang, "Alumina tie layer promotes environmental durability of FEP adhesion to EVA," *J. Adhes.*, vol. 87, no. 6, pp. 558–578, 2011, doi: 10.1080/00218464.2011.583585.
- [94] M. Kim *et al.*, "FEP encapsulated crack-based sensor for measurement in moisture-laden environment," *Materials (Basel)*, vol. 12, no. 9, p. 1516, 2019, doi: 10.3390/ma12091516.
- [95] J. D. Broder and G. A. Mazaris, "The use of FEP Teflon in solar cell cover technology," in *10th Photovoltaic Specialists Conference*, Palo Alto, 1973.
- [96] The Chemours Company, "Teflon FEP film properties bulletin," The Chemours Company. Accessed: Feb. 21, 2019. [Online]. Available: <https://www.teflon.com/en/-/media/files/teflon/teflon-fep-film-properties-bulletin.pdf>
- [97] DuPont, "DuPont Teflon Films for Photovoltaic Modules," United States of America, 2006. Accessed: Aug. 01, 2018. [Online]. Available: <https://www.photovoltaics.dupont.com>
- [98] I. Nayshevsky, Q. Xu, and A. M. Lyons, "Hydrophobic-Hydrophilic Surfaces Exhibiting Dropwise Condensation for Anti-Soiling Applications," *IEEE J. Photovoltaics*, vol. 9, no. 1, pp. 302–307, 2019, doi: 10.1109/JPHOTOV.2018.2882636.
- [99] I. Nayshevsky, Q. Feng, G. Barahman, and A. M. Lyons, "Fluoropolymer coatings for solar cover glass : Anti-soiling mechanisms in the presence of dew," *Sol. Energy Mater. Sol. Cells*, vol. 206, p. 110281, 2020, doi: 10.1016/j.solmat.2019.110281.
- [100] Uni-Solar, "Uni-Solar Bankability report," Uni-Solar, 2011. Accessed: Dec. 02, 2019. [Online]. Available: http://www.uni-solar.com/wp-content/uploads/pdf/Bankability_Report.pdf
- [101] J. Pern, "Module Encapsulation Materials, Processing and Testing (workshop slides)," Colorado, USA, 2008. Accessed: Dec. 02, 2019. [Online]. Available: <https://www.nrel.gov/docs/fy09osti/44666.pdf>
- [102] A. Badiie, I. A. Ashcroft, and R. D. Wildman, "The thermo-mechanical degradation of ethylene vinyl acetate used as a solar panel adhesive and encapsulant," *Int. J. Adhes. Adhes.*, vol. 68, pp. 212–218, 2016, doi: 10.1016/j.ijadhadh.2016.03.008.
- [103] A. W. Czanderna and F. J. Pern, "Encapsulation of PV modules using ethylene vinyl acetate copolymer as a pottant : A critical review," *Sol. Energy Mater. Sol. Cells*, vol. 43, pp. 101–181, 1996, doi: 10.1016/0927-0248(95)00150-6.
- [104] F. J. Pern, "Ethylene-Vinyl Acetate (EVA) encapsulants for photovoltaic modules: Degradation and discoloration mechanisms and formulation modifications for improved photostability," *Die Angew. Makromol. Chemie*, vol. 252, no. 1, pp. 195–216, 1997, doi: <https://doi.org/10.1002/apmc.1997.052520114>.

- [105] N. K. Shivaprakash, J. Zhang, A. Panwar, C. Barry, Q. Truong, and J. Mead, "Continuous manufacturing of reentrant structures via roll-to-roll process," *J. Appl. Polym. Sci.*, vol. 136, no. 1, p. 46980, 2019, doi: 10.1002/app.46980.
- [106] T. Mäkelä, T. Haatainen, P. Majander, J. Ahopelto, and V. Lambertini, "Continuous double-sided roll-to-roll imprinting of polymer film," *Jpn. J. Appl. Phys.*, vol. 47, no. 6, pp. 5142–5144, 2008, doi: 10.1143/JJAP.47.5142.
- [107] R. Lohmann *et al.*, "Are Fluoropolymers Really of Low Concern for Human and Environmental Health and Separate from Other PFAS?," *Environ. Sci. Technol.*, vol. 54, no. 20, pp. 12820–12828, 2020, doi: 10.1021/acs.est.0c03244.
- [108] S. H. Korzeniowski *et al.*, "A critical review of the application of polymer of low concern regulatory criteria to fluoropolymers II: Fluoroplastics and fluoroelastomers," *Integr. Environ. Assess. Manag.*, vol. 19, no. 2, pp. 326–354, 2023, doi: 10.1002/ieam.4646.
- [109] A. Habermehl *et al.*, "Roll-to-Roll Hot Embossing of 1D and 2D Photonic Nanostructures," *Adv. Eng. Mater.*, vol. 21, pp. 1–8, 2019, doi: 10.1002/adem.201900110.
- [110] A. Kolew, D. Münch, K. Sikora, and M. Worgull, "Hot embossing of micro and sub-micro structured inserts for polymer replication," *Microsyst. Technol.*, vol. 17, no. 4, pp. 609–618, 2011, doi: 10.1007/s00542-010-1182-x.
- [111] R. Leach, C. Giusca, M. Guttmann, P. J. Jakobs, and P. Rubert, "Development of low-cost material measures for calibration of the metrological characteristics of areal surface texture instruments," *CIRP Ann. - Manuf. Technol.*, vol. 64, no. 1, pp. 545–548, 2015, doi: 10.1016/j.cirp.2015.03.002.
- [112] T. Beikircher, M. Möckl, P. Osgyan, and G. Streib, "Advanced solar flat plate collectors with full area absorber, front side film and rear side vacuum super insulation," *Sol. Energy Mater. Sol. Cells*, vol. 141, pp. 389–406, 2015, doi: 10.1016/j.solmat.2015.06.019.
- [113] M. S. Chowdhury *et al.*, "An overview of solar photovoltaic panels' end-of-life material recycling," *Energy Strateg. Rev.*, vol. 27, p. 100431, 2020, doi: 10.1016/j.esr.2019.100431.
- [114] D. Sica, O. Malandrino, S. Supino, M. Testa, and M. C. Lucchetti, "Management of end-of-life photovoltaic panels as a step towards a circular economy," *Renew. Sustain. Energy Rev.*, vol. 82, pp. 2934–2945, 2018, doi: 10.1016/j.rser.2017.10.039.
- [115] M. Powalla *et al.*, "High-efficiency Cu(In,Ga)Se₂ cells and modules," *Sol. Energy Mater. Sol. Cells*, vol. 119, pp. 51–58, 2013, doi: 10.1016/j.solmat.2013.05.002.
- [116] M. Langenhorst *et al.*, "Freeform surface invisibility cloaking of interconnection lines in thin-film photovoltaic modules," *Sol. Energy Mater. Sol. Cells*, vol. 182, pp. 294–301, 2018, doi: 10.1016/j.solmat.2018.03.034.
- [117] Thorlabs, "Index Matching Gel (G608N3) Material Safety Data Sheet," 2013. Accessed: Feb. 21, 2018. [Online]. Available: <https://www.thorlabs.com/thorproduct.cfm?partnumber=G608N3>
- [118] W. Rasband, "ImageJ." Open source - Public domain, 1997. Accessed: Dec. 15, 2019. [Online]. Available: <https://imagej.net/ij/index.html>
- [119] A. Roslizar, J. Taddeucci, U. W. Paetzold, H. Hölscher, B. S. Richards, and S. Member, "Influence of Wind Speed on Volcano Ash Removal From Self-Cleaning Cover Films Dedicated for Photovoltaics," *IEEE J. Photovoltaics*, vol. 12, no. 1, pp. 1–8, 2021, doi: 10.1109/JPHOTOV.2021.3117913.

- [120] U.S. Department of the Interior, "Rainfall calculator, metric units. How much water falls during a storm?," U.S. Geological Survey. Accessed: May 15, 2019. [Online]. Available: <https://water.usgs.gov/edu/activity-howmuchrain-metric.html>
- [121] D. C. Miller, M. T. Muller, and L. . Simpson, "NREL Report: Review of artificial abrasion test methods for PV module technology," 2016. Accessed: Dec. 01, 2019. [Online]. Available: <https://www.nrel.gov/docs/fy16osti/66334.pdf>
- [122] A. T. Mulrone and M. C. Gupta, "Optically transparent superhydrophobic polydimethylsiloxane by periodic surface microtexture," *Surf. Coatings Technol.*, vol. 325, pp. 308–317, 2017, doi: 10.1016/j.surfcoat.2017.06.066.
- [123] M. Šuri, T. A. Huld, E. D. Dunlop, and H. A. Ossenbrink, "Potential of solar electricity generation in the European Union member states and candidate countries," *Sol. Energy*, vol. 81, no. 10, pp. 1295–1305, 2007, doi: 10.1016/j.solener.2006.12.007.
- [124] A. Roslizar *et al.*, "Hot-embossed microcone-textured fluoropolymer as self-cleaning and anti-reflective photovoltaic module covers," *Sol. Energy Mater. Sol. Cells*, vol. 214, 2020, doi: 10.1016/j.solmat.2020.110582.
- [125] S. Alamri, A. I. Aguilar-Morales, and A. F. Lasagni, "Controlling the wettability of polycarbonate substrates by producing hierarchical structures using Direct Laser Interference Patterning," *Eur. Polym. J.*, vol. 99, pp. 27–37, 2018, doi: 10.1016/j.eurpolymj.2017.12.001.
- [126] M. Nosonovsky and B. Bhushan, "Roughness optimization for biomimetic superhydrophobic surfaces," *Microsyst. Technol.*, vol. 11, no. 7, pp. 535–549, 2005, doi: 10.1007/s00542-005-0602-9.
- [127] A. Al Shehri, B. Parrott, P. Carrasco, H. Al Saiari, and I. Taie, "Accelerated testbed for studying the wear, optical and electrical characteristics of dry cleaned PV solar panels," *Sol. Energy*, vol. 146, pp. 8–19, 2017, doi: 10.1016/j.solener.2017.02.014.
- [128] R. Paolini *et al.*, "Effects of soiling and weathering on the albedo of building envelope materials: Lessons learned from natural exposure in two European cities and tuning of a laboratory simulation practice," *Sol. Energy Mater. Sol. Cells*, vol. 205, p. 110264, 2020, doi: 10.1016/j.solmat.2019.110264.
- [129] T. Weber *et al.*, "From the Impact of Harsh Climates and Environmental Conditions on PV-Modules -Development of a Soiling and Abrasion Test," in *EU PVSEC*, 2014, pp. 1–6. doi: 10.13140/2.1.3415.4244.
- [130] M. K. Smith, C. C. Wamser, K. E. James, S. Moody, D. J. Sailor, and T. N. Rosenstiel, "Effects of Natural and Manual Cleaning on Photovoltaic Output," *J. Sol. Energy Eng.*, vol. 135, no. 3, p. 034505, 2013, doi: 10.1115/1.4023927.
- [131] A. Gholami, I. Khazaee, S. Eslami, M. Zandi, and E. Akrami, "Experimental investigation of dust deposition effects on photo-voltaic output performance," *Sol. Energy*, vol. 159, pp. 346–352, 2018, doi: 10.1016/j.solener.2017.11.010.
- [132] S. Patil and H. M. Mallaradhya, "Design and implementation of microcontroller based automatic dust cleaning system for solar panel," *Int. J. Eng. Res. Adv. Technol.*, vol. 2, no. 01, pp. 183–186, 2016, doi: 10.31695/IJERAT.
- [133] D. Deb and N. L. Brahmabhatt, "Review of yield increase of solar panels through soiling prevention, and a proposed water-free automated cleaning solution," *Renew. Sustain. Energy Rev.*, vol. 82, pp. 3306–3313, 2018, doi: 10.1016/j.rser.2017.10.014.

- [134] I. Arabatzis *et al.*, “Photocatalytic, self-cleaning, antireflective coating for photovoltaic panels: Characterization and monitoring in real conditions,” *Sol. Energy*, vol. 159, pp. 251–259, 2018, doi: 10.1016/J.SOLENER.2017.10.088.
- [135] Y. D. Kim, J. Shin, J. Cho, H. Choi, and H. Lee, “Nanosized patterned protective glass exhibiting high transmittance and self-cleaning effects for photovoltaic systems,” *Phys. Status Solidi Appl. Mater. Sci.*, vol. 211, no. 8, pp. 1822–1827, 2014, doi: 10.1002/pssa.201330643.
- [136] L. J. Lane and M. H. Nichols, “Semi-arid climates and terrain,” in *Environmental Geology*, Dordrecht: Springer Netherlands, 1999, pp. 556–558. doi: 10.1007/1-4020-4494-1_300.
- [137] R. Modarres and V. de Paulo Rodrigues da Silva, “Rainfall trends in arid and semi-arid regions of Iran,” *J. Arid Environ.*, vol. 70, no. 2, pp. 344–355, 2007, doi: 10.1016/j.jaridenv.2006.12.024.
- [138] K. Ilse, M. Z. Khan, N. Voicu, V. Naumann, C. Hagendorf, and J. Bagdahn, “Advanced performance testing of anti-soiling coatings – Part I: Sequential laboratory test methodology covering the physics of natural soiling processes,” *Sol. Energy Mater. Sol. Cells*, vol. 202, 2019, doi: 10.1016/j.solmat.2019.110048.
- [139] Y. Jiang, S. Matsusaka, H. Masuda, and Y. Qian, “Characterizing the effect of substrate surface roughness on particle – wall interaction with the airflow method,” *Powder Technol.*, vol. 186, pp. 199–205, 2008, doi: 10.1016/j.powtec.2007.11.041.
- [140] B. Nasr, G. Ahmadi, A. R. Ferro, and S. Dhaniyala, “A model for particle removal from surfaces with large-scale roughness in turbulent flows,” *Aerosol Sci. Technol.*, vol. 54, no. 3, pp. 291–303, 2020, doi: 10.1080/02786826.2019.1692126.
- [141] M. Soltani and G. Ahmadi, “Particle detachment from rough surfaces in turbulent flows,” *J. Adhes.*, vol. 51, no. 1–4, pp. 105–123, 1995, doi: 10.1080/00218469508009992.
- [142] M. Götzinger and W. Peukert, “Particle adhesion force distributions on rough surfaces,” *Langmuir*, vol. 20, no. 13, pp. 5298–5303, 2004, doi: 10.1021/la049914f.
- [143] K. Ilse, M. Z. Khan, N. Voicu, V. Naumann, C. Hagendorf, and J. Bagdahn, “Advanced performance testing of anti-soiling coatings - Part II: Particle-size dependent analysis for physical understanding of dust removal processes and determination of adhesion forces,” *Sol. Energy Mater. Sol. Cells*, vol. 202, p. 110049, 2019, doi: 10.1016/j.solmat.2019.110049.
- [144] N. S. Beattie, R. S. Moir, C. Chacko, G. Buffoni, S. H. Roberts, and N. M. Pearsall, “Understanding the effects of sand and dust accumulation on photovoltaic modules,” *Renew. Energy*, vol. 48, pp. 448–452, 2012, doi: 10.1016/j.renene.2012.06.007.
- [145] H. R. Moutinho *et al.*, “Adhesion mechanisms on solar glass: Effects of relative humidity, surface roughness, and particle shape and size,” *Sol. Energy Mater. Sol. Cells*, vol. 172, pp. 145–153, 2017, doi: 10.1016/j.solmat.2017.07.026.
- [146] E. F. Cuddihy, “Theoretical considerations of soil retention,” *Sol. Energy Mater.*, vol. 3, pp. 21–33, 1980, doi: [https://doi.org/10.1016/0165-1633\(80\)90047-7](https://doi.org/10.1016/0165-1633(80)90047-7).
- [147] E. Del Bello, J. Taddeucci, J. P. Merrison, S. Alois, J. J. Iversen, and P. Scarlato, “Experimental simulations of volcanic ash resuspension by wind under the effects of atmospheric humidity,” *Sci. Rep.*, vol. 8, no. 1, pp. 1–11, 2018, doi: 10.1038/s41598-018-32807-2.
- [148] L. L. Kazmerski *et al.*, “Soiling particle interactions on PV modules: Surface and inter-particle adhesion and chemistry effects,” in *IEEE 43th Photovoltaic Specialist Conference, PVSC 2016*, 2016, pp. 1714–1717. doi: 10.1109/PVSC.2017.8366373.

- [149] D. Goossens, "Soiling of Photovoltaic Modules: Size Characterization of the Accumulated Dust," *J. Clean Energy Technol.*, vol. 7, no. 3, pp. 25–31, 2019, doi: 10.18178/jocet.2019.7.3.505.
- [150] J. F. Kok, E. J. R. Parteli, T. I. Michaels, and D. B. Karam, "The physics of wind-blown sand and dust," *Reports Prog. Phys.*, vol. 75, no. 10, 2012, doi: 10.1088/0034-4885/75/10/106901.
- [151] R. J. Isaifan, D. Johnson, L. Ackermann, B. Figgis, and M. Ayoub, "Evaluation of the adhesion forces between dust particles and photovoltaic module surfaces," *Sol. Energy Mater. Sol. Cells*, vol. 191, pp. 413–421, 2019, doi: 10.1016/j.solmat.2018.11.031.
- [152] X. Du, F. Jiang, E. Liu, C. Wu, and F. H. Ghorbel, "Turbulent airflow dust particle removal from solar panel surface: Analysis and experiment," *J. Aerosol Sci.*, vol. 130, pp. 32–44, 2019, doi: 10.1016/j.jaerosci.2019.01.005.
- [153] J. W. Cleaver and B. Yates, "Mechanism of detachment of colloidal particles from a flat substrate in a turbulent flow," *J. Colloid Interface Sci.*, vol. 44, no. 3, pp. 464–474, 1973, doi: 10.1016/0021-9797(73)90323-8.
- [154] K. K. Ilse *et al.*, "Particle size-dependent adhesion forces and wind removal efficiency of anti-soiling coatings on textured solar glasses," *MRS Commun.*, vol. 9, no. 3, pp. 964–970, 2019, doi: 10.1557/mrc.2019.105.
- [155] A. S. Kassab, V. M. Ugaz, M. D. King, and Y. A. Hassan, "High Resolution Study of Micrometer Particle Detachment on Different Surfaces," *Aerosol Sci. Technol.*, vol. 47, no. 4, pp. 351–360, 2013, doi: 10.1080/02786826.2012.752789.
- [156] B. Bayandelger, Y. Ueda, B. Batbayar, A. Adiyabat, N. Enebish, and K. Otani, "Long-term performance and degradation rate analyses of photovoltaic modules exposed in the Gobi Desert, Mongolia," *Jpn. J. Appl. Phys.*, vol. 57, p. 08RG07, 2018, doi: 10.7567/JJAP.57.08RG07.
- [157] A. Asgharzadeh, B. Marion, C. Deline, C. Hansen, J. S. Stein, and F. Toor, "A sensitivity study of the impact of installation parameters and system configuration on the performance of bifacial PV arrays," *IEEE J. Photovoltaics*, vol. 8, no. 3, pp. 798–805, 2018, doi: 10.1109/JPHOTOV.2018.2819676.
- [158] J. E. Panebianco, M. J. Mendez, D. E. Buschiazzo, D. Bran, and J. J. Gaitán, "Dynamics of volcanic ash remobilisation by wind through the Patagonian steppe after the eruption of Cordón Caulle, 2011," *Sci. Rep.*, vol. 7, pp. 1–11, 2017, doi: 10.1038/srep45529.
- [159] J. E. Stout and R. Arimoto, "Threshold wind velocities for sand movement in the Mescalero Sands of southeastern New Mexico," *J. Arid Environ.*, vol. 74, no. 11, pp. 1456–1460, 2010, doi: 10.1016/j.jaridenv.2010.05.011.
- [160] Q. Guan *et al.*, "Climatological analysis of dust storms in the area surrounding the Tengger Desert during 1960–2007," *Clim. Dyn.*, vol. 45, no. 3–4, pp. 903–913, 2015, doi: 10.1007/s00382-014-2321-3.

Acknowledgement

In the name of God, the Most Gracious the Most Merciful.

It has been a long journey to reach this point. A hard, longer than expected, difficult and lonely journey – but a journey none the less. As with any journey, there were multiple ups and downs. But I have enjoyed the learning process and the personal growth that I experienced – developing myself professionally and more importantly as a person.

From the bottom of my heart, I would like to especially express gratitude to my supervisors from KIT for their guidance, wisdom, and patience throughout my Ph.D. research journey – Prof. Dr. Bryce S. Richards, Prof. Dr. Hendrik Hölscher and Prof. Dr. Ulrich W. Paetzold. I will always remember and be grateful for all that I have learnt and the life lessons that I received; from the many talks and discussions and even from simply observing their conduct and carry, it has taught me a lot. Also not forgetting one of my earlier supervisors at the beginning of my time at KIT, Dr. Efthymios Klampaftis. May he be successful in the things that he aims for in life.

I am very grateful to Prof. Dr. Christian Greiner for having agreed to be the second reviewer of this dissertation.

I would like to also express thanks to colleagues from KIT (especially from the Institute of Microstructure Technology) who were directly involved in my research work – Dr. Stephan Dottermusch, Dr. Raphael Schmager, Dr. Malte Langenhorst, Dr. Benjamin Fritz, Dr. Felix Vüllers, Dr. Guillaume Gomard. Thank you for all the fruitful discussions, opinions and insights that have contributed towards the completion of my research work.

Colleagues from the research groups of Bryce (N4E) and Hendrik (FuE1) – too many to name here, but I will have your names written in my heart. Thank you for all the time spent together. I would cherish the friendship and hope that we will cross paths again, either professionally or in a personal manner.

I would also like to thank the people from the many support groups of IMT who helped me during my stay there. Also, thank you to Dr. Jacopo Taddeucci for the help while doing my research in Rome.

A special mention also to the Malaysian friends from AZIM, who helped me, and my family accommodate to a foreign country during our stay in Deutschland.

I would like to thank my parents (Dr. Roslizar and Nabilah) and parents-in-law (Md. Seniman and Masrol Hairiah), who gave their support and prayers throughout this journey. All the calls and advice from back home at that time gave me the energy and motivation to complete this Ph.D.

Finally, I would like to express my heartfelt appreciation to my wife, Sarah, and my 2 daughters, Nur and Lynn, that have been with me throughout this journey. Moving to a new country where we don't speak the language, patiently withstanding any hardship and challenges that this journey has given us. May the experience throughout these few years become something that helps us grow as individuals and as a family. Hopefully, this journey will bring us together and become stronger as a family. I love you guys.

List of Publications

Peer-reviewed journal publications as first author

Parts of this thesis have already been published in peer-reviewed scientific journals:

- **Aiman Roslizar**, Stephan Dottermusch, Felix Vüllers, Maryna N. Kavalenka, Markus Guttman, Marc Schneider, Ulrich W. Paetzold, Hendrik Hölscher, Bryce S. Richards, and Efthymios Klampaftis. "Self-cleaning performance of superhydrophobic hot-embossed fluoropolymer films for photovoltaic modules." *Solar Energy Materials and Solar Cells* 189 (2019): 188-196.
- **Aiman Roslizar**, Stephan Dottermusch, Raphael Schmager, Markus Guttman, Guillaume Gomard, Hendrik Hölscher, Bryce S. Richards, and Ulrich W. Paetzold. "Hot-embossed microcone-textured fluoropolymer as self-cleaning and anti-reflective photovoltaic module covers." *Solar Energy Materials and Solar Cells* 214 (2020): 110582.
- **Aiman Roslizar**, Jacopo Taddeucci, Ulrich Wilhelm Paetzold, Hendrik Hölscher, and Bryce S. Richards. "Influence of Wind Speed on Volcano Ash Removal from Self-Cleaning Cover Films Dedicated for Photovoltaics." *IEEE Journal of Photovoltaics* 12, no. 1 (2021): 453-460.

Peer-reviewed journal publications as co-author

Assistance in the fabrication of microtextured samples and characterization, especially of wetting properties of surfaces, resulted in co-authorship of the following publications:

- Stephan Dottermusch, Aina Quintilla, Guillaume Gomard, **Aiman Roslizar**, Vikas Reddy Voggu, B. A. Simonsen, J. S. Park et al. "Infiltrated photonic crystals for light-trapping in CuInSe 2 nanocrystal-based solar cells." *Optics express* 25, no. 12 (2017): A502-A514.
- Benjamin Fritz, Markus Guttman, Pere Casas Soler, **Aiman Roslizar**, Malte Langenhorst, Marc Schneider, Ulrich W. Paetzold et al. "Towards mass fabrication of hot embossed plant surface texture replicas as photovoltaic cover layers." In *Nanoengineering: Fabrication, Properties, Optics, and Devices XV*, vol. 10730, pp. 49-58. SPIE, 2018.
- Felix Vüllers, Benjamin Fritz, **Aiman Roslizar**, Andreas Striegel, Markus Guttman, Bryce S. Richards, Hendrik Hölscher, Guillaume Gomard, Efthymios Klampaftis, and Maryna N. Kavalenka. "Self-cleaning microcavity array for photovoltaic modules." *ACS applied materials & interfaces* 10, no. 3 (2018): 2929-2936.
- Malte Langenhorst, David Ritzer, Frederik Kotz, Patrick Risch, Stephan Dottermusch, **Aiman Roslizar**, Raphael Schmager, Bryce S. Richards, Bastian E. Rapp, and Ulrich W. Paetzold. "Liquid Glass for Photovoltaics: Multifunctional Front Cover Glass for Solar Modules." *ACS applied materials & interfaces* 11, no. 38 (2019): 35015-35022.

Conference contributions

Parts of this thesis have been presented at national and international scientific conferences:

- **A. Roslizar**, F. Vüllers, B. Fritz, M. N. Kavalenka, G. Gomard, H. Hölscher, B. S. Richards, and E. Klampaftis, "Bioinspired Self-Cleaning Cover Films for Photovoltaic Modules" in the 644. WE-

Heraeus-Seminar: Bio-inspired, Nano- and Microstructured Surfaces: New Functionality by Material and Structure. Bad Honnef, Germany (28-31 May 2017). Poster presentation.

- **A. Roslizar**, S. Dottermusch, F. Vüllers, M. N. Kavalenka, M. Guttman, M. Schneider, E. Klampaftis, U. W. Paetzold, H. Hölscher, and B. S. Richards, "Impact of Fabrication Parameters on the Self-cleaning Performance of Hot-embossed Fluoropolymer Films for Photovoltaic Modules," in *Light, Energy and the Environment 2018*, OSA Technical Digest (Optica Publishing Group, 2018), paper OM3D.4. Singapore (5–8 November 2018). Oral presentation.
- **A. Roslizar**, J. Taddeucci, U. W. Paetzold, H. Hölscher, B. S. Richards, "Influence of Wind Speed on Volcano Ash Removal from PV Modules possessing a Self-Cleaning Cover Film" in the *48th IEEE Photovoltaic Specialists Conference (PVSC)*. Virtual meeting. (20-25 June 2021). Poster presentation.